Novel insights into mechanisms and selectivity of the heterotrimeric G protein inhibitors BIM-46187 and FR900359

Dissertation

zur

Erlangung des Doktorgrades (Dr. rer. nat.)

der

Mathematisch-Naturwissenschaftlichen Fakultät

der

Rheinischen Friedrich-Wilhelms-Universität Bonn

vorgelegt von

Anna-Lena Schmitz geb. Netz

aus

Siegen

Bonn 2014

Angefertigt mit Genehmigung der Mathematisch-Naturwissenschaftlichen Fakultät der Rheinischen Friedrich-Wilhelms-Universität Bonn

1. Gutachter: Prof. Dr. E. Kostenis
2. Gutachter: Prof. Dr. G. M. König

Tag der Promotion: 07.04.2015

Erscheinungsjahr: 2015

Für meine Familie

Publications

Research articles:

Schmitz, A.-L., Schrage, R., Gaffal, E., Charpentier, T.H., Wiest, J., Hiltensperger, G., Morschel, J., Hennen, S., Häußler, D., Horn, V., Wenzel, D., Grundmann, M., Büllesbach, K.M., Schröder, R., Brewitz, H.H., Schmidt, J., Gomeza, J., Galés, C., Fleischmann, B.K., Tüting, T., Imhof, D., Tietze, D., Gütschow, M., Holzgrabe, U., Sondek, J., Harden, T.K., Mohr, K., and Kostenis, E. (2014). A cell-permeable inhibitor to trap Gαq proteins in the empty pocket conformation. Chem. Biol 21, 890-902.

Schrage, R., Holze, J., Klöckner, J., Balkow, A., Klause, A.S., **Schmitz, A.-L.**, Amici, M. de, Kostenis, E., Tränkle, C., Holzgrabe, U., and Mohr, K. (2014). New insight into active muscarinic receptors with the novel radioagonist [^{3}H]iperoxo. Biochem. Pharmacol 90, 307-319.

Poster Presentation:

Netz A.-L., Bock A., Schröder R., Mohr K. and Kostenis E.
(2012) Label-free impedance sensing to study pleiotropic 7TM receptor signaling

Die vorliegende Arbeit wurde in der Zeit von Juni 2011 bis November 2014 am Institut für Pharmazeutische Biologie der Rheinischen Friedrich-Wilhelms Universität Bonn unter der Leitung von Frau Prof. Dr. rer. nat. Evi Kostenis durchgeführt.

Table of Contents

Table of Contents ..... **I**

1 Introduction **1**

1.1 G protein-coupled receptors 1

1.2 G proteins and GPCR signaling 2

1.3 Pathway modulators acting on Gα subunits 6

1.4 Aim of this work 8

2 Material and methods **10**

2.1 Material 10

2.1.1 Chemicals, enzymes and reagents 10

2.1.2 Kits 12

2.1.3 Devices 13

2.1.4 Buffers and solutions 14

2.1.5 Consumables 17

2.1.6 Software 17

2.1.7 Cell culture media 18

2.1.8 Sterilization method 19

2.1.9 Plasmids, bacterial strains and cell lines 19

2.2 Methods 21

2.2.1 Molecular biology methods 21

2.2.2 Cell culture methods 24

2.2.3 Cell-based assays 26

2.2.4 Calculations and data analysis 30

3 Results **31**

3.1 BIM-46187: A pan-G protein inhibitor? 31

3.1.1 Influence on cAMP accumulation in HEK293 and COS7 cells 31

3.1.2 Exploring consequences on the $G\alpha_q$ pathway in HEK293 cells 34

3.1.3 Effect of BIM-dimer on $G\alpha_{13}$ signaling 35

3.1.4 Analyzing BIM-dimer in a CHO cell background 37

3.1.5 Characterizing the influence of BIM-dimer in the patient-derived MZ7 cells 38

3.1.6 Mechanistic link between sensitivity toward BIM inhibition and cellular context 41

3.1.7 BIM-dimer: A substrate for multidrug transporters? 44

3.1.8 Analyzing BIM-dimer in radioligand competition binding assays 47

3.1.9 Influence of BIM-dimer on GDP-dissociation 50

3.1.10 Washing experiments 51

3.1.11 Stability analysis of BIM-monomer 52

3.1.12 Kinetic studies with BIM-monomer and BIM-dimer in a HEK and a CHO cell background 56

3.1.13 Investigating monomeric BIM in HEK and CHO cell backgrounds ... 58
3.1.14 Screening of a substance library with BIM-dimer analogs ... 60
3.2 QIC (FR900359) - a suitable tool to specifically silence $G\alpha_q$ signaling? ... 61
3.2.1 Screening of *Ardisia crenata* extracts ... 61
3.2.2 Stability test ... 68
3.2.3 Kinetic studies with QIC in a HEK and a CHO cell background ... 71
3.2.4 Selectivity of QIC in second-messenger assays in a HEK cell background ... 73
3.2.5 BRET assays revealed QIC as selective inhibitor of $G\alpha_q$ and $G\alpha_{11}$ proteins ... 74
3.2.6 Analyzing the inhibitory profile of QIC in label-free assays ... 78
3.2.7 Characterizing the influence of QIC in the patient-derived MZ7 cells ... 87
3.2.8 Selectivity of QIC in second-messenger assays in CHO cells ... 89
3.2.9 Analyzing QIC in radioligand competition binding assays ... 90
3.2.10 Co-incubation of HEK293 cells with QIC and BIM-dimer ... 92
3.2.11 Characterizing QIC red, a hydrogenated derivative of QIC ... 93
3.2.12 Screening of QIC-derivatives ... 97

4 Discussion ... 101
4.1 Advantages of small molecule G protein inhibitors vs siRNA ... 101
4.2 Context-dependent pharmacology of BIM ... 101
4.3 BIM-dimer functions as GTP entry inhibitor ... 104
4.4 Mode of action and structure activity relationship of QIC ... 106
4.5 $G\alpha_q$-selective inhibitors: an important tool to study G protein signaling pathways and a promising approach for cancer treatment ... 109

5 Summary ... 112
6 Abbreviations ... 113
7 References ... 116
8 Appendix ... 125
Curriculum Vitae ... 127
Erklärung ... 128
Acknowledgment ... 129

1 Introduction

1.1 G protein-coupled receptors

For cells it is of great importance to adapt to their environment and therefore, they must be able to receive extracellular cues and elicit an appropriate intracellular response to those cues (Kimple et al., 2011). Although there are multiple receptor families, the superfamily of G protein-coupled receptors (GPCRs) represents the largest and most pharmacologically important receptor family. There are more than 800 GPCR sequences in the human genome and nearly a third of the pharmaceuticals currently on the market target one or more of these receptors (Fredriksson et al., 2003; Jacoby et al., 2006; Lagerström and Schiöth, 2008). GPCRs have the ability to bind to a broad range of ligands such as small organic compounds, eicosanoids, peptides, proteins and even photons in the case of rhodopsin (Dixon et al., 1986; Masu et al., 1987; Kobilka et al., 1987; Felder et al., 1993; Jacoby et al., 2006). With GPCR-directed drugs it is possible to cover a wide range of therapeutic indications like hypertension, asthma or cancer (Jacoby et al., 2006).

GPCRs feature an extracellular amino terminus and an intracellular carboxyl terminus. They consist of seven α-helical transmembrane stretches that span the plasma membrane in a counter-clockwise manner and therefore, GPCRs can also be termed as seven transmembrane (7TM) receptors (Fredriksson et al., 2003). The greatest homology between GPCRs can be found within the transmembrane (TM) segments. The most variable structures among the family of GPCRs are the carboxyl terminus, the intracellular loop spanning TM5 and TM6, and the amino terminus. The greatest diversity is observed in the amino terminus (Kobilka, 2007). Based on sequence similarities within the 7TM segments GPCRs can be divided into five subfamilies named after their hallmark members: glutamate- (15 members), rhodopsin- (701 members), adhesion- (24 members), frizzled- (24 members), and secretin-like receptors (15 members) (Fredriksson et al., 2003, Kobilka, 2007). The physiological function of a large fraction of GPCRs is still unknown and these receptors are referred to as orphan GPCRs (Kobilka, 2007).

1.2 G proteins and GPCR signaling

Heterotrimeric guanine nucleotide-binding proteins (G proteins) act as switches that regulate information processing circuits connecting GPCRs, which are expressed on the cell surface, to a variety of intracellular effectors (Simon et al., 1991). G proteins consist of three subunits: Gα, Gβ and Gγ. Human G proteins derive from 35 genes, 16 encoding Gα subunits, five Gβ and 14 Gγ (Milligan and Kostenis, 2006). In the basal state, the GDP-bound Gα subunit is in complex with the Gβγ dimer. The nucleotide-binding pocket of the Gα subunit is located between two distinct domains: (i) a Ras-like domain which is named due to its structural resemblance to the Ras superfamily of monomeric GTPases, and (ii) an additional α-helical domain composed of a structurally distinct six-helix bundle. Upon an agonist-induced conformational change, the GPCR acts as a guanine nucleotide exchange factor (GEF) resulting in the release of GDP and subsequent binding of GTP (Bohm et al., 1997; Wall et al., 1998; Johnston and Siderovski, 2007). Once GDP is released, a high-affinity complex is formed between the activated receptor and G protein (Rodbell et al., 1971; Emeis et al., 1982; Bornancin et al., 1989; Oldham and Hamm, 2008). This complex represents a short-lived intermediate in intact cells because high concentrations of guanine nucleotides are abundant, leading to a rapid exchange of GDP for GTP (Rodbell et al., 1971; Oldham and Hamm, 2008). Binding of GTP causes a structural rearrangement within three segments of Gα, called switch regions I-III, resulting from favorable interactions with the γ-phosphate of the newly bound GTP (Lambright et al., 1994; Wall et al., 1998). Switch I serves as one of two connections between the Ras-like and α-helical domains. Switch II assumes a partially helical conformation in the active state and affects many of the interactions of Gα with Gβγ, effectors, RGS proteins and other nucleotide-state-selective binding partners (Kimple et al., 2002; Johnston et al., 2005; Johnston et al., 2006). Switch III assumes a loop structure found ordered only in the active conformation of Gα. The structural conformations adopted by switches I-III upon GTP binding enable the Gα subunit to specifically recognize downstream effectors (Johnston and Siderovski, 2007). Thus, the binding of GTP leads to the dissociation of GTP-bound Gα from Gβγ and both are able to interact with effectors such as adenylyl cyclase, phospholipase C isoforms, RhoGEFs and ion channels (Clapham and Neer, 1997; Kozasa et al., 1998; Simonds, 1999; Lutz et al., 2007). Downstream effectors are activated until GTP is hydrolyzed by the intrinsic GTP hydrolysis activity of the Gα subunit. Upon hydrolysis of GTP, Gα rebinds Gβγ and the system returns to the inactive

state. Regulator of G protein signaling (RGS) proteins are able to dramatically enhance the rate of GTP hydrolysis as they function as GTPase-accelerating proteins (GAPs) in vitro and in vivo (Berman et al., 1996; Lambert et al., 2010) (**Fig. 1**).

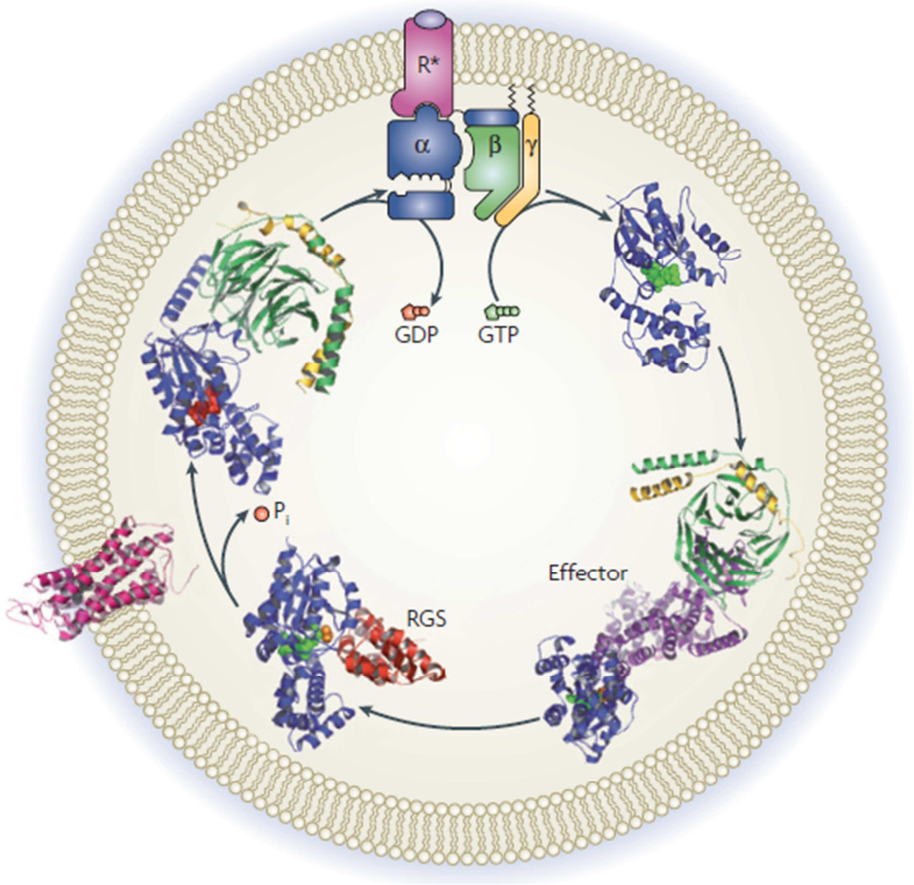

Figure 1: The G protein cycle. In the inactive state, G proteins are heterotrimers consisting of GDP-bound α, β- and γ-subunits. Upon agonist binding conformational changes of the receptor permit G protein binding and catalyze GDP release from Gα. After GDP release, a stable, high-affinity complex is formed between the activated receptor (R*) and G protein. Subsequent binding of GTP to Gα destabilizes this complex, allowing Gα(GTP) and Gβγ, to interact with downstream effector proteins The signal is terminated on hydrolysis of GTP to GDP by Gα, which may be catalyzed by RGS proteins (taken from Oldham and Hamm, 2008).

G protein heterotrimers are typically divided into four main classes based on the primary sequence similarity of their Gα subunits: $G\alpha_s$, $G\alpha_{i/o}$, $G\alpha_{q/11}$ and $G\alpha_{12/13}$ (Simon et al., 1991, Offermanns, 2003) (**Fig. 2**). GPCRs have the ability to couple selectively to members of one or more of these G protein families, thus allowing selective modulation of signaling cascades by particular GPCR ligands (Johnston and Siderovski, 2007).

The $G\alpha_s$ subclass includes the $G\alpha_s$ and $G\alpha_{olf}$ isotype. $G\alpha_{olf}$ shows 88% amino acid sequence identity with $G\alpha_s$ and both proteins share the ability to activate adenylyl cyclase to increase intracellular cAMP levels. $G\alpha_s$ proteins are ubiquitously expressed but $G\alpha_{olf}$ expression is restricted to specific neural tissues and is enriched in neurons in the olfactory epithelium (Simon et al., 1991; Milligan and Kostenis, 2006).

The $G\alpha_{i/o}$ subclass consists of the almost ubiquitously expressed $G\alpha_{i1}$, $G\alpha_{i2,}$ $G\alpha_{i3}$, $G\alpha_{oA}$ and $G\alpha_{oB}$ proteins as well as the brain- and platelet-specific $G\alpha_z$ and $G\alpha_t$, $G\alpha_{t2}$ and $G\alpha_{gust}$ which are expressed in the retina or in the taste buds (Simon et al., 1991; Milligan and Kostenis, 2006). $G\alpha_{i/o}$ proteins are able to inhibit adenylyl cyclase activity which results in reduced cAMP levels (Milligan and Kostenis, 2006).

Gα proteins belonging to the $G\alpha_{q/11}$ family activate phospholipase Cβ (PLCβ) isoforms. PLCβ hydrolyzes phosphatidylinositol bisphosphonate in the plasma membrane, generating inositol 1,4,5-trisphosphate (IP3) and diacylglycerol (DAG). IP3 activates receptors in the endoplasmatic reticulum (ER) leading to a Ca^{2+} release from intracellular Ca^{2+} stores in the ER while DAG stimulates the protein kinase C (PKC) (Cockcroft and Gomperts, 1985; Milligan and Kostenis, 2006). This subclass includes $G\alpha_q$, $G\alpha_{11}$, $G\alpha_{14}$, $G\alpha_{15}$ and $G\alpha_{16}$ proteins in which $G\alpha_{15}$ only represents a murine orthologue of $G\alpha_{16}$ (Kostenis et al., 2005). $G\alpha_q$ and $G\alpha_{11}$ are widely distributed and the amino acid sequences of these isotypes differ from each other by less than 12%. Almost all changes are confined to the NH_2-terminal region which may play an important role in determining the specificity of interaction with the βγ subunit and the relative rate of nucleotide exchange and hydrolysis. Both proteins are often found in the same cell which can be explained with the possibility to generate signals with different time constants (Simon et al., 1991). The three other isotypes of the $G\alpha_q$ family show restricted patterns of tissue specific expression. $G\alpha_{14}$ is primarily found in stromal and epithelial cells while $G\alpha_{15}$ and $G\alpha_{16}$ are found in hematopoietic cells (Simon et al., 1991; Milligan and Kostenis, 2006).

$G\alpha_{12}$ and $G\alpha_{13}$ proteins form a separate family and they are expressed ubiquitously. Activation of $G\alpha_{12}$ and $G\alpha_{13}$ proteins cannot be associated with second-messenger production but with regulation of the activity of the small GTPase Rho through guanine nucleotide exchange factor (RhoGEF). These G proteins modulate various cellular responses such as cytoskeletal changes and cellular growth. A variety of other interaction partners for $G\alpha_{12/13}$ proteins have also been reported. $G\alpha_{12/13}$ proteins can

interfere with the function of cadherins radixin, A-kinase anchoring proteins, non-receptor tyrosine kinases and protein phosphatases (Kurose 2003; Worzfeld et al., 2008).

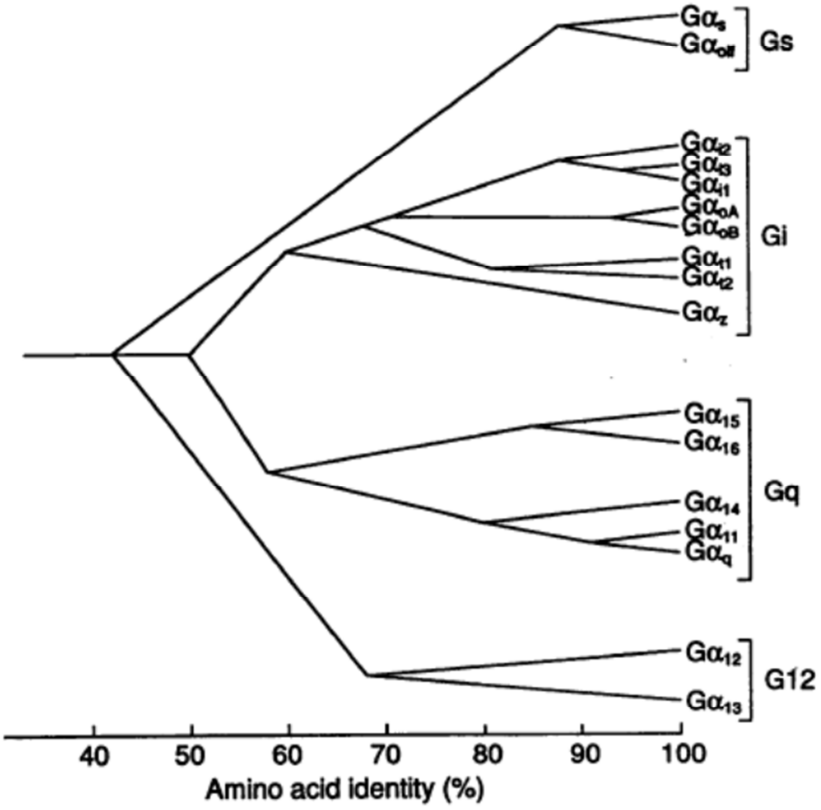

Figure 2: Relationships among mammalian Gα subunits. The α subunits are divided into four main subclasses based on the primary amino acid sequence identity (taken from Simon et al., 1991).

In addition to the signal generating process, the ligand-bound receptor initiates a second process which leads to receptor desensitization and occurs through receptor modification (Simon et al., 1991). Rapid dampening of receptor function is usually controlled by receptor phosphorylation which is mediated by second-messenger kinases (for example protein kinase A (PKA) and protein kinase C (PKC)), or by a distinct family of G protein-coupled receptor kinases (GRKs) (Pitcher et al., 1998). GRK phosphorylation promotes binding of a β-arrestin molecule to the receptor which sterically inhibits further interactions between the receptor and the G protein (Pierce et al., 2002). Arrestins can also bind to the coat structure of clathrin-coated pits, thereby promoting endocytosis of arrestin-bound receptors. After targeting to endosomal compartments, GPCRs can be rapidly de-phosphorylated and recycled back

to the plasma membrane or are delivered to lysosomal compartments for degradation (Hanyaloglu and von Zastrow, 2008).

In addition to their role in receptor internalization, β-arrestins have the ability to serve as scaffolding proteins to promote G protein-independent signaling, thereby linking GPCRs to effectors such as mitogen-activated protein kinases (MAPK), including extracellular signal-regulated kinase1/2 (ERK1/2), p38 kinase and c-Jun N-terminal kinase 3 (JNK3), as well as protein kinase B (AKT) and phosphatidylinositol 3-kinase (PI3K) pathways (Pierce et al., 2002; Defea, 2008).

1.3 Pathway modulators acting on Gα subunits

GPCRs regulate a wide range of physiological and pathophysiological processes. Thus, selective pathway modulators acting on Gα subunits enable the investigation of the contribution of G protein signaling in physiology and disease (Smrcka, 2013). The following substances are prominent examples for such pathway modulators.

$G\alpha_{i/o}$ proteins can be specifically inhibited with pertussis toxin (PTX). PTX represents a typical A-B toxin which is produced by the whooping cough-causing bacterium *Bordetella pertussis* (Pittman, 1979). The A-protomer exhibits ADP-ribosyltransferase activity while the B-oligomer can bind extracellular molecules that allow the toxin to enter the cells (Mangmool and Kurose, 2011). PTX catalyzes the ADP-ribosylation of a conserved cysteine residue located in the α subunits of the $G\alpha_{i/o}$ family (with the exception of $G\alpha_z$), thereby preventing the G proteins from interacting with their cognate GPCRs (Burns, 1988). ADP-ribosylation of the α subunit of heterotrimeric $G\alpha_{i/o}$ proteins locks the α subunit in the inactive GDP-bound form and consequently, the $G\alpha_{i/o}$ protein is unable to inhibit adenylyl cyclase resulting in an enhanced accumulation of cAMP (Mangmool and Kurose, 2011).

Another classic pathway modulator is cholera toxin (CTX), a pathologically active agent, which causes the severe watery diarrhea pathognomonic of cholera, is secreted by the bacterium *Vibrio cholerae* and can be used to explore $G\alpha_s$-mediated signaling (De Haan and Hirst, 2004; Sack et al., 2004). The toxin has an AB5 arrangement of subunits. Five identical B subunits are responsible for binding the toxin to its cell-surface receptor and have highest affinity to ganglioside GM_1. The A subunit has been shown to possess enzymatic activity and is well known for generating the toxin-specific

biological response. It binds the host co-factor GTP-ARF6 and transfers ADP-ribose from NAD to the α subunit of the $G\alpha_s$ protein to activate $G\alpha_s$, which in turn stimulates adenylyl cyclase causing a rise in cAMP concentration (Middelbrook and Dorland, 1984; Miller et al., 2008; Guichard et al., 2013). Due to the high cAMP levels, further activation of $G\alpha_s$ proteins is no longer detectable. Thus, $G\alpha_s$-mediated signaling is masked.

Suramin, a symmetric polysulphonated naphtylaminebenzamide derivative, is described as a relatively specific inhibitor of $G\alpha_s$ proteins. It inhibits GDP release but in the absence of mutagenic mapping or structural data, the detailed molecular mechanism is still unknown (Freissmuth et al., 1996; Hohenegger et al., 1998). Due to its strong negative charge, Suramin cannot cross cell membranes, which limits its utility in cell-based assay systems (Smrcka, 2013).

The cyclic depsipeptide YM-254890, isolated from the fermentation broth of *Chromobacterium* sp. QS3666, is described as a specific inhibitor of $G\alpha_q$, $G\alpha_{11}$ and $G\alpha_{14}$ proteins. YM-254890 binds directly to the Gα subunit and inhibits $G\alpha_{q/11}$-mediated signaling by preventing GDP release (Takasaki et al., 2004). It represents the only inhibitor for which structural information is available, thus allowing the understanding of its mode of action at the atomic level. The compound binds in the hydrophobic cleft between two interdomain linkers connecting the GTPase and helical domains of the $G\alpha_q$ protein. This binding stabilizes the inactive GDP-bound state through direct interactions with switch I leading to a loss of linker flexibility (Nishimura et al., 2010).

The depsipeptide FR900359 is isolated from a methanol extract of the whole plants of *Ardisia crenata*. The compound exhibits pharmacological activity as it inhibits platelet aggregation, decreases the blood pressure and is cytotoxic to cultured rat fibroblasts and myelocytic leukemia cells (Fujioka et al., 1988). The molecular structure of FR900359 closely resembles that of the bacterial metabolite YM-254890. FR900359 inhibits IP1 accumulation and Ca^{2+} release of the $G\alpha_{q/11}$-coupled cholecystokinin receptor (CCK1) as well as GTP binding (Nesterov et al., 2010). Further details concerning its mode of action are lacking.

The imidazo-pyrazine derivative BIM-46174 and its more stable, dimeric derivative BIM-46187 are reported to inhibit all G protein α subunit families equally, a feature referred to as pan-G protein inhibition. A pan-G protein inhibitor would be a promising tool to distinguish between G protein-dependent and G protein-independent signaling

pathways. BIM-46174 and BIM-46187 have been successfully analyzed in a large number of different cancer lines such as breast cancer MCF7 or melanoma A2058 cells. BIM inhibits critical functions involved in cancer progression: cell proliferation, survival and invasion. Therefore, BIM-46174 and BIM-46187 were suggested as experimental anticancer drugs (Prévost et al., 2006; Ayoub et al., 2009). The fact that monomeric BIM-46174 by itself is able to inhibit G protein signaling supports an active role for the free sulfhydryl form. A prodrug behavior has been suggested for dimeric BIM-46187 compared with the monomer (Ayoub et al., 2009). It was shown that both molecules bind directly to the Gα subunits thereby preventing the intrinsic or agonist-promoted GDP/GTP exchange (Prévost et al., 2006; Ayoub et al., 2009; Smrcka, 2013). Within these publications it has not been clarified whether BIM-46187 prevents GDP release or GTP entry.

1.4 Aim of this work

In previous publications the synthetic small molecules BIM-46174 and BIM-46187 were described to inhibit all Gα subfamilies equally. In these experiments BIM-46174 and BIM-46187 were investigated using a number of different cancer cell lines and COS7 cells (Prévost et al., 2006; Ayoub et al., 2009). However, the ability to silence all G protein pathways in frequently used immortalized cell lines such as HEK293 or CHO has not yet been examined. Therefore, one aim of this work was to investigate the influence of both BIM molecules on $G\alpha_{q/11}$-, $G\alpha_{s}$-, $G\alpha_{i/o}$- and $G\alpha_{13}$-mediated signaling in a HEK and CHO background. As these experiments revealed that BIM preferentially silences $G\alpha_{q}$ signaling in these cellular backgrounds, a possible mechanistic link between sensitivity toward BIM inhibition and cellular context should be analyzed. Additionally, it was of interest to explore the molecular mechanism underlying BIM-46187 action.

Nesterov et al. reported FR900359 (in this thesis referred to as QIC) as a specific $G\alpha_{q/11}$ inhibitor but convincing data that prove specificity are lacking (Nesterov et al., 2010). Hence, a further aim was to interrogate the specificity of FR900359 for silencing $G\alpha_{q/11}$-mediated signaling in particular and G protein signaling in general in great detail. To this end, a broad panel of assays including but not limited to second-messenger assays and label-free holistic measurements, had to be performed. Furthermore, it should be clarified whether $G\alpha_{q/11}$ inhibition caused by the depsipeptide FR900359 differs

mechanistically from that described for the structurally related $G\alpha_{q/11}$-selective inhibitor YM-254890.

2 Material and methods

2.1 Material

2.1.1 Chemicals, enzymes and reagents

Adenosine 5′-triphosphate disodium salt hydrate (ATP)	Sigma, Taufkirchen, DE, # A2383
Agar	Fluka, Hamburg, DE, #05040
Agarose UltraPure	Invitrogen™, Darmstadt, DE, #15510-27
Aluminium chloride	ZVE, Bonn, DE, #125098
Ampicillin sodium salt	Roth, Karlsruhe, DE #K029.1
BIM-dimer	Synthesized by AG Holzgrabe/Gütschow, University of Würzburg/Bonn, DE
BIM-monomer	Synthesized by AG Holzgrabe University of Würzburg, DE
Blasticidin	InvivoGen, Toulouse, FR, #ant-bl-1
Bovine serum albumin, fatty acid free	Sigma, Taufkirchen, DE, #A6003
Calcium chloride, dehydrate	Sigma, Taufkirchen, DE, #C3306
Carbachol	Sigma, Taufkirchen, DE, #C4382
Cholera toxin (CTX)	Sigma, Taufkirchen, DE, #C8052
Coelenterazine 400 a	Gold Biotechnology, St. Louis, USA, #C-320-10
Disodium hydrogen phosphate, dihydrate	Roth, Karlsruhe, DE, #4984
Dimethyl sulfoxide (DMSO)	AppliChem, Darmstadt, DE # A1584
DNA Ladder 1 kb	New England BioLabs®, MA, US, #N3272
DNA Ladder 100 bp	New England BioLabs®, MA, US, #N3231
Doxycycline hyclate	Sigma, Taufkirchen, DE, #D9891
Elacridar	Kindly provided by Prof. Gütschow, University of Bonn, DE
Ethanol	KMF Optichem, Lohmar, DE, #08-205
Ethidiumbromide	Roth, Karlsruhe, DE, #2218.1

Ethylenediaminetetraacetic acid, disodium salt dihydrate	Roth, Karlsruhe, DE, #8040.3
Fetal calf/bovine serum (FCS)	Sigma, Taufkirchen, DE, #-0804
Forskolin	Tocris, Bristol, UK, #1099
Gel loading dye, blue	New England BioLabs®, MA, US, # B7021S
D-(+)-glucose	Sigma, Taufkirchen, DE #G7021
Geneticin (G418)	Gibco, Paisley, UK, #11811
Glacial acetic acid 100%	Merck Darmstadt, DE, # 00063.2511
Glycerol	Sigma, Taufkirchen, DE, #G2025
HEPES	AppliChem, Darmstadt, DE, #A1069.0500
Hydrochloric acid	Applichem, Darmstadt, DE #0659
Hygromycin B	Invivogen, Toulouse, FR, #ant-hm-1
3-Isobutyl-1-methylxanthine (IBMX)	Tocris, Bristol, UK, #2845
Isopropanol	Merck, Darmstadt, DE, #107022
L161,982	Cayman, MI, US, #10011565
Lysophosphatidyl inositol (LPI)	Sigma, Taufkirchen, DE, #L7835
Magnesium chloride, hexahydrate	Fluka, Hamburg, DE, #63068
Magnesium sulphate, hexahydrate	Fluka Hamburg, DE, # 00627
Manganese(II) chloride	Roth Karlsruhe, DE, # T881.1
MK571	Kindly provided by Prof. Gütschow, University of Bonn, DE
(N-Morpholino)propanesulfonic acid	Sigma, Taufkirchen, DE, #M-1254
Orciprenaline	Sigma, Taufkirchen, DE, # 32237
Pertussis toxin (PTX)	Sigma, Taufkirchen, DE, #2980
Pme I	New England BioLabs®, MA, US, #R0560S
Poly-D-Lysin	Sigma, Taufkirchen, DE, #P-6407
Potassium acetate	Merck Darmstadt, DE, # 1.04820.1000
Potassium chloride	Fluka, Hamburg, DE, #60128
Potassium dihydrogen phosphate	ZVE, D-53121 Bonn; #234984
13,14-Dihydro-15-keto-prostaglandin D_2 (DK-PGD_2)	Cayman, MI, US, #12610
Prostaglandin E1 (PGE1)	Cayman, MI, US, #13010

QIC	Kindly provided by AG König, University of Bonn, DE
QIC red	Synthesized by AG Müller, University of Bonn, DE
Rubidium chloride	Merck, Darmstadt, DE, #107615
Serotonin (5-HT)	Sigma, Taufkirchen, DE, #H9523
Sodium acetate	Applichem, Darmstadt, DE, #4555
Sodium chloride	Fluka, Hamburg, DE, #71376
Sodium fluoride	ZVE, Bonn, DE, #125310
Sodium dihydrogen phosphate	Roth, Karlsruhe, DE, #T878.2
Disodium hydrogen phosphate	Roth, Karlsruhe, DE, #T876.2
Sodium hydrogen carbonate	Merck, Darmstadt, DE, #1.06323.2500
Sodium hydroxide	Fluka, Hamburg, DE, #71689
Tris(hydroxymethyl)-aminomethane	Roth, Karlsruhe, DE, #5426
Tryptone	Roth, Karlsruhe, DE, #8952.1
TUG424	Kindly provided by Dr. Trond Ulven, University of Southern Denmark, DK
Yeast extract	Applichem, Darmstadt, DE, #3732

2.1.2 Kits

cAMP dynamic 2 HTRF® kit	Cisbio Bioassays, BP 84175, France, #62AM4PEC
IP-One HTRF® assay kit	Cisbio Bioassays, BP 84175, France, # 62P1APEB
NucleoBond® Xtra Maxi	Macherey-Nagel, Düren, DE, #740414.50
innuPREP Plasmid Mini Kit	Analytik Jena, Jena, DE, #845-KS-5040250

2.1.3 Devices

Autoclave	3850 ELV, Systec Brunswick Scientific, NJ 08818-4005, USA
Balances	TE64, Sartorius, Göttingen, DE (precision balances)
	TE6101, Sartorius, Göttingen, DE (analytical balances)
Cell counting chamber	Neubauer, Brand, Wertheim, DE
Centrifuges	MiniSpin, Eppendorf, Hamburg, DE
	5810, Eppendorf, Hamburg, DE
	6K10, Sigma, Osterode, DE
Dry block heater	QBT2, Grant Instruments, Cambridge, UK
Electroporation device	Gene Pulser Xcell™, BioRad®, CA, US
Electrophoresis chambers	Mini-Sub® cell GT, Bio Rad, CA, USA
	Wide Mini-Sub® cell GT, Bio Rad, CA, USA
Freezer (-80°C)	Herafreeze, Heraeus, Hanau, DE
Incubator/shaker (bacteria)	HT-INFORS, Buch+Holm, CH
Incubator (cell culture)	HERAcell 240, Thermo Fisher, Dreieich, DE
Liquid nitrogen tank	MVE-Tec 3000, GermanCryo, Jüchen, DE
Microbiological safety cabinets	S@fe flow 1.2, Nunc™, NY, USA
Mithras LB940 Multimode reader	Berthold Technologies, Bad Wildbad, DE
Microscope	CKX31, Olympus, Hamburg, DE
Microwave	Microwave 800, Severin, Sundern, DE
Pipettes 0.5-10 µl; 10-100 µl; 20-200 µl; 100-1000 µl	Eppendorf, Hamburg, DE
Pipettes (multichannel)	Alpha, Genex, Torquay, UK
Power supply	Power Pac HC, BioRad®, CA, US
pH meter	SevenEasy, Mettler Toledo, Giessen, DE

Sterile bench (cell culture)	HeraSafe, Thermo Fisher, Schwerte, DE
Thermomixer	Thermomixer® comfort, Eppendorf, Hamburg, DE
Spectrophotometer	Smart Spec Plus, BioRad®, CA, US
Vortexer	Reaxtop, Heidolph, Schwabach, DE
Water purification system	Milli Q® Water system, Millipore, MA, US

2.1.4 Buffers and solutions

2.1.4.1 Commercially available buffers and solutions

DMEM	Invitrogen™, Darmstadt, DE, #41965039
Ham´s F-12 Nutrient Mixture GlutaMAX™	Invitrogen™, Darmstadt, DE, #21765
HBSS buffer	Invitrogen™, Darmstadt, DE, #14025
Penicillin/streptomycin solution	Invitrogen™, Darmstadt, DE, #15140
Trypsin/EDTA 0.05/0.02% in PBS	Pan Biotech GmbH, Aidenbach, DE, #P10-0231SP
Ultra pure water	Invitrogen™, Darmstadt, DE, #10977035

2.1.4.2 Other buffers and solutions

Aqua dem. was used as solvent unless otherwise stated.

Aluminium fluorid solution (AlF_4^-)

A 1.2 mM AlF_4^- solution was generated by mixing equal amounts of 2.4 mM $AlCl_3$ and 80 mM NaF, each solved in assay buffer.

Assay buffer for DMR, Impedance and BRET assays

20 mM HEPES in HBSS, pH 7.2.

$CaCl_2$ solution for calcium phosphate transfection

2 M $CaCl_2$, filter-sterilized (0.2 μm).

Coelenterazine stock solution

1 mg Coelenterazine 400a resuspended in 2500 μl of 99.9% ethanol (final conc. 1 mM).

Coelenterazine reagent

Coelenterazine stock solution diluted in assay buffer containing 30% ethanol (final concentration 100 μM).

Competent bacteria buffer 1

30 mM CH_3COOK, 50 mM $MnCl_2$ x 4 H_2O, 100 mM $CaCl_2$ x 2 H_2O, 15% glycerine, pH 5.8, filter-sterilized (0.2 μm).

Competent bacteria buffer 2

10 mM RbCl, 75 mM $CaCl_2$ x 2 H_2O, 10 mM MOPS, 15% glycerine, pH 6.8, filter-sterilized (0.2 μm).

Electroporation buffer (EB) (1x)

50 mM K_2HPO_4, 20 mM CH_3COOK, 20 mM KOH, pH 7.4 adjusted with acetic acid, filter-sterilized (0.2 μm).

Electroporation buffer (EB) (5x)

250 mM K_2HPO_4, 100 mM CH_3COOK, 100 mM KOH, pH 7.4 adjusted with acetic acid, filter-sterilized (0.2 μm).

HEPES solution (1 M)

1 M HEPES, pH 7.2, filter-sterilized (0.2 μm).

Hepes bufferd saline (HBS) (2x) for calcium phosphate transfection

50 mM HEPES, 280 mM NaCl, 1.5 mM Na_2HPO_4, pH 7.1, filter-sterilized (0.2 μm).

Luria Bertani (LB) medium

1% bactotryptone, 0.5% yeast extract, 1% NaCl, pH adjusted to 7.4 with NaOH, sterilized by autoclaving.

MgSO4 solution for electroporation

1 M $MgSO_4$ hexahydrate, filter-sterilized (0.2 μm).

Phosphate buffered saline (PBS)

150 mM NaCl, 2.5 mM KCl, 7.5 mM Na_2HPO_4, 1.5 mM KH_2PO_4, pH 7.2 adjusted with HCl, sterilized by autoclaving.

Stimulation buffer for cAMP assays

HBSS, 20 mM HEPES, 1 mM 3-isobutyl-1-methylxanthine (IBMX).

Super optimal broth (SOB)

2% Bactotryptone, 0.5% yeast extract, 10 mM NaCl, 2.5 mM KCl, pH 7.4, sterilized by autoclaving at 121°C. After autoclaving 1 ml of sterile 1 M $MgCl_2$ and 1 ml of sterile 1 M $MgSO_4$ were added to 100 ml media.

Tris acetate EDTA (TAE) buffer (50x)

40 mM Tris(hydroxymethyl)-aminomethane (Tris), 1 mM EDTA, 5.71% glacial acetic acid.

Tris-EDTA (TE) buffer for calcium phosphate transfection

10 mM Tris, 1 mM EDTA, pH 8.0 adjusted with HCl, filter-sterilized (0.2 μm).

2.1.5 Consumables

CellKey 384-well biosensor cell assay microplate	Molecular Devices, CA, US, #1030787
Cryogenic vials 1.5 ml	Nalgene, Thermo Fisher Scientific, NY, USA, #5012
Dishes: 6, 10 and 15 cm	Corning®, NY, US, #430161, 430167, 430599
Disposable filter unit 0.2 µl	Whatman®
Epic 384-well biosensor cell assay microplate, fibronectin-coated	Corning®, NY, US, #5042
Epic compound plate	Corning®, NY, US, #3657
Falcon tubes 15 and 50 ml	Corning®, NY, US430791, 430829
Flasks: 25, 75 and 175 cm^2	Corning®, NY, US, #430168, 430720, 431079
Gene Pulser cuvette, 0.4cm,	BioRad®, CA, US, #1652088
384-well LIA-plate, white, TC, F-form, Greiner bio one 4550	Greiner, Frickenhausen, DE, #632102
Microtubes 1.5 and 2 ml	Labomedic, Bonn, DE, #115105, 115106
Optiplate, 96-well, flat bottom, white	Perkin Elmer, Rodgau, DE, #6005500
Pasteur pipettes, glass	Labomedic, Bonn, DE, #447016
Pipette tips: Oxygen crystal tips 10 µl Yellow 200 µl tips Blue 1000 µl tips	 Labomedic Bonn, DE, # 110727 Greiner Frickenhausen, DE, #685290 Greiner Frickenhausen, DE, # 686290
Tiptrays 384 for Epic	CyBio, Jena, DE, #3800-25-513-N
Tiptrays 384 for CellKey	Molecular Devices, CA, US, #1031046

2.1.6 Software

Citavi 3.0	Swiss Academic Software GmbH, Zürich, CH
DeVision G v1.0	Decon Science Tec GmbH, Hohengandern, DE
Office Excel® 2010	Microsoft Corporation, Unterschleißheim, DE

Office PowerPoint® 2010	Microsoft Corporation, Unterschleißheim, DE
Office Word® 2010	Microsoft Corporation, Unterschleißheim, DE
Prism® 5	GraphPad Software, Inc, CA, USA
Microplate Analyzer v1.5	Corning® Incorporated, NY, USA
MicroWin 2000 AdvII v4.41	Mikrotek Laborsysteme GmbH, Overath, DE

2.1.7 Cell culture media

HEK293 and COS7 Medium

Constituent	Volume [ml]	Final Concentration
Dulbecco's Modified Eagle Medium (DMEM)	500	-
Fetal Bovine Serum	50	~10%
Penicillin-Streptomycin	5	~ 100 U/ml Penicillin, 0.1 mg/ml Streptomycin

CRTH2-HEK and GPR55-HEK Medium

Constituent	Volume [ml]	Final Concentration
Dulbecco's Modified Eagle Medium (DMEM)	500	-
Fetal Bovine Serum	50	~10%
Penicillin-Streptomycin	5	~ 100 U/ml Penicillin, 0.1 mg/ml Streptomycin
G418	2	0.4 mg/ml

FFA1-HEK Medium

Constituent	Volume [ml]	Final Concentration
Dulbecco's Modified Eagle Medium (DMEM)	500	-
Fetal Bovine Serum	50	~10%
Penicillin-Streptomycin	5	~ 100 U/ml Penicillin, 0.1 mg/ml Streptomycin
Blasticidin	0.75	15 µg/ml
Hygromycin B	0.5	100 µg/ml

CHO-K1 Medium

Constituent	Volume [ml]	Final Concentration
Ham´s F-12 Nutrient Mix GlutaMAX™	500	-
Fetal Bovine Serum	50	~10%
Penicillin-Streptomycin	5	~ 100 U/ml Penicillin, 0.1 mg/ml Streptomycin

CHO-M1 Medium

Constituent	Volume [ml]	Final Concentration
Ham´s F-12 Nutrient Mix GlutaMAX™	500	-
Fetal Bovine Serum	50	~10%
Penicillin-Streptomycin	5	~ 100 U/ml Penicillin, 0.1 mg/ml Streptomycin
G418	1	0.2 mg/ml

2.1.8 Sterilization method

For molecular and cellular biological experiments all heat stable materials, equipments, solutions and media were autoclaved in a Varioklav® (H+P Labortechnik AG, Oberschleißheim) at 121°C and 1.2 bar for 21 min. Sterilization of heat sensitive solutions and buffers was accomplished by the use of sterile filters (pore wide 0.2 µm).

2.1.9 Plasmids, bacterial strains and cell lines

Vectors:

pcDNA3.1+

pcDNA3.1+ was purchased from Invitrogen™, Darmstadt, DE, #V790-20

hGPR55 in pcDNA3.1+

cDNA of hGPR55 was kindly provided by Dr. Maria Waldhoer, Institute for Experimental and Clinical Pharmacology, Medical University of Graz, Austria

hM3 in pcDNA3.1+

cDNA of human M3 receptor was kindly provided by the group of Prof. Dr. Klaus Mohr, University of Bonn, Germany.

$G\alpha_q$ tagged with an internal hemagglutinin (HA)-epitope tag in pcDNA3.1+

$G\alpha_q$ tagged with an internal hemagglutinin (HA)-epitope tag in pcDNA3.1+ in the pcDNA3.1 expression vector was purchased from the UMR cDNA resource center (http://www.cdna.org).

BRET constructs:

$G\alpha_{13}$-106*R*Luc8, $G\alpha_q$-97*R*Luc8, $G\gamma_2$-GFP[10], and unlabeled $G\beta_1$ (all in pcDNA3.1) were kindly provided by Céline Galés, Université Toulouse, (Saulière et al., 2012).

Bacteria:

XL1-Blue

This *E.coli* strain obtained from Agilent Technologies (200249) was used for the amplification of recombinant plasmids.

Mammalian cell lines:

HEK293 cells

The used HEK293 cell line was from an internal source: research group of Prof. Dr. Evi Kostenis, Institute of Pharmaceutical Biology, University of Bonn, Germany.

HEK293 cells stably expressing CRTH2 (CRTH2-HEK)

The HEK293 cell line stably expressing CRTH2 was from an internal source: research group of Prof. Dr. Evi Kostenis, Institute of Pharmaceutical Biology, University of Bonn, Germany. Cells include cDNA of CRTH2 (gene bank accession-number NM_004778) fused to a FLAG-tag at the N-terminus. Cells were selected by resistance towards geneticin (G418).

HEK293-Flp-In™ T-REx™ cells stably expressing FFA1 (FFA1-HEK)

HEK293-Flp-In™ T-REx™ expressing FFA1 (FFA1-HEK) cells were from an internal source: research group of Prof. Dr. Evi Kostenis, Institute of Pharmaceutical Biology, University of Bonn, Germany. The cDNA of FFA1 (also referred to as FFAR1 or GPR40) corresponds to the gene bank accession-number NM_005303. Cells were selected by resistance towards blasticidin and hygromycin B. To induce receptor expression on demand, cells were treated with 1 µg/ml of doxycyline for 16 hours.

AD-HEK cells stably expressing GPR55 (GPR55-HEK)

AD-HEK cells stably expressing GPR55 (Henstridge, et al., 2009) were kindly provided by Prof. Dr. Andy Irving (University of Dundee, UK).

CHO-K1 cells

The used CHO-K1 cell line was from an internal source: research group of Prof. Dr. Evi Kostenis, Institute of Pharmaceutical Biology, University of Bonn, Germany.

CHO-K1 cells stably expressing muscarinic M1 receptor

The used cell line was kindly provided by the group of Prof. Dr. Klaus Mohr University of Bonn, Germany.

2.2 Methods

2.2.1 Molecular biology methods

2.2.1.1 Preparation of LB plates

First LB medium was prepared as described in section 2.1.4.2 and 1.5% agar was added. The mixture was autoclaved and allowed to cool down to about 50°C prior to the addition of ampicillin (100 µg/ml). The mixture was slewed and approximately 25 ml were poured per 10 cm petri dish. The plates were cooled to room temperature and then stored at 4°C.

2.2.1.2 Preparation of rubidium chloride competent *E.coli*

E. coli XL-blue cells were scratched out onto an LB plate in and incubated overnight at 37°C. A single colony was inoculated into a 5 ml culture of SOB and incubated for 16 h at 37°C under vigorous shaking (220 rpm). The following day 1 ml of this preparatory culture was used to inoculate 100 ml SOB. The cell suspension was incubated at 37°C and 220 rpm until the optical density at 550 nm reached the value of 0.5. The culture was centrifuged in ice-cold falcons for 10 min at 4°C (3000 g). The supernatant was removed and pellet was resuspended in 25 ml ice-cold competent bacteria buffer 1 and the bacteria were centrifuged again for 10 min at 4°C (3000 g). Then cell pellet was resuspended in 8 ml competent bacteria buffer 2, bacteria were aliquoted (100 µl), frozen in liquid nitrogen and stored at -80°C.

2.2.1.3 Transformation of chemically competent bacteria

Competent bacteria (100 µl) were thawn on ice and 50 ng of plasmid DNA were added. Then cells were incubated on ice for 20 min. After that cells were subjected to a heat shock at 42°C for 90 seconds and returned on ice for 2 min. 500 µl of LB without antibiotic was added. 100 µl of the cell suspension was scratched out onto LB plates containing an appropriate selective antibiotic and plates were incubated overnight at 37°C.

2.2.1.4 Cryoconservation of bacterial strains

A single colony of transformed *E. coli* cells grown on an LB plate was picked with a sterile pipette tip and 5 ml of LB media containing the appropriate antibiotic were inoculated. The cell suspension was incubated for 16-18 h at 37°C under vigorous shaking (220 rpm). 800 µl of the bacterial suspension were supplemented with 200 µl glycerol and stored in a cryovial at –80°C.

2.2.1.5 Isolation of plasmid DNA

2.2.1.5.1 Analytical plasmid preparation (mini-preparation)

To analyze the plasmids for inserts by restriction analysis, the plasmid DNA was isolated on a small scale using innuPREP Plasmid Mini Kit. 2-10 colonies were picked

and cultured for 16-18 h at 37°C in 5 ml LB medium containing an appropriate selective antibiotic. 2 ml of the cell suspension were centrifuged and plasmid DNA was isolated according to the manufacturer´s instructions. The remaining bacteria suspension could be used to generate glycerol stocks (see 2.2.1.4).

2.2.1.5.2 Preparative plasmid preparation (maxi-preparation)

To obtain high-purity and high-concentration plasmid DNA for further transfection experiments plasmid DNA was isolated on a larger scale using a NucleoBond® Xtra Maxi kit according to the manufacturer's instructions. In preparation 300 ml LB medium containing appropriate selective antibiotic were inoculated with the bacteria harboring the appropriate plasmid left over from the mini-preparation or from a glycerol stock. Then cell suspension was incubated for 16-18 h at 37°C with vigorous shaking (220 rpm).

2.2.1.6 Restriction endonuclease digestion

For restriction digests 500 ng DNA, 0.3 µl of the appropriate restriction enzyme, 2 µl of the appropriate buffer specified by the manufacturer, BSA, and purified water (UltraPure, Invitrogen®) were mixed in a total volume of 20 µl. Micro tubes were incubated at 37°C for 1 h and fragments were visualized by the use of agarose gel electrophoresis.

2.2.1.7 Agarose gel electrophoresis

DNA fragments were separated via agarose gel electrophoresis. Therefore 6-fold concentrated DNA loading buffer was added to digested samples and samples together with an 1 kb ladder were loaded on a 1% agarose gel which was prepared by mixing agarose with 1x TAE and boiling the solution in a microwave until the agarose was completely melted. The solution was cooled down to about 60°C before 0.5 µg/ml ethidium bromide was added. Electrophoresis was performed at a voltage of 100 V for 30-45 min. The DNA fragments were detected using ultraviolet light and the size of each fragment was determined by comparison with 1 kb DNA ladder. Results were photographically recorded with the photo documentation system DeVision G v1.0.

2.2.1.8 Quantification of nucleic acid concentration

Quantification of DNA samples were determined photometrically by examining the absorbance of the sample at 260 nm. Following equation was used for calculations:

$$c\ [\mu g/ml] = OD_{260} \times D \times F$$

c = concentration

OD_{260} = optical density at 260 nm

D = dilution factor

F = multiplication factor (for DNA 50)

The OD_{280} value of the sample was also determined to estimate the purity. A DNA solution with OD_{260}/OD_{280} ratio between 1.7 and 2.0 was considered pure enough for transfections.

2.2.2 Cell culture methods

Cell lines were grown in an incubator at 37°C with an atmosphere of 5% CO_2 and 96% humidity. Before use all cell culture solutions and media were prewarmed up to 37°C in a water bath.

2.2.2.1 Passaging cell lines

After cells were grown to confluence, media was removed and cells were washed with PBS. Then trypsin was added and cells were incubated until cells have detached (at 37°C for CHO cells). Trypsinization was stopped by addition of medium, cells were resuspended and desired share of the suspension was transferred into new culture flasks or dishes filled with fresh cell medium.

2.2.2.2 Cryoconservation and thawing of cells

For cryoconservation, cells were washed, detached, resuspended in medium and centrifuged (800 rpm, 4 min). The medium was removed and replaced by freezing medium (cell medium with 10% DMSO). 1 ml cell suspension (25 cm^2 per aliquot) was transferred into each cryogenic vial and placed into a -80°C freezer for 24 h. After that cryogenic vials were transferred into a liquid nitrogen tank for long-term storage.

Liquid nitrogen frozen cells were rapidly thawed and cells were immediately transferred to a 15 ml falcon containing 10 ml of pre-warmed medium. The cell suspension was centrifuged 800 rpm, 4 min), the supernatant was removed, cells were resuspended in fresh cell medium (without selective antibiotics for 24 h) and transferred to a 25 cm^2 culture flask.

2.2.2.3 Counting cells

10 µl cell suspension were pipetted between the surface of a Neubauer counting chamber and a cover slip. The cell number of one big square was counted. The cell density was determined by the following terms: Cell density [cells/ml] = counted cells x dilution factor x 10^4.

2.2.2.4 Coating with Poly-D-lysine

In order to avoid cell detachment in washing procedures, surfaces of CellKey plates were pretreated with poly-D-lysine. The desired amount of wells was completely covered with PDL solution (0.1 mg/ml, 12 µl per well) and incubated at 37°C for 30 min. After that PDL was aspirated, wells were washed three times with PBS and then dried under laminar air flow.

2.2.2.5 Transient calcium phosphate transfection of HEK293 cells

For gene dosing experiments cells were seeded 24 hours prior to transfection at a density of $4.2x10^6$ cells per 10 cm dish in DMEM with 10% FCS to achieve 50-60% confluence the next day. 20 µg of DNA (total amount, $G\alpha_q$ + pcDNA 3.1) were mixed in 500 µl TE buffer together with 60 µl 2 M $CaCl_2$ solution and precipitates were formed via drop-by-drop addition of this DNA/$CaCl_2$ solution into a round bottom

falcon filled with 500 µl 2xHBS at minimum speed vortexing the round bottom falcon. The suspension was incubated for 20 min at room temperature and then precipitates were added drop-by-drop into the cell medium. After 4-6 h incubation the medium was removed, cells were washed two times with PBS and fresh medium was added. Transiently transfected cell were used 48 h after transfection.

2.2.2.6 Transient transfection of HEK293 cells via electroporation

For BRET assays, $5x10^6$ cells were resuspended in 30 µl EB (1x) and 50 µl of this suspension were added to a mixture of 20 µl EB (5x), 4 µl $MgSO_4$ (1 M), 2 µg pcDNA 3.1, 0.5 µg $G\alpha_q$-*R*Luc8 or $G\alpha_{13}$-*R*luc8, 0.5 µg $G\gamma_2$-GFP[10], 1 µg β_1, 2 µg GPR55 or M3 receptor DNA and filled up to 100 µl with H_2O. After 15 min incubation at room temperature the transfection mix was transferred into a 0.4 cm electroporation cuvette and pulsed using the Gene Pulser Xcell with following settings:

Program: exponential decay

voltage: 250 (V)

capacity: 500 (µF)

resistance: ∞ (Ω)

cuvette: 4 (mm)

After electroporation, cells were removed from the cuvette and resuspended in media without antibiotics. Cells were grown for 48 hours prior to the assay.

2.2.3 Cell-based assays

2.2.3.1 Homogenous time resolved fluorescence assays (cAMP and IP1)

The HTRF cAMP and IP1 assay kits are based on time-resolved resonance energy transfer (HTRF) which demonstrates a competition immunoassay where cellular cAMP or IP1 competes with a labeled form of cAMP or IP1 for binding to an anti-cAMP or anti-IP1 antibody. The antibodies used as donor are labeled with europium cryptate, and cAMP or IP1 labeled with the dye d2 is used as acceptor. Light excitation (320 nm) at anti-cAMP or anti-IP1 conjugates leads to fluorescence caused emission of light (620 nm). When the cAMP-d2 or IP1-d2 molecule binds to the anti-cAMP or anti-IP1

conjugate, fluorescence resonance energy transfer (FRET) between the europium cryptate and the dye d2 occurs, resulting in fluorescence caused emission of light (655 nm). Results were calculated from the ratio of absorbance at 665 nm/620 nm. Obtained ratio values were corrected by a negative control, consisting of buffer and europium cryptate. Calculations were performed according to following formula:

$$\text{Delta F} = [\text{Ratio}_{\text{sample}} - \text{Ratio}_{\text{neg}} / \text{Ratio}_{\text{neg}}] \times 100$$

Beacause of the inverse relationship between signal and cAMP or IP1 concentration, accumulation of cAMP or IP1 resulted in a decreased signal.

cAMP assay protocol

Changes of cAMP levels were monitored with the MithrasLB 940 multimode reader using the HTRF-cAMP dynamic kit according to the manufacturer's instructions. For the assay, cells were resuspended in cAMP assay buffer (Hanks' balanced salt solution, 20 mM HEPES, 1 mM 3-isobutyl-1-methylxanthine), transferred to 384-well small volume microplates at a density of 50,000 cells/well in a volume of 5 µl (5,000 cell/well for COS7 cells) and settled by centrifugation (800 rpm, 10 sec). Plates were incubated for 15 min at 37°C before $G\alpha_q$ inhibitors or antagonists (2.5 µl, 3-fold concentrated) were added and incubated for 1 h at 37 C (2 h for BIM-monomer and BIM-dimer). Then compounds were added (2.5 µl, 4-fold concentrated), for inhibition approaches in the presence of indicated concentrations of forskolin. After further incubation for 30 min at 37°C (10 min for CRTH2-HEK cells), the reactions were stopped by adding 5 µl of 1.25% Triton X-100 containing HTRF reagents. Plates were then incubated for 60 min at room temperature, and time resolved FRET signals were measured.

IP1 assay protocol

The amount of intracellular IP1 was measured in a 384-well format using the HTRF-IP1 kit as per manufacturer's instructions. Therefore the cell suspension was dispensed with a density of 100,000 cells/well in volume of 7 µl in IP1 stimulation buffer containing 50 mM LiCl. Then cells were centrifuged to settle down with 800 rpm for 10 sec. After 20 min incubation at 37°C, 3.5 µl stimulation buffer containing $G\alpha_q$ inhibitors or multidrug transporter inhibitors (3-fold concentrated) was added and incubated for 1 h (2 h for BIM-monomer and BIM-dimer) at 37°C. Then 3.5 µl stimulation buffer

containing various concentrations of ligand (4-fold concentrated) was added. After further incubation at 37°C for 30 min, 3 µl IP1-d2 conjugate followed by 3 µl europium cryptate-labeled anti-IP1 antibody was added. Time-resolved fluorescence at 620 and 665 nm was measured with the Mithras LB 940 multimode reader after incubation at room temperature for 60 min, and the ratios of the signals were calculated as described above. For the wash experiments, cells were preincubated with QIC or BIM-dimer in micro tubes. Then the cells were washed three times for five minutes with a volume of 750 µl PBS. After that cells were resuspended in fresh stimulation buffer and seeded into a 384-well plate.

2.2.3.2 BRET assay

The principle of the bioluminescence resonance energy transfer (BRET) technology is based on an energy transfer between a bioluminescent donor, the enzyme *Renilla* luciferase, and a fluorescent acceptor, green fluorescent protein (GFP), which can be detected if donor and acceptor are in sufficiently proximity to each other. The experiments were performed with *R*luc8 or *R*LucII which are mutant and more sensitive forms of *R*luc (Loening et al., 2006; Breton et al., 2010). The $G\alpha_q$ or $G\alpha_{13}$ subunit was labelled with the energy donor *R*Luc8 and $G\gamma_2$ was labelled with the energy acceptor GFP[10]. Addition of the substrate coelenterazine 400a (DeepBlueC), substrate of the luciferase, led to an oxidation of coelentarazine 400a and as a consequence blue light was emitted which overlapped with the excitation spectrum of GFP, which then produces green light. The BRET signal was determined with the Mithras LB 940 multimode reader thereby determining the ratio of green light (515 nm) over blue light (410 nm). HEK293 cells were transiently transfected via electroporation to express $G\alpha_q$-*R*Luc8 or $G\alpha_{13}$-*R*Luc8, $G\gamma_2$-GFP[10], $G\alpha_{12/13}$-sensitive GPR55 or $G\alpha_q$-sensitive M3 receptors along with unlabeled β_1. On the day of the assay 180,000 cells per well (170 µl) resuspended in assay buffer were seeded into a 96-well plate. Then 5 µl BIM-dimer or buffer was added and cells were incubated at 28°C on a plate shaker (300 rpm) for 2 h. After that cells were challenged with 5 µl agonist and incubated for 5 min on a plate shaker (28°C) before 20 µl coelenterazine 400a (50 µM) were injected by the Mithras LB injector. After a short shaking process of 2 sec BRET ratios were determined. Pathway activation could be detected as a decrease in BRET because the Gα-helical domain was separated from the N terminus of Gγ.

2.2.3.3 DMR assay

Dynamic mass redistribution (DMR) leads to changes in local optical density and therefore enables label-free monitoring of GPCR-mediated signaling. DMR was recorded with the Corning Epic biosensor. Cells were seeded into a 384-well fibronectin-coated biosensor cell plate 18-24 h before the assay (15,000 cells/well for HEK293 cells, 18,000 cells/well for CRTH2-HEK and FFA1-HEK cells, 12,500 cells/well for CHO-M1 cells) and grown to confluence at 37°C. For GPR55-HEK 12,000 cells/well were seeded 48 h before the assay and after 24 h cell culture media was replaced by assay buffer to obtain starvation conditions. In experiments with pertussis toxin (PTX) and cholera toxin (CTX) cells were preincubated with 50 ng/ml PTX or 100-200 ng/ml CTX for 16-18 h. On the day of experiment cells were washed twice with assay buffer and cells were allowed to rest at least 1 h at 28°C. In experiments with QIC or AlF_4^- they were added after the washing procedure and incubated for 1 h (1.5 h for AlF_4^-). After a baseline read of 300 s agonists were added and DMR responses were monitored at 28°C for at least 3600 s. If compounds were solubilized in dimethyl sulfoxide (DMSO), cells were washed in assay buffer containing the same percentage of DMSO as the later added compounds in order to avoid bulk refractive index differences. Data were evaluated using the Corning Microplate Analyzer v1. All optical DMR recordings were buffer corrected.

2.2.3.4 Impedance assay

Bioimpedance measures the electrical impedance of cell layers positioned over electrode arrays. The short-term effects of receptor activation, manifested as changes in cell adherence to their substrate, changes in cell volume and shape, and changes in cell–cell interactions, are the focus of the CellKey system. In brief, the CellKey system measures a cell layer’s ability to impede the flow of electrical current to a greater or lesser extent as a result of receptor activation (McGuinness, 2007). One day before the assay cells were seeded at a density of 11,000 cells per well (13,000 cells/well for CRTH2-HEK and FFA1-HEK cells) on PDL-coated 384-well biosensor plates to obtain confluent monolayers. GPR55-HEK cells were seeded 48 h before the assay. After 24 h culture medium was removed and replaced by assay buffer for starvation (Hank's buffered salt solution (HBSS) with 20 mM HEPES). On the day of experiment cell culture medium or assay buffer was removed and cells were washed twice with assay

buffer and allowed to equilibrate at least for 1 h at 28°C. In experiments with PTX and CTX cells were preincubated with 50 ng/ml PTX or 100-200 ng/ml CTX for 16-18 h. QIC or AlF_4^- were added after the washing procedure and incubated for 1 h (1.5 h for AlF_4^-). Then the cell plate was transferred to the CellKey and a baseline read was recorded for 5 min before the compound addition. Bioimpedance changes were detected for 3600 s. If compounds were solubilized in dimethyl sulfoxide (DMSO), assay buffer for the washing procedure contained the same percentage of DMSO as the later added compounds. All impedance recordings were buffer corrected.

2.2.4 Calculations and data analysis

Results are expressed as mean values ± SEM and were analyzed using GraphPad Prism 5.04 (Graph Pad). Concentration-response curves were fitted by non-linear sigmoidal regression. Pharmacological parameters of plotted sigmoidal concentration-response curves such as EC_{50} value and E_{max} value were calculated by the GraphPad Prism software.

For the binding experiments data points from single experiments were either fitted to the four parameter logistic function or a two phase competition (membrane binding with carbachol) and inflection points were further transformed according to the Cheng-Prusoff correction (Cheng and Prusoff ,1973) yielding (apparent) equilibrium binding affinity constants KD and Ki.

Comparison between two experimental groups was based on a two-tailed student t-test. P values were considered as significant (*) if $P<0.05$, as very significant (**) if $P<0.01$ and as extremely significant (***) if $P<0.001$.

3 Results

3.1 BIM-46187: A pan-G protein inhibitor?

The first part of this thesis deals with BIM-46187 (hereafter referred to as BIM-dimer) (**Fig. 3**), a compound which was published as a specific pan-G protein inhibitor (Ayoub et al., 2009). The goal of this work is to elucidate its inhibiting influence on G Protein-dependent signaling in commonly used cellular backgrounds.

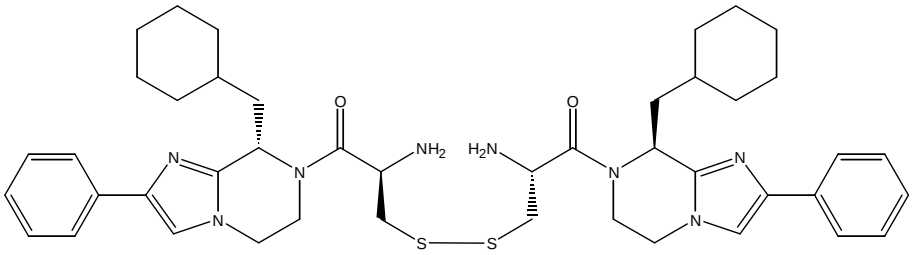

Figure 3: Chemical structure of the BIM-dimer.

3.1.1 Influence on cAMP accumulation in HEK293 and COS7 cells

As a first approach it was of interest to test whether preincubation with BIM-dimer affects cAMP production mediated by the direct adenylyl cyclase activator forskolin (**Fig. 4A)**. Therefore, HEK293 cells were pretreated with increasing amounts of BIM-dimer (2.5 h) and then stimulated with 10 µM forskolin. The results show no reduction of cAMP accumulation provoked by BIM-dimer.

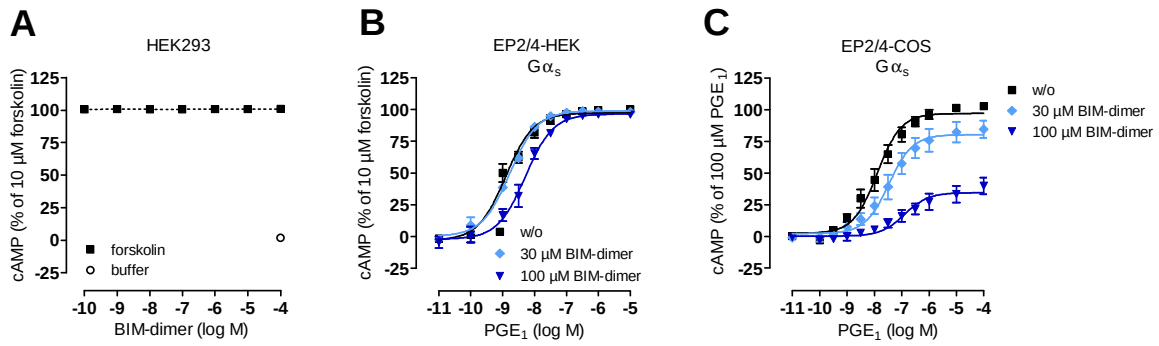

Figure 4: Effects of BIM-dimer on cellular cAMP levels in HEK293 and COS7 cell backgrounds.
(**A**) Increasing concentrations of BIM-dimer did not lower forskolin-mediated cAMP production in HEK293 cells. Data were kindly provided by Stephanie Hennen, Institute for Pharmaceutical Biology, University of Bonn, Germany.
(**B**) BIM-dimer was not able to silence cAMP signaling of the $G\alpha_s$-sensitive EP2/4 receptors in HEK293 cells. pEC_{50} (w/o) = 8.91 ± 0.07; pEC_{50} (30 µM BIM-dimer) = 8.78 ± 0.04; pEC_{50} (100 µM BIM-dimer) = 8.29 ± 0.06. w/o, without.
(**C**) BIM-dimer largely suppressed PGE_1-mediated cAMP production in COS7 cells. pEC_{50}/E_{max} (w/o) = 7.90 ± 0.08/97%; pEC_{50}/E_{max} (30 µM BIM-dimer) = 7.47 ± 0.12/80%; pEC_{50}/E_{max} (100 µM BIM-dimer) = 6.90 ± 0.18/35%.
(**A**)-(**C**) are mean values ± SEM of three to ten independent experiments, each performed in triplicate.

Because BIM-dimer was published as a pan-G protein inhibitor (Ayoub et al., 2009) its effect on stimulating $G\alpha_s$ proteins was analyzed. Therefore, HEK293 cells endogenously expressing $G\alpha_s$-linked EP2/4 receptors were preincubated with BIM-dimer in two different concentrations (30 and 100 µM) and after stimulation with prostglandin E_1 (PGE_1) cAMP levels were determined. cAMP levels were nearly unaffected by BIM-dimer (**Fig. 4B**). Based on the results of Ayoub et al. the influence of BIM-dimer in a COS7 cell background was tested to find that however, BIM-dimer significantly dampened $G\alpha_s$-coupled signaling via EP2/4 receptors in this cell line (**Fig. 4C**). To exclude failures in the assay system, HEK293 cells were incubated in the presence of EP2/4 antagonists, which completely blunted cAMP production (**Fig. 5**). These findings confirmed proper functionality of our BIM-dimer and led to the conclusion that BIM-dimer might interfere with G protein signaling in a cell-type-specific manner.

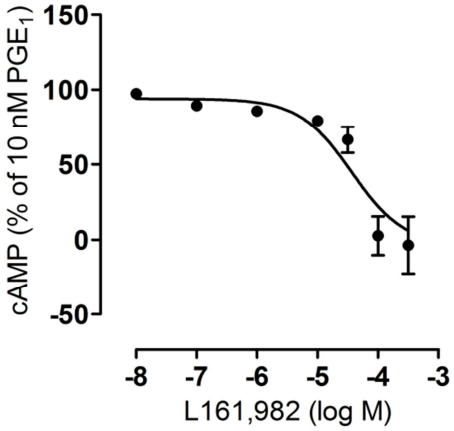

Figure 5: EP2/4 receptor antagonist L161,982 completely blunted PGE_1-mediated cAMP production. HEK293 cells endogenously expressing the E prostanoid receptors EP2 and EP4 were pretreated for 30 min with the EP2/EP4 antagonist L161,982 and cAMP production was quantified. pIC50 = 4.44 ± 0.12. Data shown are mean values ± SEM of four independent experiments, each performed in triplicate.

To get further insight into this postulated mechanism the influence of BIM-dimer on $G\alpha_i$-mediated signaling was investigated. Therefore, the free fatty acid receptors 2 (FFA2) and 3 (FFA3) were chosen. The FFA2 receptor couples via $G\alpha_i$ and $G\alpha_q$ proteins and the FFA3 receptor is $G\alpha_i$-sensitive (Brown et al., 2003; Le Poul et al., 2003; Nilsson et al., 2003; Stoddart et al., 2008). HEK293-Flp-In™ T-REx™ cells stably transfected with FFA2 and FFA3 (FFA2-HEK and FFA3-HEK) were induced to express FFA2 and FFA3 by pretreatment with doxycycline (**Fig. 6A-B**). The receptors were activated with propionic acid and cAMP levels were measured. BIM-dimer was not able to silence $G\alpha_i$-mediated signaling in this cellular background. To explore another $G\alpha_i$-coupled receptor a HEK293 cell line stably expressing the receptor for 5-oxo-eicosatetraenoic acid, OXE-R, as well as the promiscuous Gα subunit G_{16} (OXE-HEK) was used (**Fig. 6C**). After pretreatment with BIM-dimer the OXE receptor was stimulated with its endogenous ligand 5-oxo-ETE. Again, the agonist induced cAMP reduction was hardly affected by BIM-dimer preincubation.

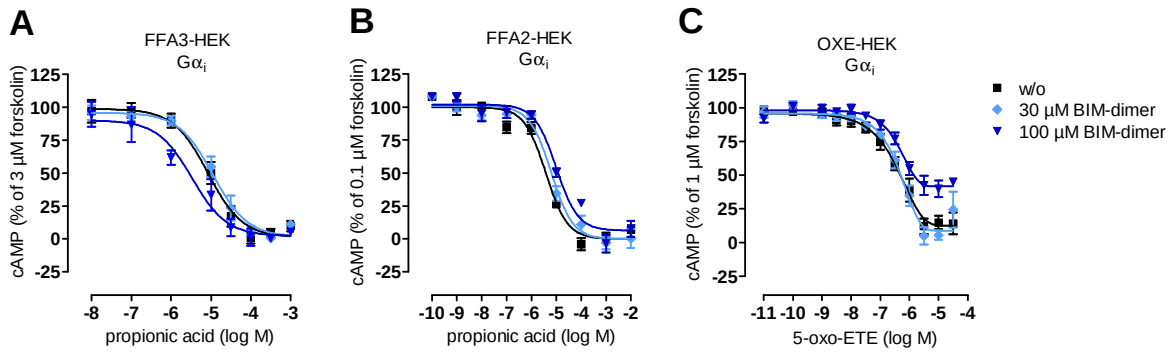

Figure 6: BIM-dimer was no silencer of Gα$_i$ signaling in HEK293 cells.
(**A**) HEK293 cells stably transfected with FFA2 receptors were induced with doxycycline for 16-18 h and incubated with BIM-dimer for 2 h. After that the cells were stimulated with the agonist propionic acid in the presence of 0.1 µM forskolin. pEC$_{50}$ (w/o) = 5.08 ± 0.12; pEC$_{50}$ (30 µM BIM-dimer) = 4.95 ± 0.10; pEC$_{50}$ (100 µM BIM-dimer) = 5.48 ± 0.19. Data were kindly provided by Manuel Grundmann, Institute for Pharmaceutical Biology, University of Bonn, Germany.
(**B**) HEK293 cells were stably transfected to express FFA3 receptors. The cells were induced with doxycycline for 16-18 h and incubated with BIM-dimer for 2 h. Then the cells were stimulated with the agonist propionic acid in the presence of 3 µM forskolin. pEC$_{50}$/E$_{max}$ (w/o) = 5.42 ± 0.10/0%; pEC$_{50}$/E$_{max}$ (30 µM BIM-dimer) = 5.20 ± 0.09/0%; pEC$_{50}$/E$_{max}$ (100 µM BIM-dimer) = 5.00 ± 0.11/6%. Data were kindly provided by Manuel Grundmann, Institute for Pharmaceutical Biology, University of Bonn, Germany.
(**C**) HEK293 cells stably expressing the OXE receptor and Gα$_{16}$ were pretreated with BIM-dimer (2 h), stimulated with 5-oxo-ETE in the presence of 1 µM forskolin and then cAMP accumulation was measured. pEC$_{50}$/E$_{max}$ (w/o) = 6.38 ± 0.12/8%; pEC$_{50}$/E$_{max}$ (30 µM BIM-dimer) = 6.35 ± 0.08/7%; pEC$_{50}$/E$_{max}$ (100 µM BIM-dimer) = 6.35 ± 0.10/40%. Data were kindly provided by Katrin Büllesbach, Institute for Pharmaceutical Biology, University of Bonn, Germany.
(**A**)-(**C**) BIM-dimer hardly affected Gα$_i$ interaction of FFA2, FFA3 and OXE-R.
Data shown are means ± SEM of three independent experiments, each conducted in triplicate.

3.1.2 Exploring consequences on the Gα$_q$ pathway in HEK293 cells

To explore the consequences of BIM-dimer exposure on Gα$_q$-mediated signaling three different Gα$_q$-linked receptors were analyzed by measuring IP1 accumulation. HEK293 cells endogenously expressing the muscarinic M3 receptor (M3-HEK) were preincubated with BIM-dimer and then receptors were stimulated with increasing concentrations of carbachol, a synthetic muscarinic receptor agonist (**Fig 7A**). In this approach BIM-dimer completely silenced Gα$_q$ activation. Similar results were obtained investigating the influence of BIM-dimer on endogenously expressed P2Y receptors stimulated with ATP (**Fig. 7B**) and on HEK293 cells stably transfected with the FFA2 receptor activated with its agonist propionic acid (**Fig. 7C**). In summary, it can be stated

that preincubation with 100 µM BIM-dimer completely abolished signaling of three independent $G\alpha_q$-sensitive receptors in a HEK293 background.

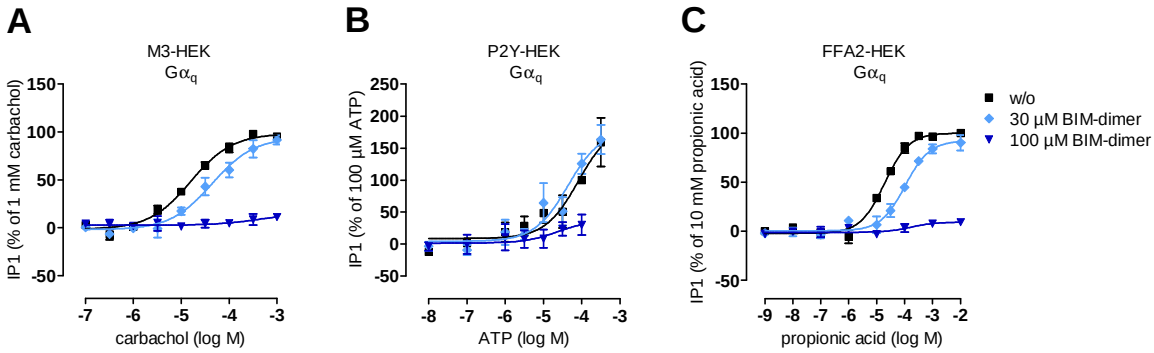

Figure 7: BIM-dimer interdicted $G\alpha_q$ signaling in HEK cells.
(**A**)-(**C**) In a concentration of 100 µM BIM-dimer silences $G\alpha_q$ activation induced by stimulation of three $G\alpha_q$-sensitive receptors.
(**A**) After pretreatment with BIM-dimer (2 h) HEK293 cells endogenously expressing the muscarinic M3 receptor were stimulated with increasing concentrations of carbachol. Data were normalized to the maximal concentration of carbachol (1 mM). pEC_{50} (w/o) = 4.80 ± 0.05; pEC_{50} (30 µM BIM-dimer) = 4.36 ± 0.11.
(**B**) Endogenously expressed P2Y receptors in HEK293 cells were used to detect $G\alpha_q$-mediated IP1 production in the presence of BIM-dimer. P2Y receptors were activated with its agonist ATP. Data were normalized to a concentration of 100 µM ATP. pEC_{50} (w/o) = 4.08 ± 0.25; pEC_{50} (30 µM BIM-dimer) = 4.36 ± 0.27.
(**C**) HEK293 cells were induced with doxycycline (1 µg/ml for 16 h) to express the FFA2 receptor, preincubated with BIM-dimer and stimulated with increasing concentrations of propionic acid. The concentration effect curve was normalized to 10 mM propionic acid. pEC_{50} (w/o) = 4.71 ± 0.07; pEC_{50} (30 µM BIM-dimer) = 3.98 ± 0.09. Data were kindly provided by Manuel Grundmann, Institute for Pharmaceutical Biology, University of Bonn, Germany.
(**A**)-(**C**) Data shown are means ± SEM of three independent experiments, each conducted in triplicate.

3.1.3 Effect of BIM-dimer on $G\alpha_{13}$ signaling

Activation of the $G\alpha_{13}$ pathway can be detected by bioluminescence resonance energy transfer (BRET) assays (Saulière et al., 2012). Therefore, the influence of 100 µM BIM-dimer was analyzed using lysophosphatidylinositol (LPI) and its target receptor GPR55 (**Fig.8A**) which represents a $G\alpha_{13}$-sensitive receptor. It was possible to measure an agonist-promoted decrease in BRET in HEK293 cells coexpressing GPR55, along with the energy donor $G\alpha_{13}$106*R*Luc8, the energy acceptor $G\gamma_2$-GFP[10,] and unlabeled $G\beta_1$. The BRET decrease reflects the separation of the Gα-helical domain from the N terminus of Gγ which then enables GDP exit and GTP entry (Galés et al., 2006; Saulière

et al., 2012). Data in **Figure 8A** show that there was no significant difference in the BRET decrease in the presence or absence of BIM-dimer. Hence, pretreatment with BIM-dimer had no effect on GPR55-$G\alpha_{13}$ activation. In order to validate our BRET approach $G\alpha_q$ signaling was examined using carbachol which stimulated the transiently expressed muscarinic M3 receptor (**Fig. 8B**). HEK293 cells were transfected to coexpress the energy donor $G\alpha_q$97*R*Luc8, the energy acceptor $G\gamma_2$-GFP[10], and unlabeled $G\beta_1$. Pretreatment with 100 µM BIM-dimer significantly blunted activation of the $G\alpha_q$-$\beta_1\gamma_2$ heterotrimer thereby demonstrating that the BRET partners used were suitable for examining inhibition of G protein signaling by BIM-dimer.

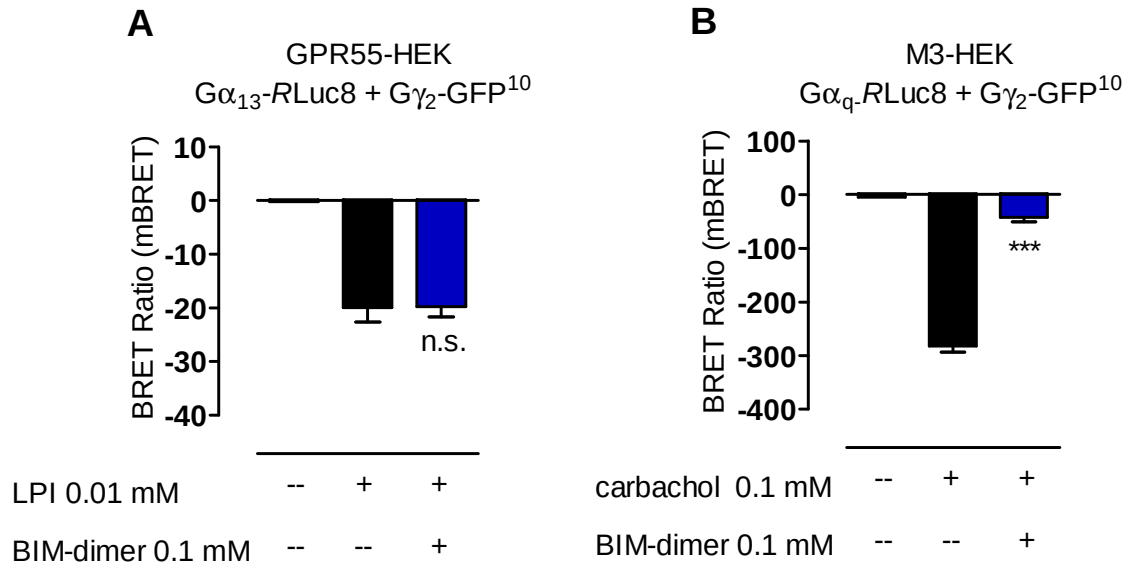

Figure 8: $G\alpha_{13}$ signaling was not affected by BIM-dimer preincubation.
(**A**) BIM-dimer did not block molecular rearrangement of activated $G\alpha_{13}$. BRET decrease was measured after GPR55 activation in HEK293 cells transfected to express $G\alpha_{13}$106*R*Luc8 + $G\gamma_2$-GFP[10] and unlabeled $G\beta_1$. n.s., not significant.
(**B**) BIM-dimer efficiently dampened activation of the $G\alpha_q$-BRET biosensor. Opening of the nucleotide binding pocket was detected as BRET decrease after muscarinic M3 receptor activation in HEK293 cells transfected to express $G\alpha_q$97*R*Luc8 + $G\gamma_2$-GFP[10] and unlabeled $G\beta_1$. ***$p < 0.001$
(**A**)-(**B**) Data are means + SEM of three to six independent experiments, each performed in triplicate.

3.1.4 Analyzing BIM-dimer in a CHO cell background

Concerning the fact that BIM-dimer did not function as a pan-G protein inhibitor in the HEK cell background, its G protein-mediated signaling inhibition profile should be investigated in another frequently used immortalized cell line. Therefore, the influence of BIM-dimer on second-messenger pathways was additionally analyzed in a CHO cell background.

CHO cells stably transfected to express the muscarinic M1 receptor were chosen to study $G\alpha_q$-mediated signaling (**Fig. 9A**). After preincubation with dimeric BIM, the cells were stimulated with carbachol and IP1 accumulation was detected. In the presence of 100 µM BIM-dimer, IP1 production was entirely blocked. CHO-K1 cells endogenously expressing EP2/4 receptors were used to evaluate the influence of BIM-dimer on $G\alpha_s$ proteins by measuring cAMP accumulation (**Fig. 9B**). After an incubation of 2 h in the presence of BIM-dimer and a following stimulation with increasing concentrations of PGE_1 there was still a strong cAMP accumulation detectable. 30 µM BIM-dimer showed almost no inhibitory effect on $G\alpha_s$-mediated signaling whereas pretreatment with 100 µM BIM-dimer resulted in a decreased efficacy and a rightward shift of the $logEC_{50}$ value. To explore the effect of BIM-dimer on $G\alpha_i$ proteins, CHO-K1 cells endogenously expressing $G\alpha_i$-sensitive serotonin receptors, were pretreated with dimeric BIM for 2 h and then stimulated with serotonin (5-HT). BIM-dimer did not block $G\alpha_i$-mediated signaling (**Fig. 9C**).

In summary, BIM-dimer did not display pan-G protein inhibitory activity in a CHO cell background, but showed a clear preference for inhibition of $G\alpha_q$ signaling.

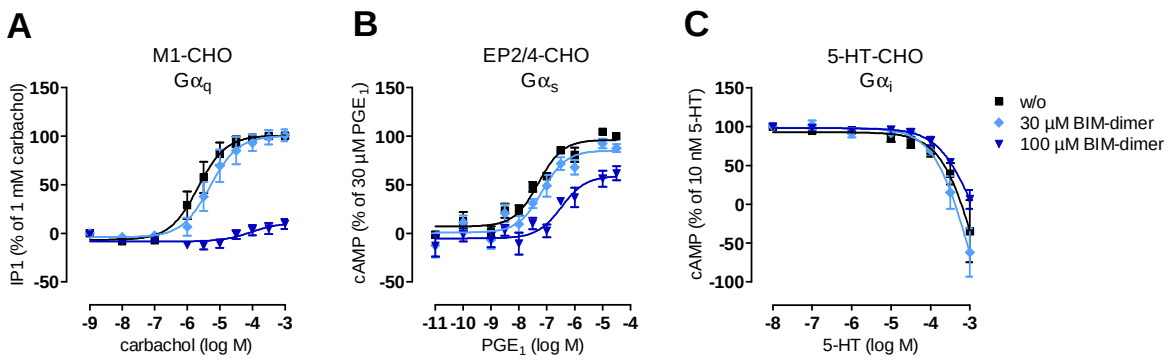

Figure 9: BIM-dimer preferentially silenced $G\alpha_q$ signaling in a CHO cell background.
(**A**) Dimeric BIM almost completely blunted $G\alpha_q$ signaling in CHO cells stably transfected to express the muscarinic M1 receptor. pEC_{50}/E_{max} (w/o) = 5.67 ± 0.10/100%; pEC_{50}/E_{max} (30 µM BIM-dimer) = 5.30 ± 0.13/100%; pEC_{50}/E_{max} (100 µM BIM-dimer) = 4.04 ± 0.43/11%.
(**B**) cAMP accumulation via endogenously expressed EP2/4 receptors stimulated with increasing concentrations of PGE_1 was nearly unaffected in the presence of 30 µM BIM-dimer. Pretreatment with 100 µM BIM-dimer decreased the efficacy and caused a rightward shift of the concentration response curve. EC_{50}/E_{max} (w/o) = 7.30 ± 0.10/96%; pEC_{50}/E_{max} (30 µM BIM-dimer) = 7.17 ± 0.16/85%; pEC_{50}/E_{max} (100 µM BIM-dimer) = 6.48 ± 0.19/59%.
(**C**) $G\alpha_i$ signaling activated with endogenously expressed serotonin 5-HT receptors was not influenced by BIM-dimer preincubation.
(**A**)-(**C**) Data are means ± SEM of at least three independent experiments, each performed in triplicate.

3.1.5 Characterizing the influence of BIM-dimer in the patient-derived MZ7 cells

Ayoub et al. demonstrated the pan-G protein inhibitory effect of BIM in COS7 cells and in different cancer cell lines (e.g. HCT8/S119). The first experiments of this thesis revealed that BIM-dimer interdicted $G\alpha_q$-mediated signaling in a HEK293 and CHO cell background but $G\alpha_s$, $G\alpha_i$ and $G\alpha_{13}$ signaling was largely unaffected by pretreatment with BIM-dimer. Subsequently, BIM-dimer and its influence on G protein signaling was analyzed in the patient-derived MZ7 cell line to ascertain whether these findings differ from our results in the HEK293 and CHO cells.

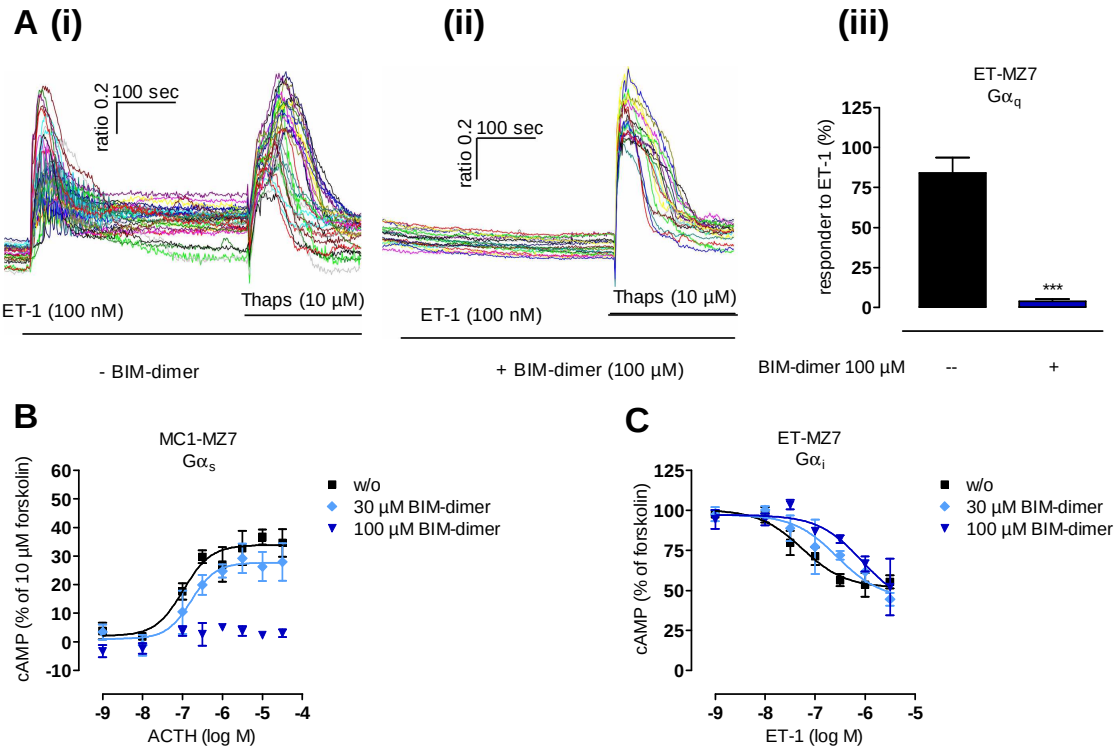

Figure 10: Dimeric BIM inhibited second-messenger production in the patient derived MZ7 cancer cell background.
(**A**) (**i**) untreated MZ7 cells responded to both the $G\alpha_q$-stimulus endothelin 1 (ET-1) and thapsigargin (Thaps). (**ii**) BIM-dimer completely blunted Ca^{2+} mobilization triggered with ET-1 but did not impair Thaps–induced release of Ca^{2+} from the endoplasmatic reticulum. (**iii**) Quantification of Ca^{2+} traces in the absence and presence of BIM-dimer in single cells. Data in (i) and (ii) show representative traces, data in (iii) are means + SEM of n=159 cells. sec, seconds. ***p < 0.001. Data were kindly provided by Daniela Wenzel, Institute of Physiology I, Life and Brain Center, University of Bonn, Germany.
(**B**) BIM-dimer (100 µM) silenced $G\alpha_s$-mediated cAMP production induced via ACTH and its cognate $G\alpha_s$-linked and endogenously expressed MC1 receptor. pEC_{50}/E_{max} (w/o) = 6.99 ± 0.21; pEC_{50}/E_{max} (30 µM BIM-dimer) = 6.79 ± 0.27.
(**C**) Dimeric BIM diminished $G\alpha_i$ coupling of endogenous ET-1 receptors. pEC_{50}/E_{max} (w/o) = 7.26 ± 0.21/52%; pEC_{50}/E_{max} (30 µM BIM-dimer) = 6.56 ± 0.31/45%; pEC_{50}/E_{max} (100 µM BIM-dimer) = 6.08 ± 0.37/40%.
(**B**)-(**C**) Data shown are means ± SEM of three to ten independent experiments, each conducted in triplicate. Data were kindly provided by Ramona Schrage, Pharmacology and Toxicology Section, Institute of Pharmacy, University of Bonn, Germany.

To explore $G\alpha_q$ dependent signaling MZ7 cells were analyzed in single cell Ca^{2+} assays using endogenously expressed endothelin receptors (**Fig 10A**). Therefore, MZ7 cells were pretreated with 100 µM BIM-dimer, stimulated with endothelin 1 (ET-1) and the Ca^{2+} response was detected. Untreated MZ7 cells responded to both the $G\alpha_q$ stimulus ET-1 and thapsigargin (Thaps) (**i**). Prior addition of BIM-dimer completely blocked the ET-1-mediated response but not the thapsigargin-induced Ca^{2+} mobilization (**ii**). These

findings were specifically caused at the level of the G proteins because BIM-dimer preincubation had no effect on the G protein-independent thapsigargin-induced Ca^{2+} mobilization from the endoplasmatic reticulum.

The influence of BIM-dimer on the $G\alpha_s$ und $G\alpha_i$ pathway was investigated by determining changes in cAMP levels. MZ7 cells were stimulated with the adrenocorticotropic hormone (ACTH), an agonist for the $G\alpha_s$-sensitive melanocortin1 (MC1) receptor. 100 µM BIM-dimer completely prevented cAMP accumulation (**Fig. 10B**). BIM-dimer did not prevent cAMP production triggered with forskolin (**Fig. 11**) which underlined that BIM inhibition occurred specifically at the level of G proteins. BIM-dimer alone dampened the basal cAMP level which can be explained by its ability to silence $G\alpha_s$-mediated signaling through constitutively active GPCRs endogenously expressed in MZ7 cells. Endogenous ET-1 receptors were stimulated with endothelin to verify the effect of BIM-dimer on $G\alpha_i$ dependent signaling (**Fig 10C**). The results indicate that BIM-dimer diminished $G\alpha_i$ coupling of ET-1 receptors in a MZ7 cell background. In contrast to the results obtained in the HEK29 and CHO cell lines, BIM-dimer was able to silence all three second-messenger pathways in this cancer cell line.

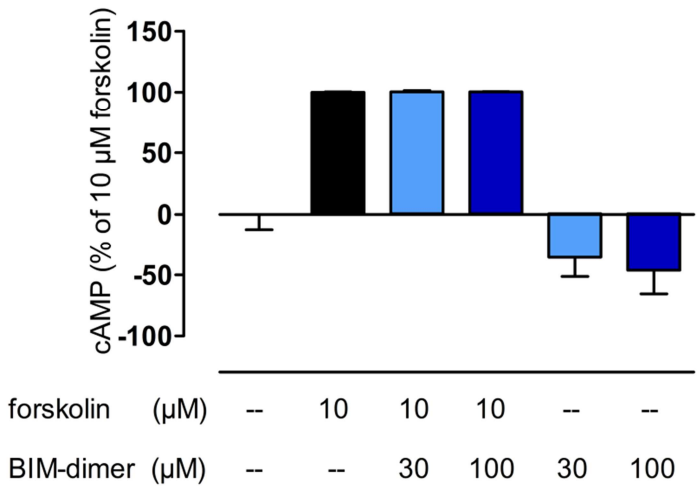

Figure 11: BIM-dimer did not lower cAMP production stimulated with the direct adenylyl cyclase activator forskolin in MZ7 cells. MZ7 skin cancer cells were pretreated for 2 h with the indicated concentrations of BIM-dimer prior to stimulation of cAMP synthesis with forskolin. Shown are mean values + SEM of three experiments, each performed in triplicate. Data were kindly provided by Ramona Schrage, Pharmacology and Toxicology Section, Institute of Pharmacy, University of Bonn, Germany.

3.1.6 Mechanistic link between sensitivity toward BIM inhibition and cellular context

The fact that BIM-dimer is able to silence only $G\alpha_q$ proteins in a HEK and CHO background led to the question whether these findings might have something to do with the level of expression of its target protein. Context-dependent pharmacology of GPCR ligands is a well-known phenomenon and could be due to the relative amount of signaling components or its stoichiometry to each other in different cell lines (Kenakin, 2013).

To study this hypothesis HEK293 cells were transfected (calcium phosphate precipitation) with increasing amounts of HA-tagged $G\alpha_q$ cDNA in a gene dosing approach. To ensure an appropriate, higher $G\alpha_q$ protein expression an immunoblot detection was conducted (**Fig. 12A-B**). In parallel, IP1 accumulation was detected utilizing the endogenously expressed muscarinic M3 receptor after stimulation with carbachol (**Fig. 12C**). A clear correlation between BIM inhibition and $G\alpha_q$ expression could be detected. BIM inhibition was reversed when the expression of $G\alpha_q$ proteins was raised. These data support the hypothesis of the existence of a link between the expression level of BIM target proteins and the extent of BIM inhibition.

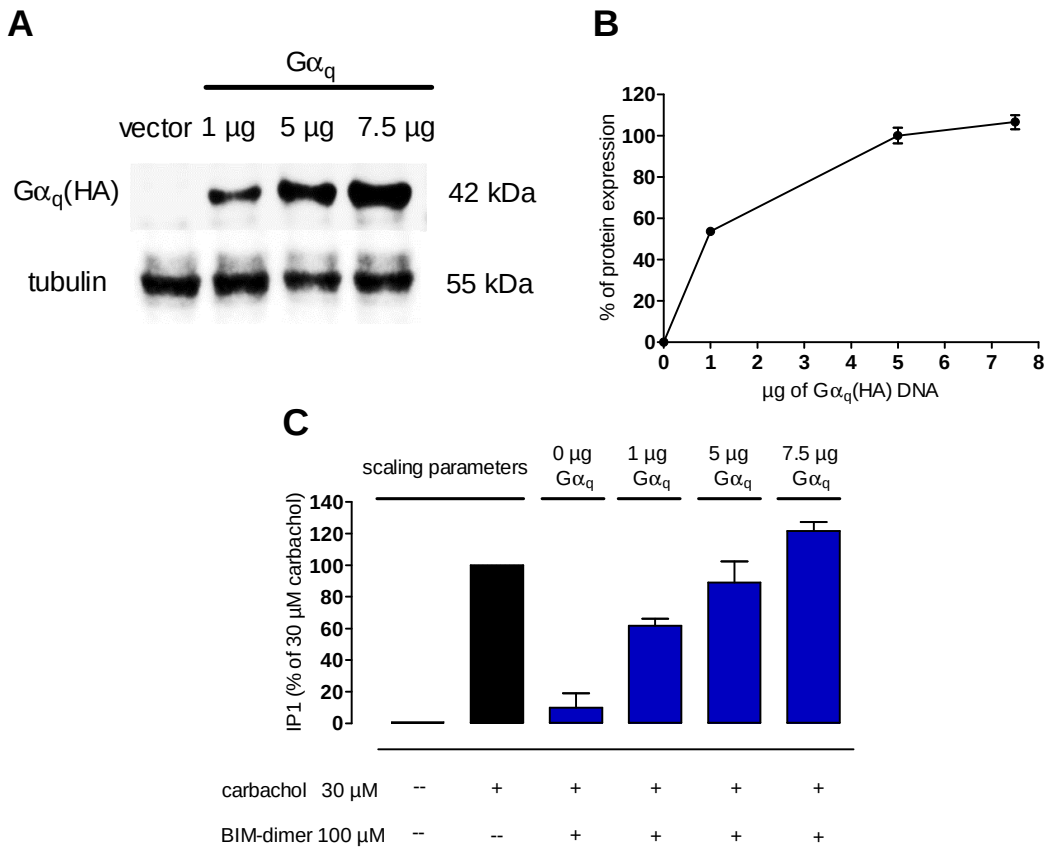

Figure 12: Investigating context-dependent influence of BIM-dimer with a gene dosing approach.

(**A**) Immunoblot detection of HEK293 lysates prepared after transfection with increasing amounts of HA-tagged $G\alpha_q$ cDNA. Membranes were reprobed for tubulin to ensure equal sample loading and transfer. Membranes were incubated in primary antibody solution (1:1000) containing anti-HA or anti-β-tubulin. Bound antibodies were detected with an anti-rabbit horseradish-peroxidase-conjugated secondary antibody (1:10,000). Shown is one representative experiment of four independent experiments.

(**B**) Densitometric analysis of the immunoblot experiments depicted in (A). Shown are means ± SEM of four independent experiments.

(**B**)-(**C**) Data were kindly provided by Julia Morschel, Institute for Pharmaceutical Biology, University of Bonn, Germany.

(**C**) HEK293 cells were transfected with increasing amounts of $G\alpha_q$(HA) cDNA and IP1 accumulation was detected using the endogenously expressed muscarinic M3 receptor in the presence or absence of BIM-dimer. Enrichment with $G\alpha_q$ proteins was inversely related to BIM inhibition. Data are means ± SEM of four independent experiments.

The diverse G protein inhibition profiles between HEK293 and MZ7 cells might also be related to different levels of target proteins. Therefore, the expression levels of $G\alpha_q$, $G\alpha_s$ and $G\alpha_i$ proteins were quantified in both cell lines (**Fig. 13**). The expression level of $G\alpha_q$ proteins was equal between both cell lines which fit well to the hypothesis seeing as BIM-dimer silenced $G\alpha_q$-mediated signaling in both cellular backgrounds. For $G\alpha_s$ proteins immunoblot quantification revealed significantly lower expression levels in the MZ7 cells and these data also supported the mechanistic link between sensitivity towards BIM and Gα subunit expression. In contrast, expression levels of $G\alpha_i$ proteins in MZ7 cells were enhanced in comparison to HEK293 cells. These findings were not in line with the expected results that the expression of $G\alpha_i$ proteins would have been reduced in MZ7 cells because BIM-dimer diminished $G\alpha_i$-dependent signaling in MZ7 cells (**Fig. 10C**). Taken together, different intracellular levels of Gα proteins might be one aspect to explain the absence of pan-G protein inhibition across different cell lines but other considerations regarding the cell-type dependent pharmacology of BIM-dimer have to be taken into account.

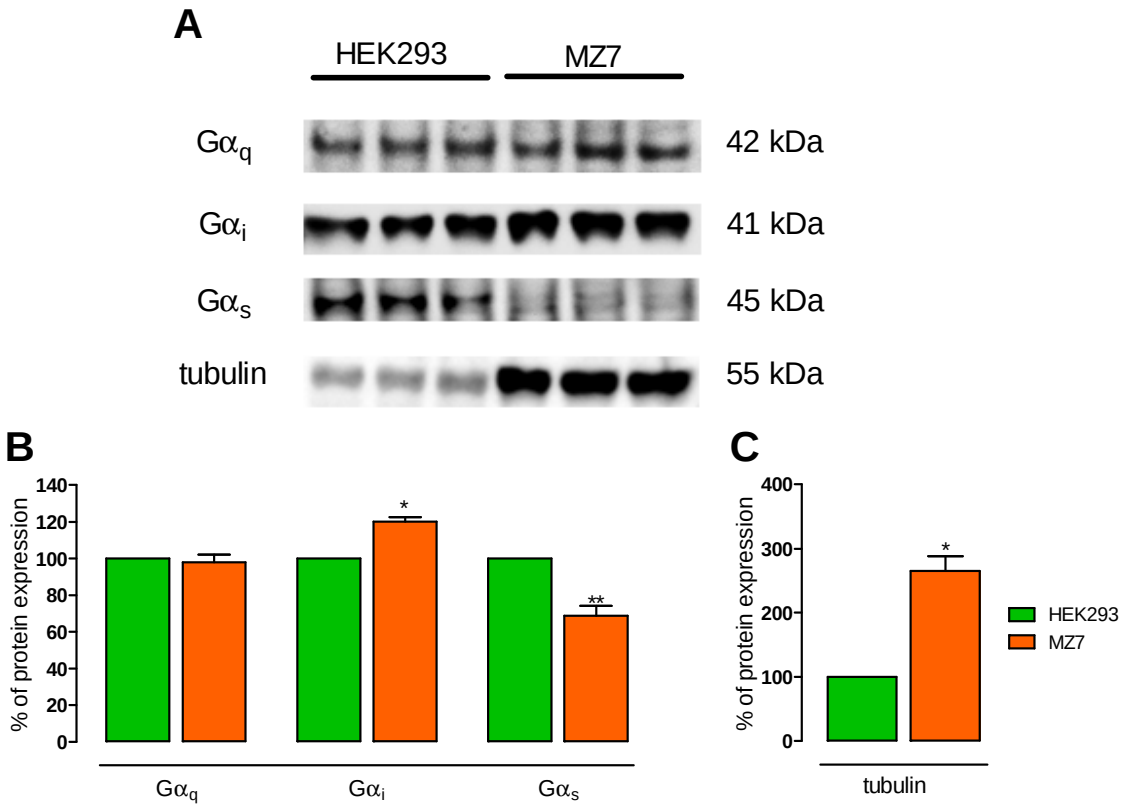

Figure 13: Quantification of Gα protein subunits in HEK293 versus MZ7 cells.
(**A**) Immunoblot detection of lysates prepared from native HEK293 and MZ7 cells evaluating $G\alpha_q$, $G\alpha_s$ and $G\alpha_i$ proteins. Membranes were reprobed for tubulin to ensure equal sample loading and transfer. Membranes were incubated in primary antibody solution (1:1000) containing: anti-$G\alpha_{q/11}$, anti-$G\alpha_s$, anti-$G\alpha_{i3}$ or anti-β-tubulin, respectively. Bound antibodies were detected with an anti-rabbit horseradish-peroxidase-conjugated secondary antibody (1:10,000). Shown is one representative experiment of three independent experiments.
(**B**)-(**C**) Densitometric analysis of the experiments depicted in (**A**). Shown are means + SEM of three independent experiments.
(**A**)-(**C**) Data were kindly provided by Julia Morschel, Institute for Pharmaceutical Biology, University of Bonn, Germany.

3.1.7 BIM-dimer: A substrate for multidrug transporters?

Another explanation for the absence of pan-G protein inhibition in certain cell lines might be that BIM-dimer acts as a substrate for active outward transport via multidrug transporters. Therefore HEK293 cells, which endogenously express multidrug transporters, were incubated with a combination of BIM-dimer and either elacridar (**Fig. 14A**) or MK571 (**Fig. 14B**) as transport inhibitors. Endogenously expressed muscarinic M3 receptors were stimulated with carbachol and the IP1 accumulation was detected. Elacridar inhibits P-glycoprotein (P-gp) and breast cancer resistance protein

(BCRP). P-gp transports hydrophobic compounds while BCRP prefers diverse and nonconjugated compounds (Ahmed-Belkacem et al., 2005). MK571 inhibits MRP1 and MRP2, two transporters that export hydrophilic molecules and GSH conjugates (Wortelboer et al., 2013, Leyers et al., 2008). Pretreatment with elacridar alone increased the pEC_{50} value. This effect was comparable to that mediated by pretreatment with 30 µM BIM-dimer. The combination of 30 µM BIM-dimer and elacridar shifted the pEC_{50} value in an additive manner. 100 µM BIM-dimer or the combination of 100 µM BIM-dimer and elacridar completely inhibited IP1 accumulation (**Fig. 14A**). In the presence of the multidrug transporter MK571 alone (10 µM), the concentration response curve was unaltered concerning its potency and efficacy in comparison to no pretreatment. 30 µM BIM-dimer and the combination of 30 µM BIM-dimer and MK571 shifted the pEC_{50} value to the right in the same range. 100 µM BIM-dimer alone and the combination of 100 µM BIM-dimer and MK571 completely blocked IP1 accumulation (**Fig. 14B**). Together, neither elacridar nor MK571 was able to improve the capacity of 30 µM BIM-dimer to silence $G\alpha_q$-mediated signaling. Based on these findings one could conclude that export of BIM-dimer via multidrug transporters had no influence on the cell-type specific differences between G protein inhibition profiles.

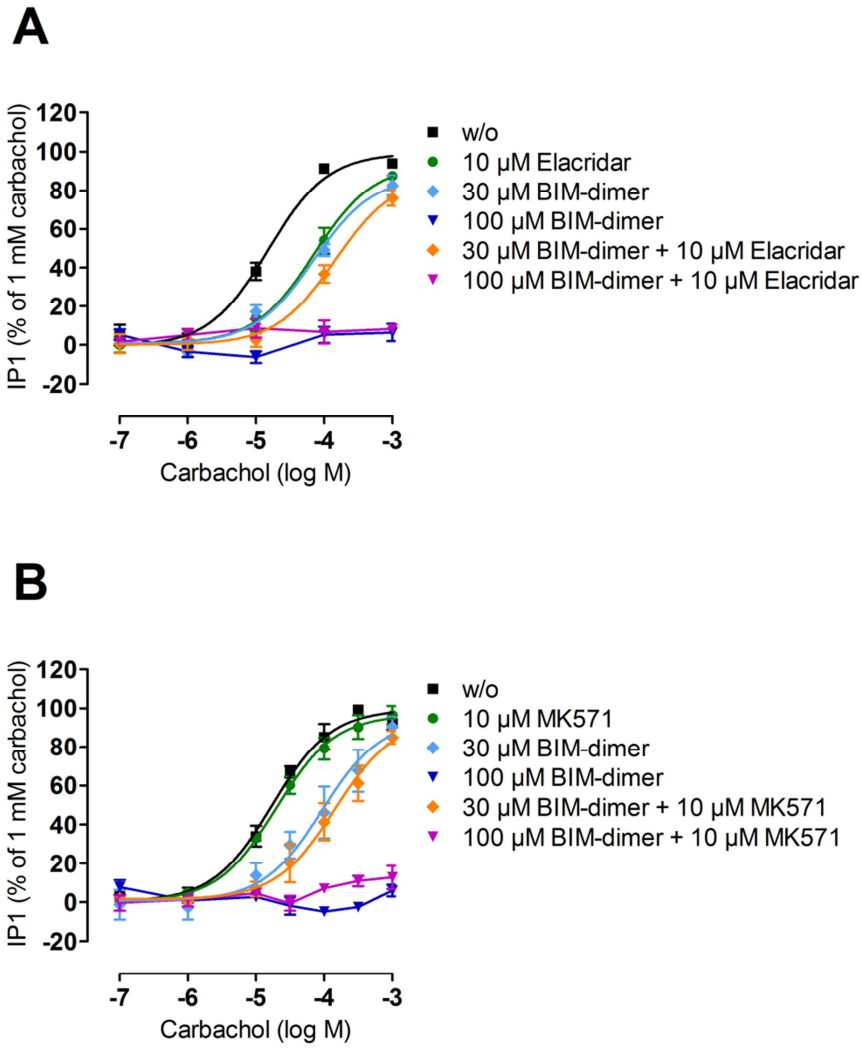

Figure 14: Inhibition of multidrug transporters did not improve the capacity of BIM to silence $G\alpha_q$ signaling.

(**A**)-(**B**) HEK293 cells endogenously expressing the $G\alpha_q$-sensitive muscarinic M3 receptor were pretreated with the indicated concentrations of BIM-dimer for 2 h in the absence or presence of the multidrug transport inhibitors elacridar (**A**) or MK571 (**B**) and inositol phosphate IP1 accumulation was quantified as a measure of M3 receptor activity. Shown are mean values ± SEM of three independent experiments, each performed in triplicate.

(**A**) pEC_{50}/E_{max} (w/o) = 4.82 ± 0.11/99%; pEC_{50}/E_{max} (10 µM elacridar) = 4.15 ± 0.12/93%; pEC_{50}/E_{max} (30 µM BIM-dimer) = 4.15 ± 0.11/87%; pEC_{50}/E_{max} (30 µM BIM-dimer + 10 µM elacridar) = 3.84 ± 0.13/87%.

(**B**) pEC_{50}/E_{max} (w/o) = 4.77 ± 0.08/99%; pEC_{50}/E_{max} (10 µM MK571) = 4.71 ± 0.07/97%; pEC_{50}/E_{max} (30 µM BIM-dimer) = 4.03 ± 0.18/94%; pEC_{50}/E_{max} (30 µM BIM-dimer + 10 µM MK571) = 3.84 ± 0.16/94%.

3.1.8 Analyzing BIM-dimer in radioligand competition binding assays

The findings that BIM-dimer silenced $G\alpha_q$ signaling in different cellular environments led to the question whether BIM-dimer could interfere with the agonist binding. In a first experiment it was tested whether BIM-dimer had an influence on the antagonist recognition of the muscarinic M1 receptor (**Fig. 15**). The results depict that BIM-dimer did not interfere with antagonist recognition.

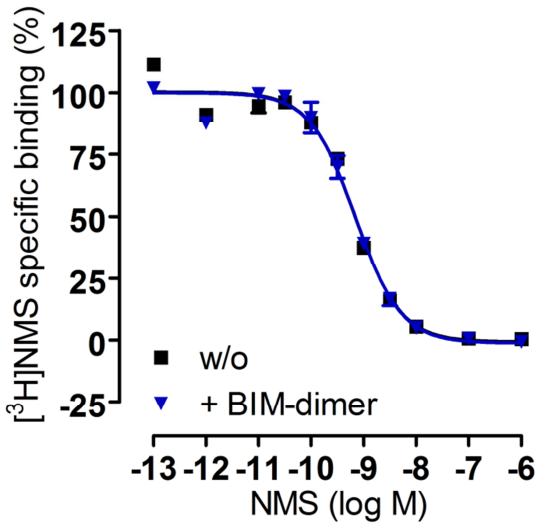

Figure 15: Influence of BIM-dimer on antagonist recognition. CHO-M1 membranes were labelled with 0.2 nM [^{3}H]NMS and homologous competition experiments were conducted after a preincubation with 100 µM BIM-dimer (2 h). Data are means ± SEM of 2-9 experiments performed in duplicates and were kindly provided by Ramona Schrage, Pharmacology and Toxicology Section, Institute of Pharmacy, University of Bonn, Germany.

Next, whole CHO-M1 cells were investigated in radioligand competition assays using carbachol as a ligand (**Fig 16A**). BIM-dimer did not impair carbachol displacement of the radio-antagonist [^{3}H]NMS but rather enhanced agonist binding. From these data it seems reasonable that the inhibition of $G\alpha_q$-mediated signaling was not due to BIM interference with agonist binding but with agonist function.

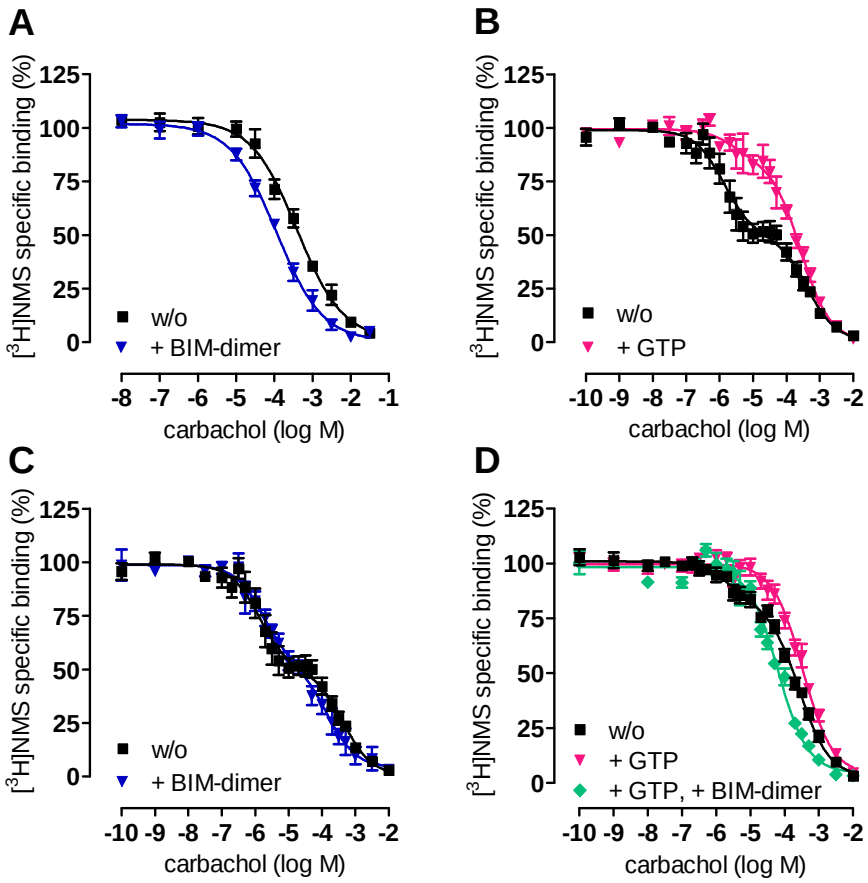

Figure 16: Effect of BIM-dimer on carbachol recognition of the muscarinic M1 receptor.
(**A**) 100 µM BIM dimer enhanced carbachol affinity to muscarinic M1 receptors labeled with [^{3}H]NMS in whole CHO-M1 cells: pKi (w/o) = 3.61 ± 0.08; pKi (BIM-dimer) = 4.09 ± 0.09.
(**B**) Carbachol competed for [^{3}H]NMS sites with high and low affinity in membrane preparations from CHO-M1 cells. If 1 mM GTP were present, 49% of the high-affinity sites were converted to the low-affinity sites.
(**C**) In CHO-M1 preparations 100 µM BIM-dimer did not impair formation of high-affinity complexes.
(**D**) BIM counteracted the effect of GTP on high-affinity agonist binding in membrane preparations from CHO cells stably expressing the muscarinic M1 receptor. pKi_{high} (w/o) = 6.02 ± 0.23; pKi_{low} (w/o) = 3.75 ± 0.06, fraction (w/o) = 19% ± 3; pKi (GTP) = 3.67 ± 0.10; pKi (GTP + BIM) = 4.34 ± 0.04.
(**A**)-(**D**) Data are means ± SEM of at least three independent experiments, each conducted at least in duplicates and were kindly provided by Ramona Schrage, Pharmacology and Toxicology Section, Institute of Pharmacy, University of Bonn, Germany.

Ayoub et al. used [^{35}S]GTPγS binding assays to show that BIM prevented G protein activation independent of the activating stimulus. They activated GPCRs with a direct ligand, the direct G protein activators AlF_4^- and mastoparan or the $G\alpha_i$ mimetic

FUB132. In all cases BIM-dimer blocked G protein activation and these data led to the hypothesis that BIM achieved its effect through direct interaction with the Gα protein (Ayoub et al., 2009). These findings did not clarify the mode of action and did not answer the question whether BIM affects GDP exit or GTP entry. To get further insight into the mechanism radio-ligand binding studies were performed with CHO-M1 cell membranes using [^{3}H]NMS as radio-antagonist.

CHO-M1 membranes were analyzed in competition binding assays in which membranes were labelled with 0.2 nM [^{3}H]NMS and then increasing amounts of the M1 agonist carbachol were added. With this approach it was possible to discriminate between the two possibilities for a mode of action of BIM: (1) BIM acts as guanine-nucleotide dissociation inhibitor (GDI) or (2) BIM functions as GTP entry inhibitor. For the first postulated situation BIM would have inhibited high-affinity agonist binding which is a conformational receptor state that is stabilized by the nucleotide-free empty-pocket G protein (De Lean et al., 1980; Oldham and Hamm, 2008; Rodbell et al., 1971). It is important to know that the high-affinity state is only detectable in the absence of guanine nucleotides and represents only a short-lived intermediate state in whole cells since guanine nucleotides are abundant (De Lean et al., 1980; Oldham and Hamm, 2008; Rodbell et al. 1971). **Figure 16B** shows binding data generated in the presence and absence of 1 mM GTP. In the absence of GTP one could detect high-affinity binding of carbachol to coupled GPCRs and low-affinity binding to uncoupled M1 receptors. If the cells were treated with GTP 49% of the high-affinity sites were converted to low-affinity sites (**Tab. 1**) because of a rapid exchange from GDP to GTP and thus the empty pocket conformation was no longer measureable. A preincubation with 100 µM BIM-dimer had no effect on the high-affinity sites (**Fig. 16C, Tab. 1**) meaning that BIM-dimer was not able to uncouple receptors from their G proteins. Based on the results in **Fig. 16C** one could conclude that GDP can exit. If BIM permits GDP exit but inhibits G protein function it consequently must function as GTP entry inhibitor. This postulated hypothesis was challenged with a further experiment, in which membranes were preincubated with a combination of BIM-dimer and GTP (**Fig. 16D**). In the presence of BIM-dimer and GTP, BIM-dimer counteracted the effect of GTP on high-affinity agonist binding. This indicates that GTP cannot enter and receptors are not uncoupled from their cognate G protein because BIM “freezes” $G\alpha_q$ in the empty pocket conformation. Thus, these data fit well to the postulated mode of action.

Condition	log (Ki) high	SEM	log (Ki) low	SEM	fraction	SEM	n
w/o	-6.04	0.16	-3.54	0.02	0.51	0.05	4
BIM-dimer 100 µM	-5.96	0.25	-3.96	0.12	0.49	0.01	3
GTP 1 mM	-5.70	0.55	-3.66	0.09	0.26	0.08	4

Table 1: Related to **Figure 16**. Binding affinities of carbachol to [^{3}H]NMS-labelled CHO-M1 receptors as determined in membrane preparations in the absence or presence of 100 µM BIM or 1 mM GTP. Data were kindly provided by Ramona Schrage, Pharmacology and Toxicology Section, Institute of Pharmacy, University of Bonn, Germany.

3.1.9 Influence of BIM-dimer on GDP-dissociation

To underpin the present findings BIM-dimer was investigated in [^{3}H]GDP dissociation assays with purified recombinant $G\alpha_q$ proteins (**Fig. 17**). For this assay a recombinant $G\alpha_q$, lacking the first 34 residues ($G\alpha_q\Delta34$) was used. This protein was purified after expression from a pFastBacI vector in insect cells (Waldo et al., 2010). This construct was expressed as a chimera containing the first 28 residues of rat $G\alpha_{i1}$ connected to mouse $G\alpha_q\Delta34$. An intervening TEV cleavage site between the $G\alpha_{i1}$ and $G\alpha_q$ sequences enables removal of the $G\alpha_{i1}$ sequence by the use of TEV protease. Thus, it is possible to obtain soluble chimeric proteins that could be purified in sufficient amounts (Tesmer et al., 2005; Kreutz et al., 2006). $G\alpha_q$-bound GDP dissociates very slowly (Chidiac et al., 1999) and to avoid this problem the assays were performed in the presence of 750 mM $(NH_4)_2SO_4$, a chemical substance which speeds up the dissociation process and thus enabled its visualization. After 120 min the dissociation process was complete but completely unaffected by the presence of BIM-dimer.

These results were strongly in line with the hypothesis that BIM-dimer enables GDP exit but prevents GTP entry.

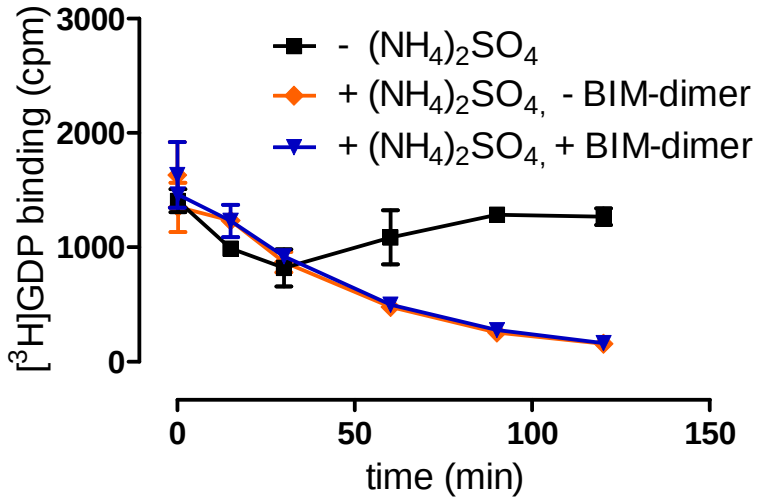

Figure 17: [^{3}H]GDP dissociation from purified Gα_q proteins. G$\alpha_q\Delta$34 proteins were incubated with 1 µM [^{3}H]GDP for 18 h and then dissociation was detected in the presence of 750 mM $(NH_4)_2SO_4$. BIM-dimer had no effect on [^{3}H]GDP dissociation. Data were kindly provided by Thomas Charpentier, Department of Pharmacology, School of Medicine, University of North Carolina, Chapel Hill, USA. Data are means ± SEM of at least three experiments.

3.1.10 Washing experiments

These experiments were designed to investigate whether BIM-dimer irreversibly binds to the Gα_q protein. HEK293 cells were analyzed in IP1 accumulation assays (**Fig. 18**) after preincubation with 100 µM BIM-dimer for 2 h. After the incubation cells were washed three times for 5 min with PBS and then stimulated with carbachol. In parallel the assay was performed without the washing procedure to exclude influences on the cells by the washing process itself. As depicted in Figure 16 the washing procedure had no effect on the concentration response curve in the absence of BIM-dimer. When the cells were washed in the presence of BIM-dimer the inhibitory effect on the Gα_q pathway was strongly diminished. From these results one can conclude that BIM-dimer did not bind irreversibly to Gα_q proteins because it was possible to wash out the Gα_q-inhibitory effect.

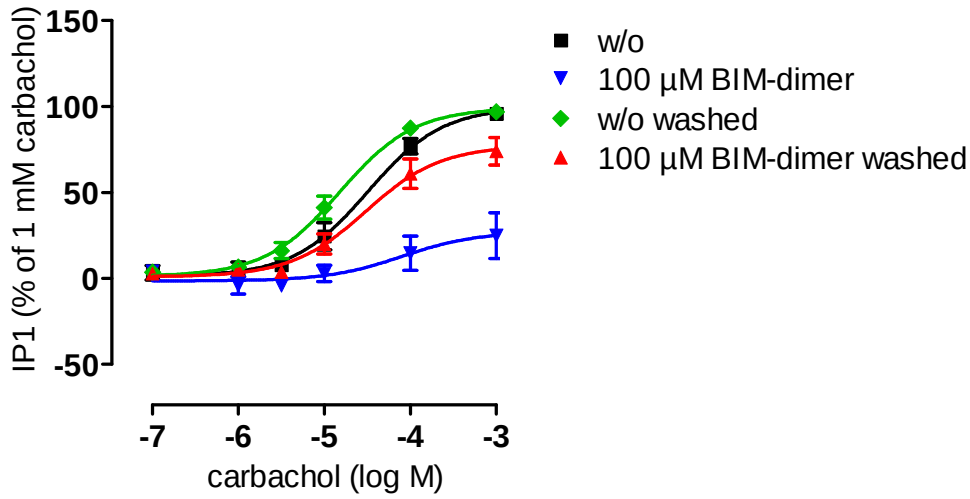

Figure 18: BIM effect showed no irreversibility in washing experiments. HEK293 cells endogenously expressing muscarinic M3 receptors were preincubated with BIM-dimer (100 µM) and subsequently washed three times for 5 minutes with PBS. Then cells were stimulated with the muscarinic agonist carbachol in increasing concentrations and IP1 accumulation was assessed. As a control IP1 accumulation was also determined without the washing procedure. pEC_{50}/E_{max} (w/o) = 4.50 ± 0.12/100%; pEC_{50}/E_{max} (100 µM BIM-dimer) = 4.10 ± 0.61/27%; pEC_{50}/E_{max} (w/o washed) = 4.82 ± 0.08/99%; pEC_{50}/E_{max} (100 µM BIM-dimer washed) = 4.52 ± 0.17/77%. Data shown are means ± SEM of at least three independent experiments, each performed in triplicate.

3.1.11 Stability analysis of BIM-monomer

In 2006 Prévost et al. ascribed the properties of a pan-G protein inhibitor to a compound named BIM-46174 (hereafter referred to as BIM-monomer). Before analyzing its effect on Gα subunits it was necessary to investigate the stability of monomeric BIM. Based on the structure of BIM-monomer it was hypothesized that the free thiol group should be intrinsically sensitive to oxidation and therefore stability was investigated in aqueous solution (D_2O) over time by nuclear magnetic resonance (NMR) spectroscopy (**Fig. 19**). The protons in position 2 and 16 were well suited to study stability and enabled the differentiation between BIM-monomer and BIM-dimer.

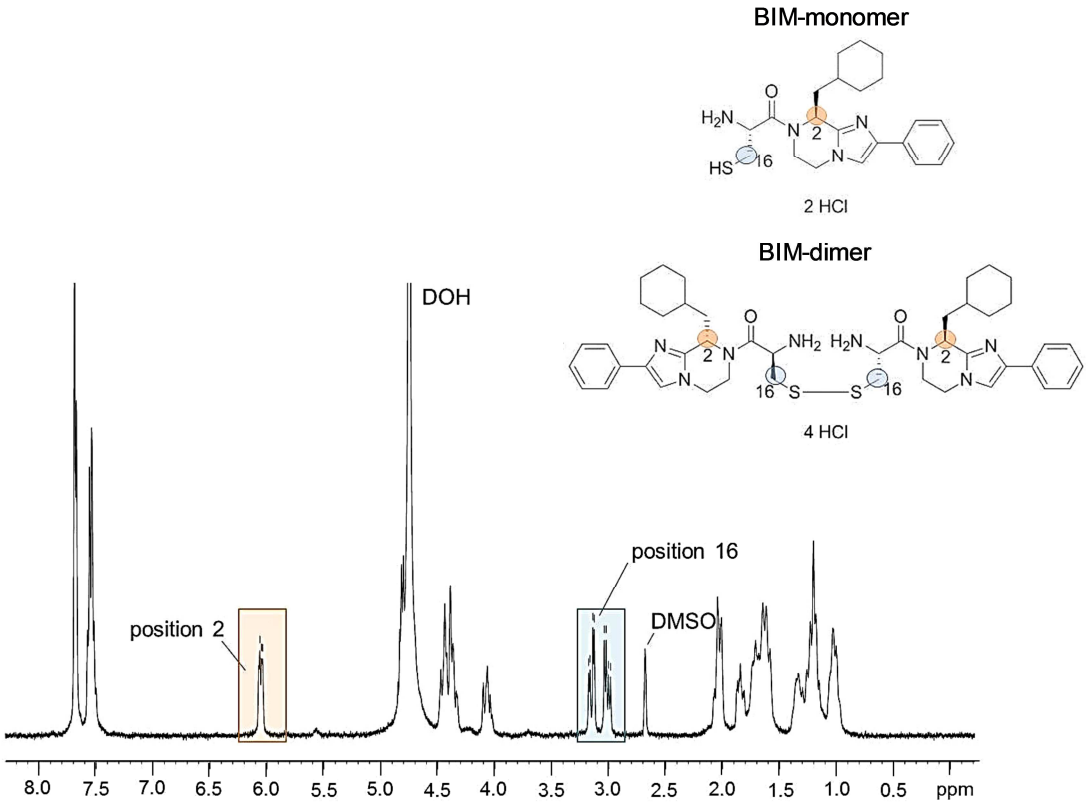

Figure 19: Structures of BIM-monomer and BIM-dimer and NMR analysis in aqueous solution. ^{1}H-NMR of the BIM-monomer: The signals at δ = 7.4-7.8 ppm correlate to the protons of the aromatic moiety and the imidazole ring. The signal at δ = 6.0 ppm corresponded to the proton in position 2 and the area from δ = 4.0-5.0 ppm compromised the protons of position 12, 13 and 15 partially overlayed by the residual solvent (DOH) signal. At about δ = 3 ppm, the diasterotopic methylene protons next to the thiol group resonate (position 16), followed by the DMSO signal and the high-field shifted protons of the cyclohexylmethyl group. Data were kindly provided by Georg Hiltensperger, Pharmaceutical and Medicinal Chemistry, Institute of Pharmacy and Food Chemistry, University of Würzburg, Germany.

NMR spectra were detected at different time points between 0 and 48 h (**Fig. 20**) and were clearly indicative of BIM-monomer oxidation in a time-dependent manner. After 48 h BIM-monomer was no longer detectable. The integrated area of the signals (**Tab. 2**) correlated with the concentration of BIM-monomer and allowed for the deduction of a 11.4 h half-life for this first order reaction (**Fig. 21**).

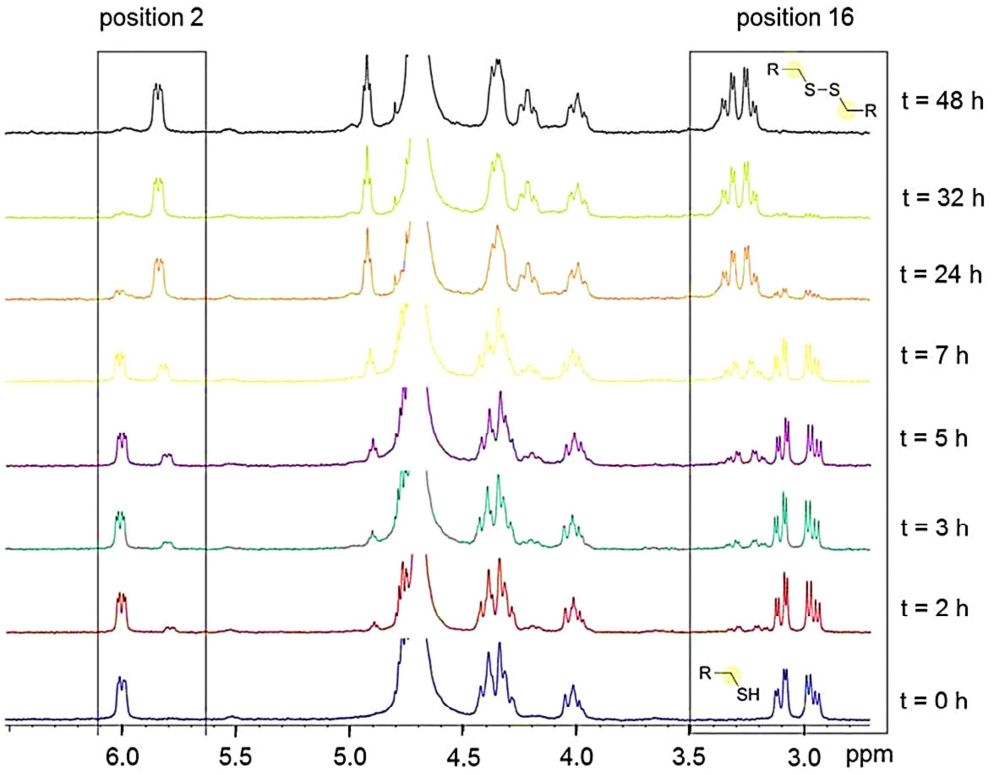

Figure 20: NMR spectroscopy of BIM-monomer over time. The oxidation process could be observed using the protons in position 2 and 16. At t = 0 h, only the proton signals of BIM-monomer were observed. Within 48 h the integrated areas of the signal of the monomer protons decreased while the dimer signals increased until 100% dimer was observed at t = 48 h. Data were kindly provided by Georg Hiltensperger, Pharmaceutical and Medicinal Chemistry, Institute of Pharmacy and Food Chemistry, University of Würzburg, Germany.

Time [h]	Integration area	Concentration [mg/ml]	Ln c
0	0.99	2.50	0.92
2	0.88	2.24	0.80
3	0.84	2.13	0.76
5	0.71	1.80	0.59
7	0.62	1.57	0.45
24	0.22	0.56	-0.58
32	0.14	0.36	-1.03

Table 2: Related to **Figure 20**. Decreasing integration areas (proton 2) and corresponding concentrations of BIM-monomer. Data were kindly provided by Georg Hiltensperger, Pharmaceutical and Medicinal Chemistry, Institute of Pharmacy and Food Chemistry, University of Würzburg, Germany.

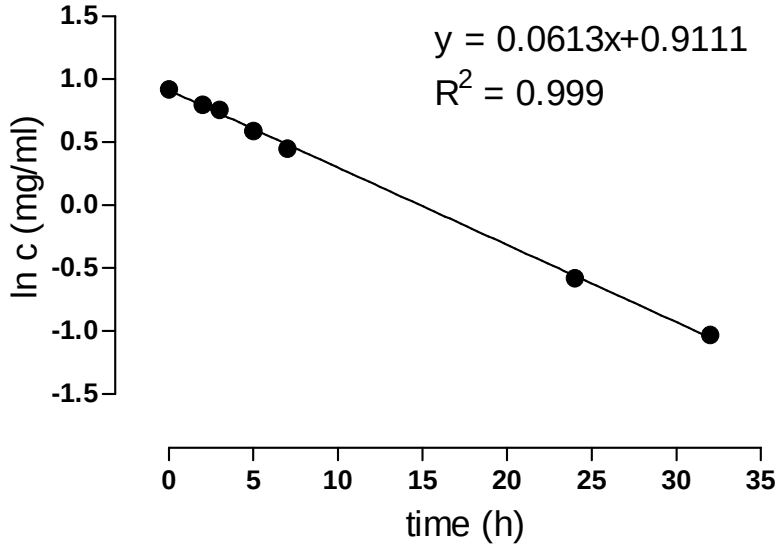

Figure 21: A diagram of the natural logarithm of the concentration (ln c) of BIM-monomer versus time. Since the integration area of the signals in Figure 18 correlated with concentration of the BIM-monomer, a half-life of 11.4 h is calculated for this first-order reaction. Data were kindly provided by Georg Hiltensperger, Pharmaceutical and Medicinal Chemistry, Institute of Pharmacy and Food Chemistry, University of Würzburg, Germany.

Due to the short preincubation time during the second-messenger assays (2 h), a half-life of 11.4 h of monomeric BIM is sufficiently long to test its Gα subunit-inhibiting profile. Nonetheless it is important to remember that BIM-monomer might partially convert to BIM-dimer during the assay period although the greater portion will be present as monomeric BIM.

3.1.12 Kinetic studies with BIM-monomer and BIM-dimer in a HEK and a CHO cell background

To compare BIM-monomer and BIM-dimer concerning their kinetic profiles IP1 accumulation assays were performed. Therefore HEK293 (**Fig. 22A**) and CHO-M1 (**Fig. 22B**) cells were preincubated with BIM-monomer or BIM-dimer for 0.5 to 3 h and IP1 levels were determined after the stimulation with carbachol. The findings within the different cellular backgrounds were very similar for both inhibitory compounds. The inhibitory effect increased with a longer preincubation time and had its maximum after three hours. Notably, after three hours preincubation the assay window was reduced, probably caused by lowered cell viability, and therefore it was decided that incubation for 2 h would be the best suitable duration for further experiments with BIM-monomer. In addition to this the results in **Figure 22** show that dimeric BIM was superior to BIM-monomer in its ability to silence $G\alpha_q$-mediated signaling independently of the preincubation time.

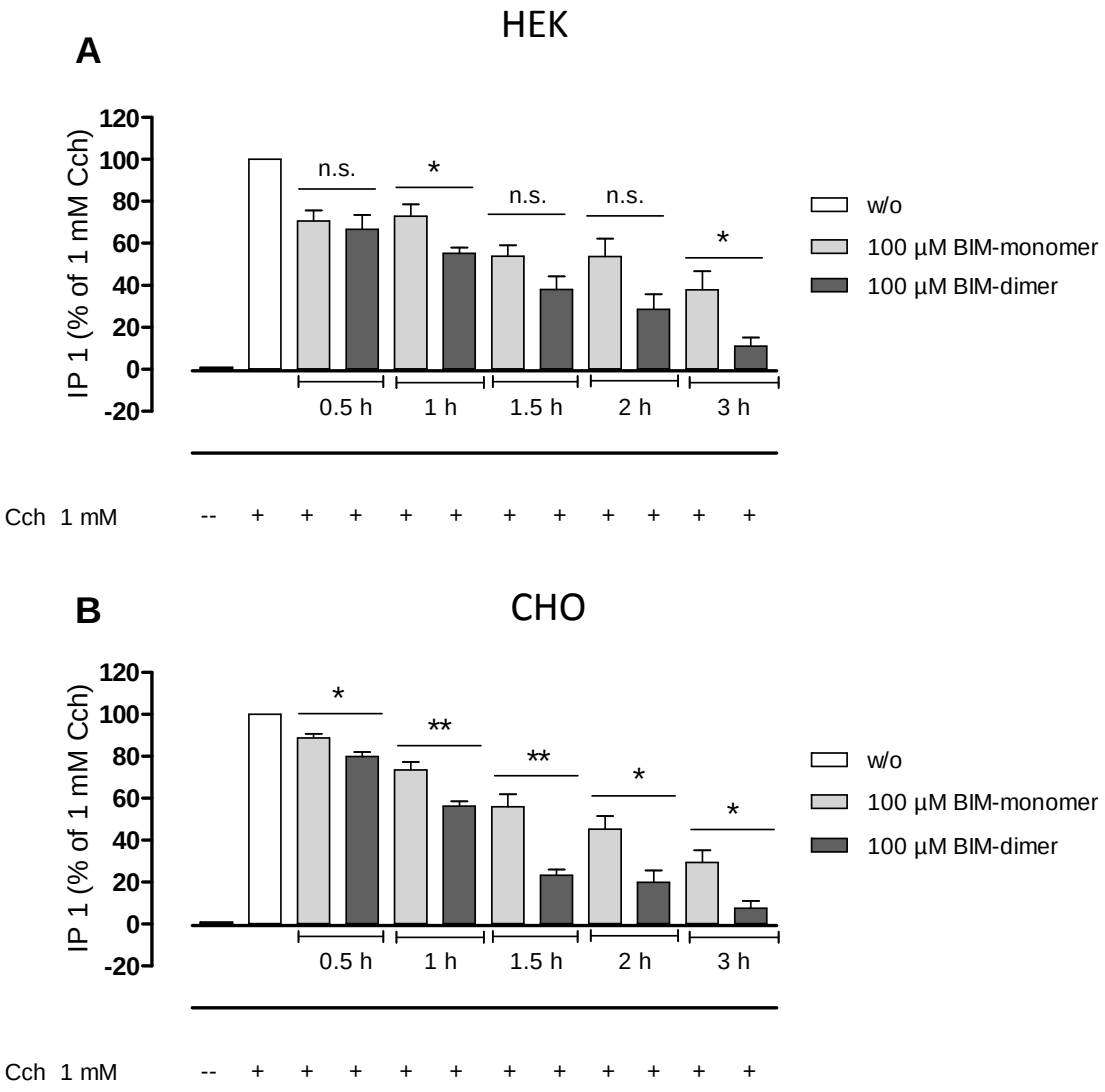

Figure 22: Kinetic studies with BIM-monomer and BIM-dimer.
(**A**) HEK293 cells endogenously expressing muscarinic M3 receptors were used to determine IP1 levels after different preincubation times for BIM-monomer and BIM-dimer. The cells were stimulated with 1 mM carbachol.
(**B**) IP1 accumulation was detected in CHO cells stably transfected to express the muscarinic M1 receptor. BIM-monomer and BIM-dimer were preincubated for 0.5-3 h and then receptors were stimulated with 1 mM carbachol.
(**A**)-(**B**) Cch = carbachol. Data shown are means + SEM of at least three independent experiments.

3.1.13 Investigating monomeric BIM in HEK and CHO cell backgrounds

The following experiments helped answer the question whether BIM-monomer shows a similar preference for inhibition of $G\alpha_q$ proteins in HEK and CHO cell backgrounds. Therefore, BIM-monomer was analyzed in second-messenger assays analogous to experiments conducted for BIM-dimer. As depicted in Figure 21 BIM-monomer partially silenced $G\alpha_q$-mediated signaling (**Fig. 23A**) of the endogenously expressed muscarinic M3 receptor in HEK293 cells. However, $G\alpha_s$ signaling via endogenously expressed EP2/4 receptors (**Fig 23B**) and $G\alpha_i$ signaling via stably transfected CRTH2 receptors (**Fig. 23C**) was completely unaffected.

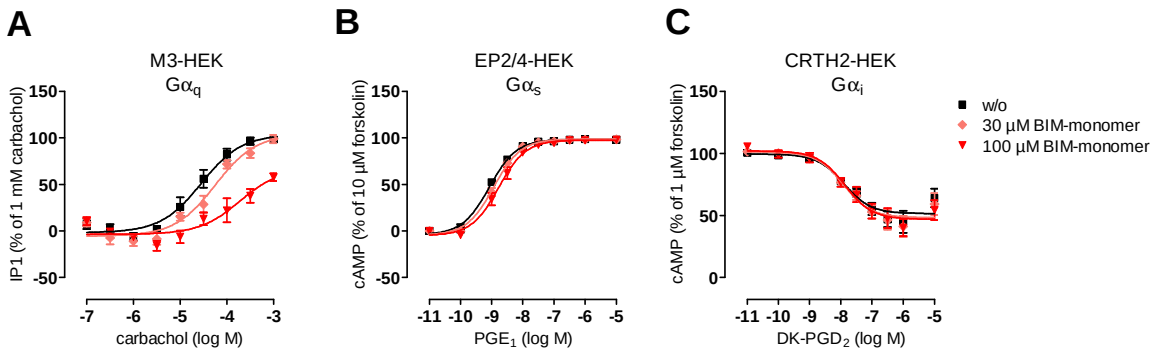

Figure 23: BIM-monomer preferentially silenced $G\alpha_q$ signaling in HEK cells.
(**A**) In HEK293 cells IP1 levels were determined in the presence or absence of BIM-monomer. $G\alpha_q$ signaling of the endogenously expressed M3 receptor was partially inhibited. pEC_{50}/E_{max} (w/o) = 4.55 ± 0.10/104%; pEC_{50}/E_{max} (30 µM BIM-monomer) = 4.25 ± 0.11/104%; pEC_{50}/E_{max} (100 µM BIM-monomer) = 3.72 ± 0.24/68%.
(**B**) Signaling via $G\alpha_s$ proteins was detected with cAMP accumulation assays. BIM-monomer showed no inhibitory effect on $G\alpha_s$-sensitive EP2/4 receptors. pEC_{50}/E_{max} (w/o) = 9.07 ± 0.03/98%; pEC_{50}/E_{max} (30 µM BIM-monomer) = 8.93 ± 0.03/99%; pEC_{50}/E_{max} (100 µM BIM-monomer) = 8.78 ± 0.05/98%.
(**C**) $G\alpha_i$-sensitive CRTH2 receptors were unaffected by BIM-monomer pretreatment. pEC_{50}/E_{max} (w/o) = 7.90 ± 0.18/51%; pEC_{50}/E_{max} (30 µM BIM-monomer) = 7.91 ± 0.17/48%; pEC_{50}/E_{max} (100 µM BIM-monomer) = 7.87 ± 0.17/47%.
(**A**)-(**C**) Means ± SEM of at least three independent experiments are shown.

Similar results were obtained in the CHO cell background: After a preincubation with BIM-monomer for 2 h IP1 production mediated via muscarinic M1 receptors was reduced (**Fig. 24A**). $G\alpha_s$ and $G\alpha_i$ signaling was determined using $G\alpha_s$-sensitive EP2/4 receptors (**Fig. 24B**) and $G\alpha_i$-sensitive serotonin receptors (**Fig. 24C**) but cAMP production was unaffected by a preincubation with BIM-monomer.

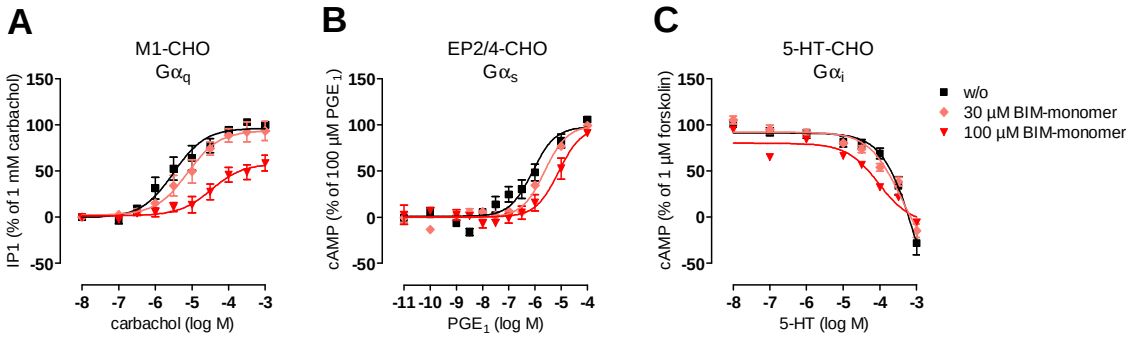

Figure 24: BIM-monomer preferentially diminished $G\alpha_q$ signaling in a CHO background.
(**A**) $G\alpha_q$ signaling of the muscarinic M1 receptor in CHO cells was partially silenced in IP1 accumulation assays. pEC_{50}/E_{max} (w/o) = 5.51 ± 0.13/96%; pEC_{50}/E_{max} (30 µM BIM-monomer) = 5.12 ± 0.13/94%; pEC_{50}/E_{max} (100 µM BIM-monomer) = 4.47 ± 0.19/58%.
(**B**)-(**C**) cAMP levels were detected to analyze the influence of BIM-monomer on $G\alpha_s$-coupled EP2/4 receptors (pEC_{50}/E_{max} (w/o) = 6.09 ± 0.13/98%; pEC_{50}/E_{max} (30 µM BIM-monomer) = 5.63 ± 0.08/99%; pEC_{50}/E_{max} (100 µM BIM-monomer) = 5.10 ± 0.15/98%) (**B**) and $G\alpha_i$-coupled serotonin (5-HT) receptors (**C**). BIM-monomer did not diminish signaling of these pathways.
(**A**)-(**C**) Data shown are means ± SEM of at least three independent experiments, each performed in triplicates.

In summary, monomeric BIM as well as BIM-dimer, had a clear preference for diminishing signaling via $G\alpha_q$ proteins. In a CHO and HEK cell background BIM-dimer was superior to BIM-monomer in its potential to silence $G\alpha_q$-mediated signaling. From these data one can conclude that the cellular context-dependent inhibition of $G\alpha_q$ signaling was not related to the inability of the cells to convert BIM-dimer into BIM-monomer or the different reductive potentials of the cells.

3.1.14 Screening of a substance library with BIM-dimer analogs

In a large substance library of the working group of Prof. Gütschow (Pharmaceutical Chemistry I, Institute of Pharmacy, University of Bonn, Germany) several compounds with structural similarity to BIM-dimer were available (chemical structures see Appendix). All of them contained a disulfide structure and showed symmetry. The aim of this screening was to clarify whether the disulfide structure demonstrated an important element for the $G\alpha_q$-inhibitory effect and to ascertain whether it would be possible to explore other structures which could potentially be applied at lower concentrations than 100 µM. To this end, IP1 assays were performed: The cells were preincubated with 30 or 100 µM of the potential inhibitors followed by stimulation of M1 receptors with 30 µM carbachol (**Fig. 25**). None of the screened compounds was able to silence $G\alpha_q$-mediated signaling indicating that the disulfide structure alone could not be responsible for the inhibitory interaction with $G\alpha_q$ proteins.

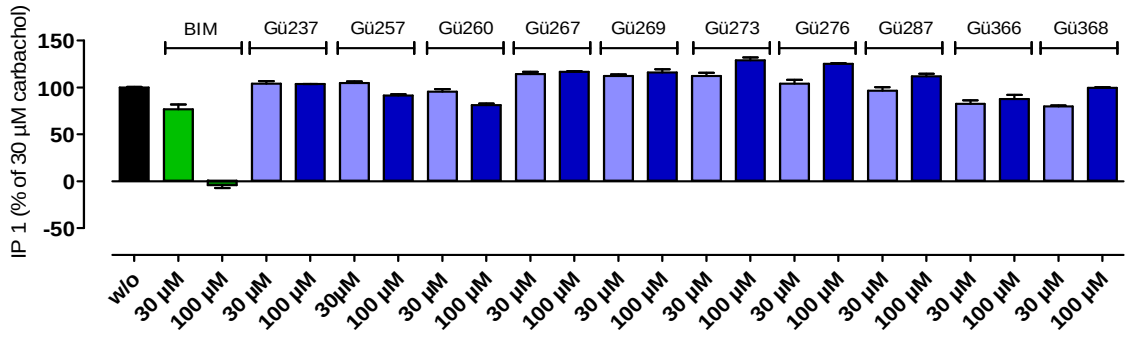

Figure 25: Screening of BIM-dimer analogs. CHO cells stably transfected to express muscarinic M1 receptors were used to test several substances for their ability to silence $G\alpha_q$ signaling in IP1 accumulation assays after 2 h preincubation. Each substance was tested in a concentration of 30 and 100 µM. BIM-dimer was used as a positive control. Inhibitory effects were not observed in any of the substances analyzed. Data are means + SEM of one to three experiments, each conducted in triplicate.

3.2 QIC (FR900359) - a suitable tool to specifically silence $G\alpha_q$ signaling?

The second part of this thesis deals with the depsipeptide FR900359 (hereafter referred to as QIC) which was described by Nesterov et al. as a specific $G\alpha_q$ protein inhibitor. The chemical structure (**Fig. 26**) is very similar to the structure of YM-254890 (hereafter referred to as YM) a well-known selective $G\alpha_q$ silencer (Takasaki et al., 2004; Nishimura et al., 2010). With a great variety of assays QIC should be investigated in detail to examine its specificity to silence Gα subunits and its mode of action.

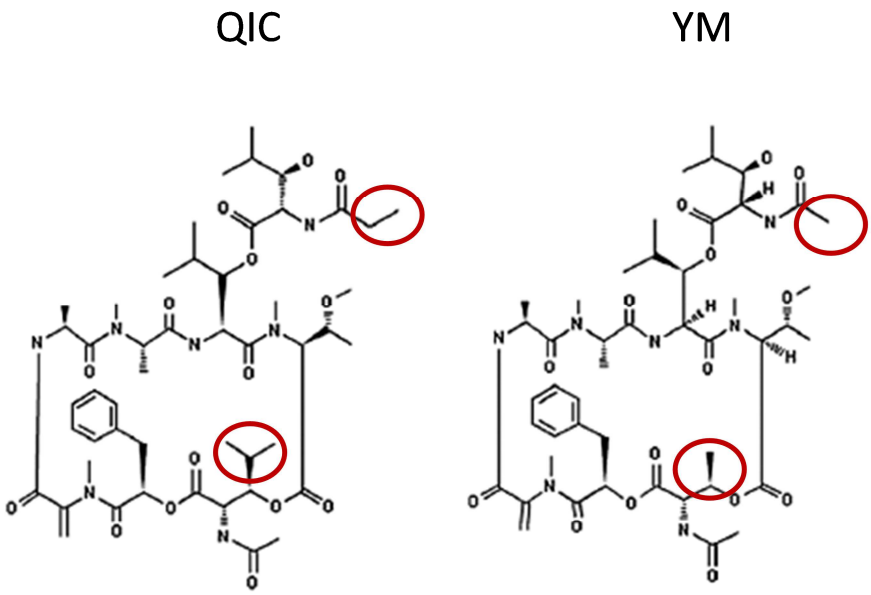

Figure 26: Chemical structure of QIC and YM (modified from Nesterov et al., 2010). QIC and YM are cyclic heptadepsipeptides with ester bonds via C-termini of amino acids with beta-hydroxy carbonic acids (e.g. Phenyllactic acid) or beta-hydroxy amino acids. They consist of six non-proteinogenic amino acids and two cis-peptide bonds. Structural differences are highlighted with red circles.

3.2.1 Screening of *Ardisia crenata* extracts

QIC was isolated from the leaves of the evergreen plant *Ardisia crenata.* The extraction was conducted by Dr. Stefan Kehraus (Institute for Pharmaceutical Biology, University of Bonn, Germany). Several extracts were tested in IP1 accumulation assays to detect QIC containing fractions. In a first step leaves were extracted with methanol (3-4 times) to obtain the primary leaf extract. This primary leaf extract was further fractionated via liquid-liquid distribution between water (extract E1) and butanol. Then the butanolic residuent was separated with liquid-liquid extraction between acetonitrile and hexane

obtaining extract E2 and E3. For the first approach three leaf extracts of *Ardisia crenata* were analyzed: E1 (H_2O), E2 (acetonitrile) and E3 (hexane). These extracts were tested in a concentration of 0.3% (**Fig. 27A**) in CHO cells stably expressing the muscarinic M1 receptor which is coupling via $G\alpha_q$ proteins. The cells were stimulated with the synthetic muscarinic agonist carbachol. IP1 production was inhibited by extract E1 and E2. Two further assays were performed with lower concentrations of E1 to E3 (**Fig. 27B-C**). Inhibitory activity was still detectable in E2 in a concentration of 0.03% while the other extracts lost their ability to silence $G\alpha_q$ signaling with further dilution.

Based on these findings E2 was further separated via vacuum liquid chromatography (VLC) and five fractions F1 to F5 were obtained. These fractions were tested in a concentration of 1% (**Fig 28A**) and it seemed that the $G\alpha_q$ inhibitory compound was distributed over the whole eluate with the exception of fraction F2. To elucidate quantitative differences within the fractions further diluted concentrations were analyzed. An inhibitory effect was exclusively found in fraction F4 and F5 (**Fig. 28B**) but the Delta F levels were decreased in comparison to unfractionated extract E2 which could be explained with the enrichment of colored components interfering with FRET-based IP detection. With further dilutions this effect was no longer detectable while the $G\alpha_q$-inhibitory compound was still enriched enough to silence $G\alpha_q$-mediated IP1 production (**Fig. 28**C).

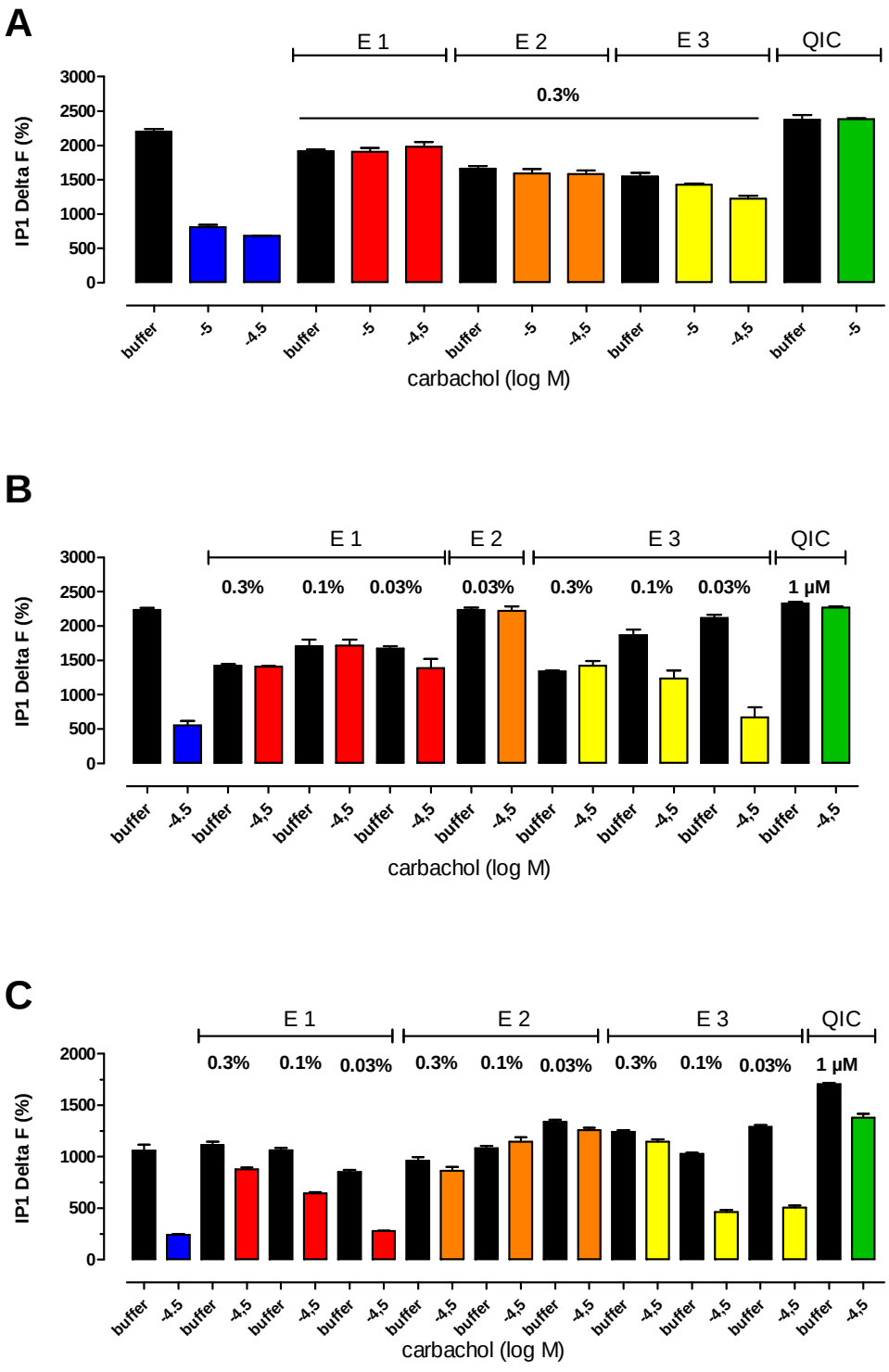

Figure 27: E2 leaf extract contained Gα_q protein inhibitory compound.
(**A**)-(**C**) CHO-M1 cells were preincubated with various concentrations of extracts E1 (H_2O), E2 (acetonitrile) and E3 (hexane) and IP1 levels were detected after stimulation with 30 µM carbachol. Data shown are means + SEM, experiments were performed in triplicate.

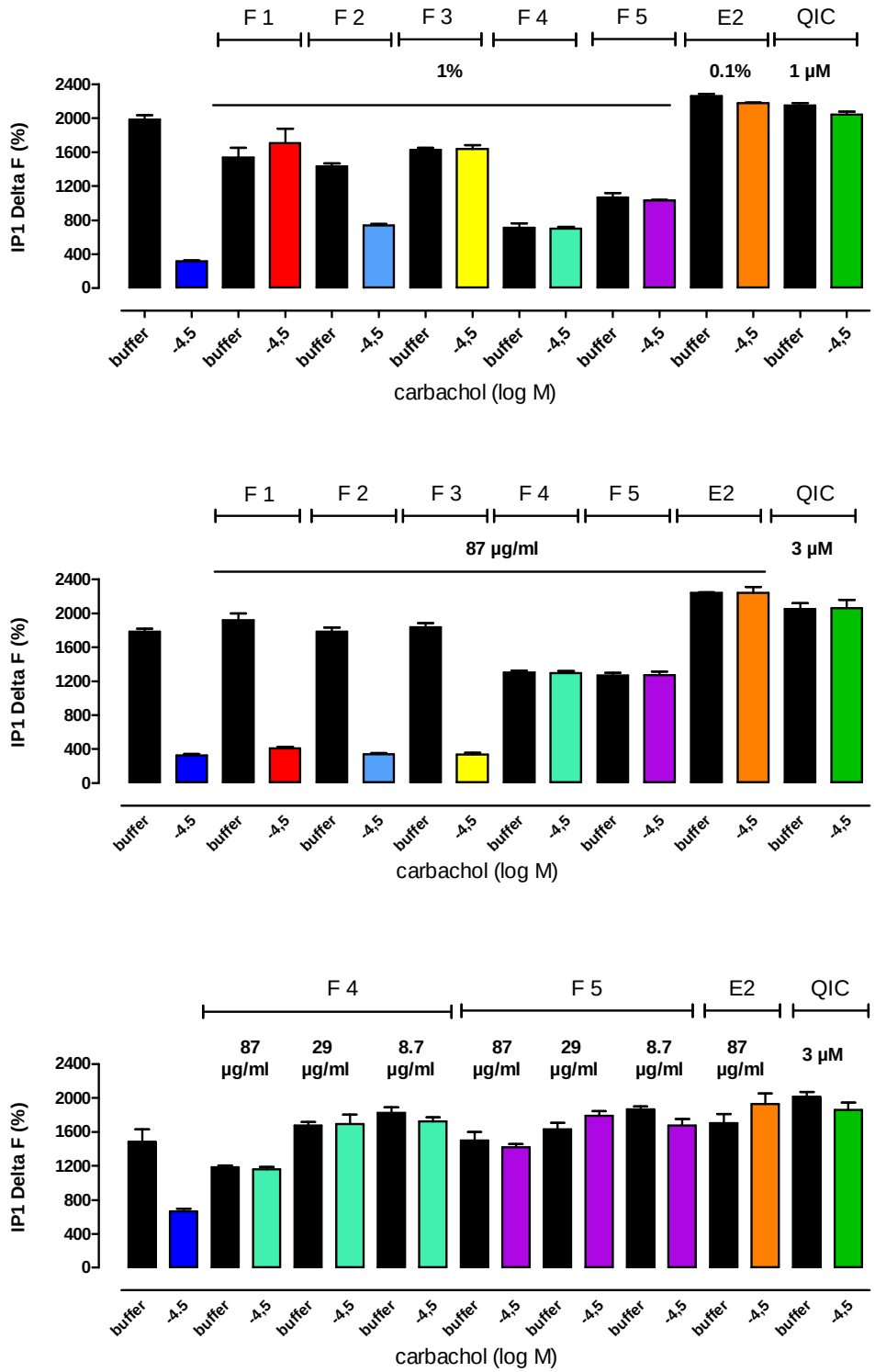

Figure 28: VLC Fraction F4 and F5 of the leaf extract were enriched with the Gα_q protein inhibitory compound.

(**A**)-(**C**) CHO-M1 cells were preincubated with various concentrations of VLC fractions F1 to F5 and IP1 levels were detected after stimulation with 30 µM carbachol. Data shown are means + SEM, experiments were performed in triplicate.

For the following experiments the primary shoot extract of *Ardisia crenata* was treated in the same way as leave extract ending up with three analogous secondary shoot extracts: E1 (H_2O), E2 (acetonitrile) and E3 (hexane). Extract E2 was further separated via VLC and six fractions F1 to F6 were obtained. As expected from the leaf extract results, enrichment of the $G\alpha_q$ inhibitor could be detected in further fractions of extract E2 (**Fig. 29A-B**), namely in fraction F4-F6 which fitted to the results in leaf fractions. Extract E1 did not contain significant amounts of the $G\alpha_q$ inhibitor but extract E3 seemed to contain inhibitory activity. Further dilution of fractions F4-F6 and E3 revealed that the greatest portion of the $G\alpha_q$ inhibitor was enriched in fraction F4 and F5, with a slightly higher enrichment in fraction F5 (**Fig. 29C**). The amount of the $G\alpha_q$-inhibitory compound formerly detected in extract E3 and fraction F6 seemed to be negligible because further dilutions did not show an inhibition of IP1 production anymore.

Based on these findings fraction F5 was further separated via high performance liquid chromatography (HPLC) ending up with 9 fractions HF0 to HF8. Fractions HF2, HF3 and HF4 seemed to contain the $G\alpha_q$-inhibitory compound (**Fig. 30A**). After a further dilution of HF2-HF4 the inhibitory effect was reduced for HF4 (**Fig. 30B**) and from dilutions up to 0.03% one could conclude that HF2 contained most of the $G\alpha_q$ inhibitor (**Fig. 30C**). Therefore fraction HF2 was selected for a further experiment in dynamic mass redistribution (DMR) assays. As depicted in **Figure 31** a treatment with HF2 alone as well as a treatment with QIC alone did not cause a cell response which was indicative that HF2 did not contain any activating components leading to changes in DMR. If CHO-M1 cells were stimulated with carbachol after pretreatment with HF2 or QIC the $G\alpha_q$-mediated signal was completely silenced but a negative DMR response was detectable. This response could be explained with the ability of the M1 receptor to couple also via $G\alpha_s$ proteins (Burford and Nahorski, 1996) but in the absence of a $G\alpha_q$-inhibitory compound this signal is masked by the $G\alpha_q$-mediated response.

In summary, it was possible to work out fractions with a high enrichment of the $G\alpha_q$-inhibitory compound without major differences between extracts originating from leaf or shoot of *Ardisia crenata*. Due to the fact that it is much easier to prepare leaf extracts it was decided to work with leaf extracts in further approaches.

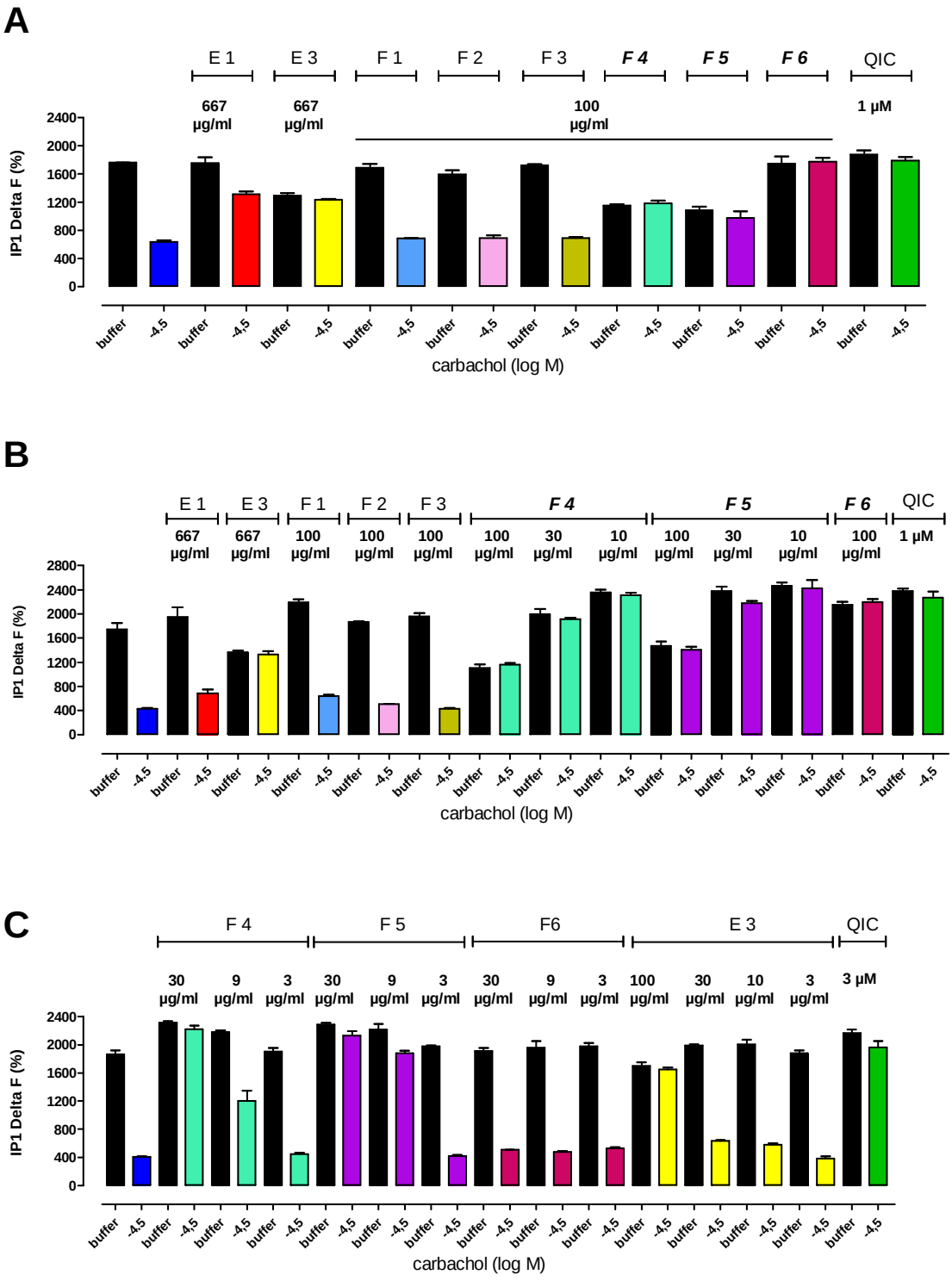

Figure 29: VLC Fraction F4 and F5 of the shoot extract were able to silence Gα_q signaling.
(**A**)-(**C**) CHO-M1 cells were preincubated with various concentrations of extract E1 and E3 or VLC fractions F1 to F6 and IP1 levels were detected after stimulation with 30 µM carbachol. Data shown are means + SEM, experiments were performed in triplicate.

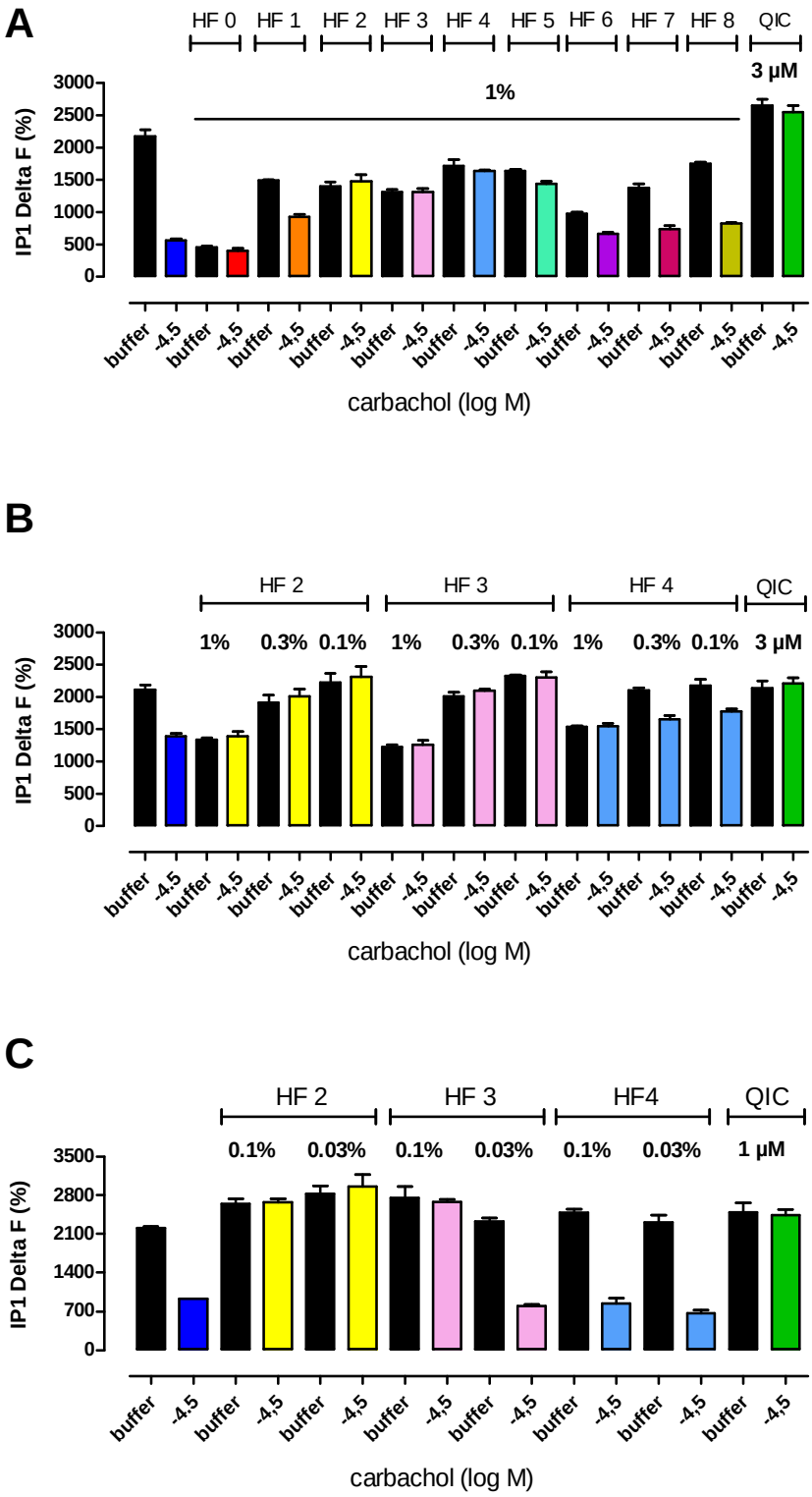

Figure 30: HPLC fraction HF2 and to a minor extent HF3 and HF4 of the shoot extract contained the Gα_q inhibitor.
(**A**)-(**C**) CHO-M1 cells were preincubated with various concentrations of extract E1 and E3 or VLC fractions F1 to F6 and IP1 levels were detected after stimulation with 30 µM carbachol. Data shown are means + SEM, experiments were performed in triplicate.

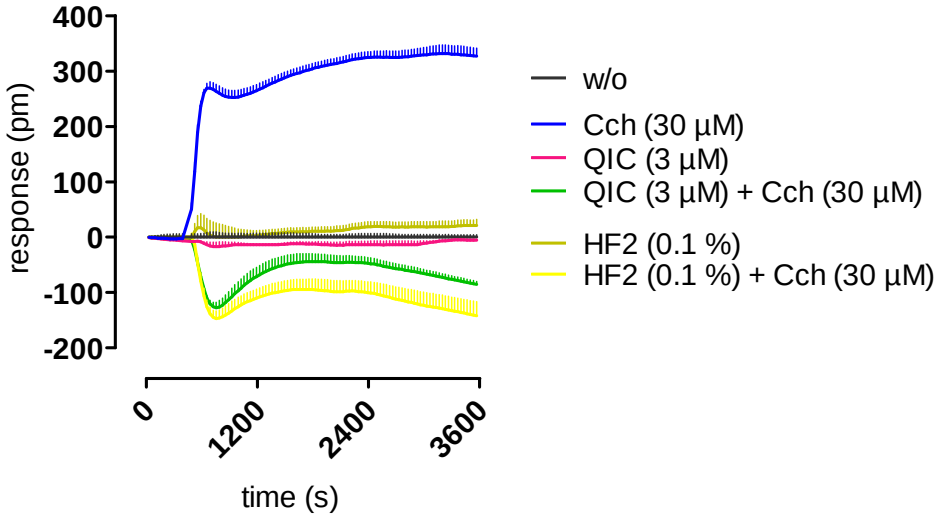

Figure 31: DMR revealed that HPLC fraction HF2 contained the $G\alpha_q$-inhibitory compound. CHO-M1 cells were pretreated with HF2 or QIC and wavelength shift was monitored as a measure of receptor activation. M1 receptors were stimulated with the synthetic agonist carbachol. Cch = carbachol. Shown are representative data means + SEM.

3.2.2 Stability test

Due to the fact that it was planned to explore QIC effects in long-term assays the stability of QIC was analyzed with DMR and calcium mobilization assays. For the DMR assays QIC was solubilized in assay buffer (Hank's buffered salt solution (HBSS) with 20 mM HEPES) and stored for up to eight days at 37°C. As a control assay buffer alone was also stored for this time period. On the day of the assay CHO-M1 cells were preincubated with either the collected assay buffer (**Fig. 32A**) or the stored QIC solutions (**Fig. 32B**) and M1 receptors were stimulated with carbachol. The addition of carbachol caused a positive wavelength shift and preincubation with the collected assay buffer had no effect on the cell response (**Fig. 32A**). This preincubation served as a control to check whether there are artifacts caused by the incubation process itself. If the CHO-M1 cells were preincubated with the different QIC solutions a similar negative wavelength shift was detectable (**Fig. 32B**), indicating that QIC was unaffected by the storage conditions at 37°C. The negative cell response could be explained with the ability of the M1 receptor to couple also via $G\alpha_s$ proteins (Burford and Nahorski, 1996) which becomes visible through a negative wavelength shift in a CHO cell background (Schröder et al., 2010). In the absence of $G\alpha_q$-inhibitory compounds this effect is superimposed by the positive $G\alpha_q$-mediated signal, because the M1 receptor preferentially couples via $G\alpha_q$ proteins (Caulfield and Birdsall., 1998).

As depicted in **Figure 32C-D** CHO-M1 cells were also stimulated with forskolin, a direct activator of the adenylyl cyclase to analyze whether QIC preincubation or possibly existing degradation products influence receptor-independent signaling as well as cell viability. The negative DMR was enhanced in the presence of QIC. This phenomenon could be explained with the crosstalk between the $G\alpha_q$ and $G\alpha_s$ signaling pathway, an effect which is well-described in literature. In the absence of QIC, endogenously expressed and constitutively active $G\alpha_q$-coupled receptors can cause a Ca^{2+} release and for calcium ions it is described that they can either activate or inactivate isoforms of adenylyl cyclase (Defer et al., 2000; Cordeaux and Hill, 2002). In this case calcium ions seem to show inhibitory effects on the adenylyl cyclase. QIC inhibits the $G\alpha_q$-mediated signaling via constitutively active receptors. Therefore, in the presence of QIC Ca^{2+} release is suppressed and inhibitory effects on the adenylyl cyclase are reversed.

Calcium mobilization assays were performed to detect whether QIC stability was influenced through the presence of adherent growing cells or media components. The assays were performed with (1) 1 µM QIC diluted in HEK-ratGPR17 media and stored for up to eight days in reaction tubes at 37°C and (2) 1 µM QIC diluted in HEK-ratGPR17 media was given into a cell culture flask with splitted HEK-ratGPR17 cells and samples were collected for up to eight days from the cell supernatant. The presence of growing cells or media showed no negative impact on the stability of QIC (**Fig. 32E**) because calcium mobilization was completely blocked independently of their storage duration.

From these findings one could conclude that the $G\alpha_q$-inhibitory effect of QIC was stable for a term of at least eight days at 37°C and therefore it is seems to be unnecessary to repeatedly dispense QIC in long-term assays.

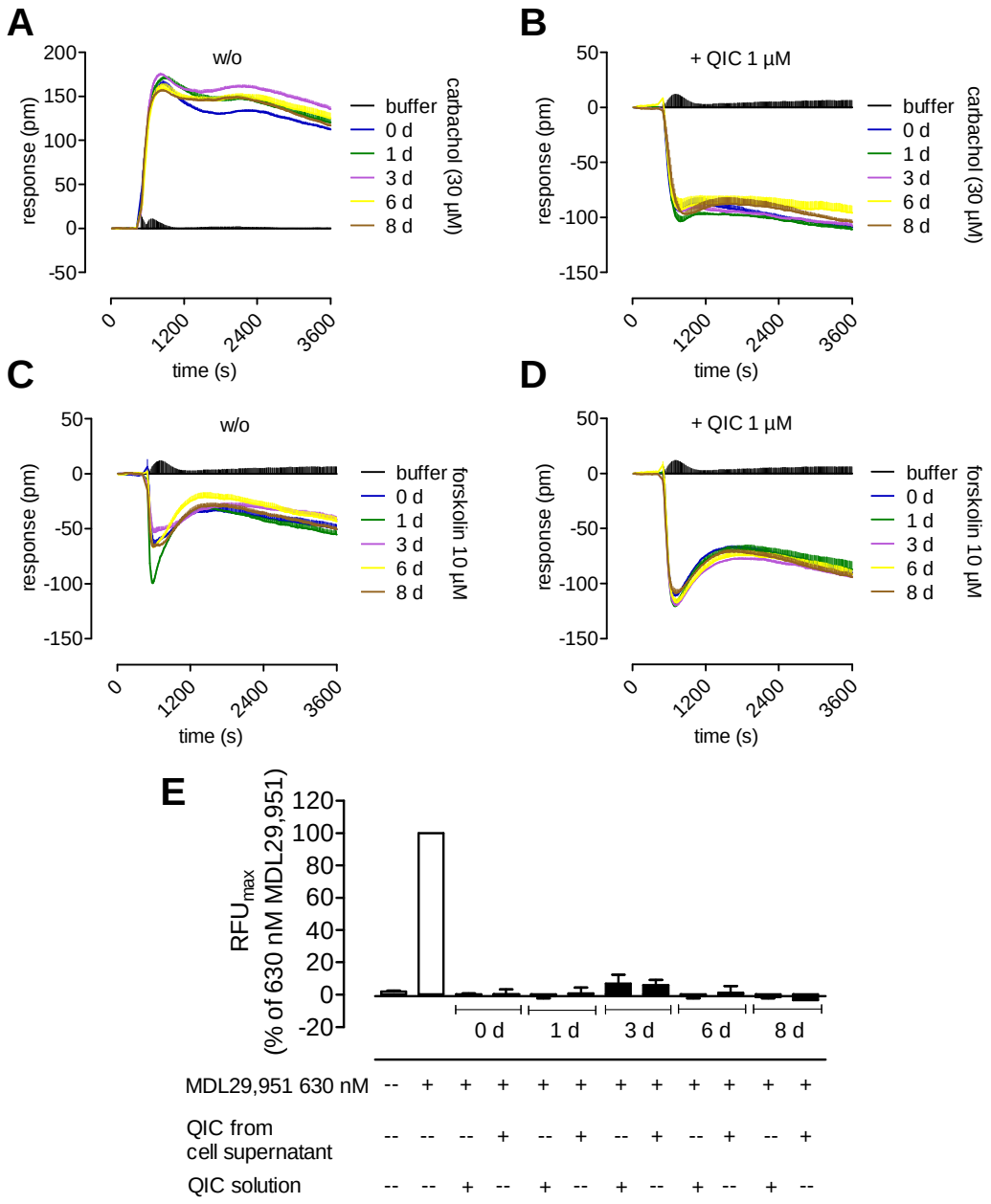

Figure 32: QIC activity was stable over a period of up to eight days in DMR and calcium mobilization assays.

(**A**)+(**C**) CHO-M1 cells were preincubated with assay buffer collected from day zero to day eight. M1 receptors were activated with 30 µM carbachol (**A**) or the direct adenylylcyclase activator forskolin (**C**) and wavelength shift was detected over time.

(**B**)+(**D**) CHO-M1 cells were pretreated with QIC solutions in assay buffer (final concentration1 µM) collected from day zero to day eight and stimulated with carbachol.(**B**) or forskolin (**D**). Wavelength shift was monitored as a measure of receptor activation.

(**A**)-(**D**) Data are represented as means + SEM of one representative experiment.

(**E**) HEK-ratGPR17 cells were preincubated with a QIC solution or QIC from cell supernatant, stimulated with the GPR17 agonist MDL29,951 (Hennen et al., 2013) and calcium mobilization was detected. Data shown are means + SEM of two independent experiments. Data were kindly provided by Dr. Stefanie Blättermann, Institute for Pharmaceutical Biology, University of Bonn, Germany.

3.2.3 Kinetic studies with QIC in a HEK and a CHO cell background

To explore the kinetic profile of QIC IP1 accumulation assays were performed in two commonly used cell lines. HEK293 cells endogenously expressing the muscarinic M3 receptor (**Fig. 33A**) and CHO cells stably transfected to express muscarinic M1 receptors (**Fig. 33B**) were preincubated for five to 15 min and then cells were stimulated with carbachol. The inhibitory effect seemed to occur a little bit faster in the HEK cells, because already after five minutes preincubation time IP1 production was reduced by approximately 80% whereas in the CHO cells it was just 20%. After 15 min pretreatment with QIC in both cell lines the IP1 levels were decreased close to 0%. These data indicate that QIC reliably silenced $G\alpha_q$-mediated signaling within 15 min in this second-messenger assay and therefore reached an inhibitory effect substantially faster than BIM-dimer and BIM-monomer (see chapter 3.1.12).

In order to facilitate comparison between the different assays types it was decided to work with a preincubation of 1 h in further second-messenger experiments.

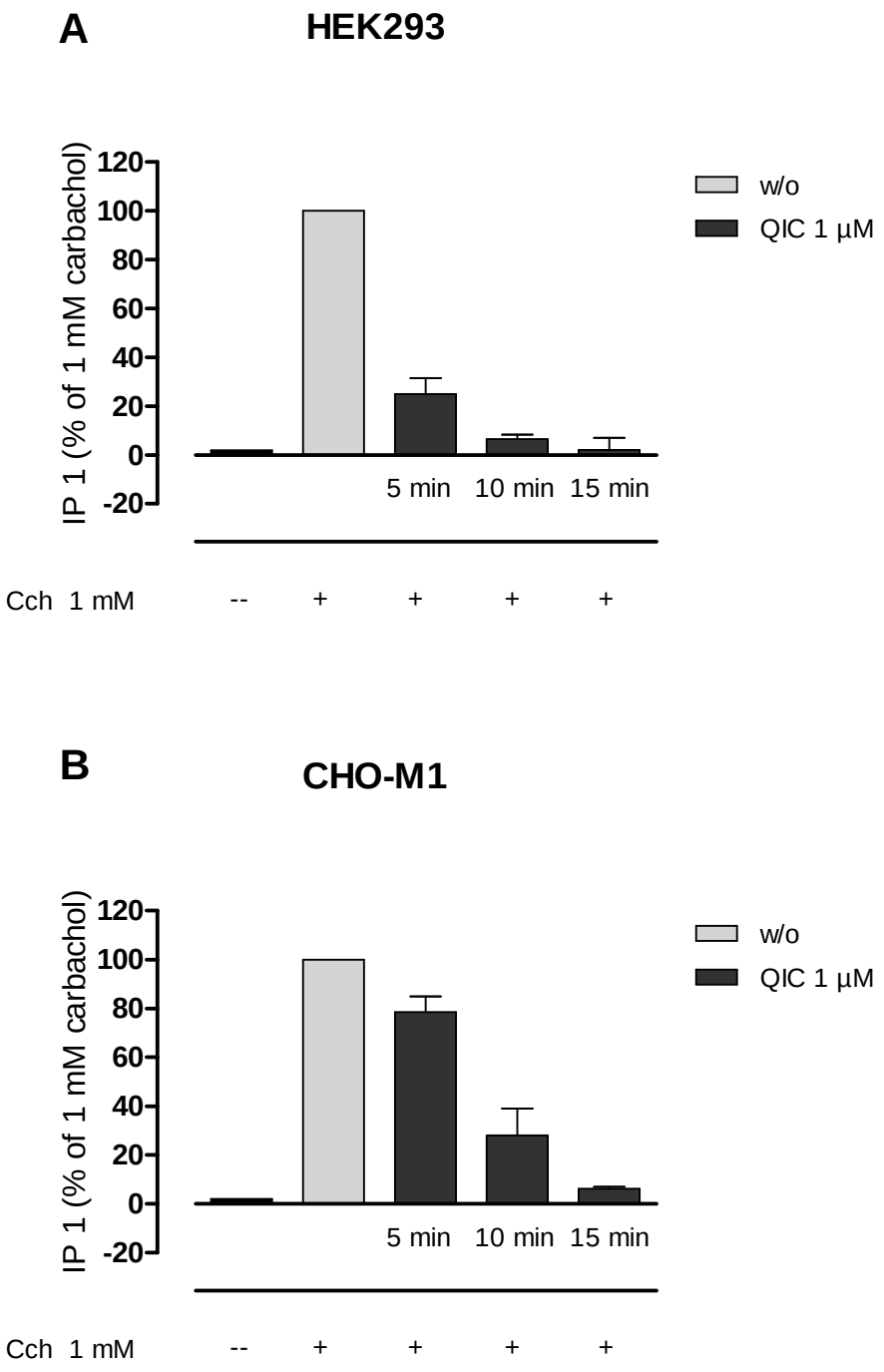

Figure 33: Analyzing the kinetic profile of QIC.
(**A**)-(**B**) HEK293 cells (**A**) and CHO-M1 cells (**B**) were pretreated with QIC (1 µM) for the indicated time periods. Then M3 or M1 receptors were stimulated with 1 mM carbachol and IP1 levels were determined. Data shown are means + SEM of at least three independent experiments, each conducted in triplicate.

3.2.4 Selectivity of QIC in second-messenger assays in a HEK cell background

In order to explore whether QIC specifically silences $G\alpha_q$-mediated signaling in second-messenger assays IP1 and cAMP levels were determined in the presence or absence of QIC. HEK293 cells were preincubated with various concentrations of QIC and endogenously expressed M3 receptors were stimulated with the synthetic muscarinic agonist carbachol. As depicted in **Figure 34A** 300 nM and 1 µM QIC were sufficient to silence IP1 production completely. 0.1 nM and 1 nM had no impact on IP1 accumulation and concentrations between 1 nM and 300 nM only partly affected the IP1 levels. Notably, in a concentration-dependent manner QIC decreased basal IP1 production which could be explained by the presence of constitutively active GPCRs in HEK293 cells coupling via $G\alpha_q$ proteins.

The effect of QIC on stimulating $G\alpha_s$ proteins was analyzed in HEK293 cells endogenously expressing $G\alpha_s$-linked EP2/4 receptors. Therefore, cells were preincubated with QIC in two different concentrations (0.3 µM and 1 µM) and after stimulation with prostglandin E_1 (PGE_1) cAMP levels were determined (**Fig. 34B**). cAMP production was completely unaffected by pretreatment with QIC.

Similar results were obtained in assays which detect the influence on $G\alpha_i$ proteins (**Fig. 34C**). In these assays HEK cells stably transfected to express $G\alpha_i$-sensitive CRTH2 receptors (CRTH2-HEK) were pretreated with QIC for 1 h and then stimulated with increasing concentrations of DK-PGD_2. There was still a strong cAMP reduction detectable indicating that QIC was not able to inhibit $G\alpha_i$-mediated signaling.

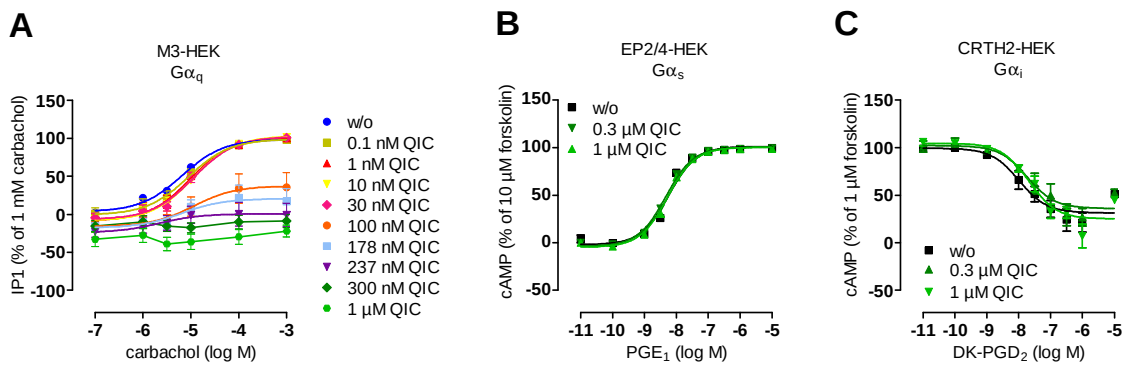

Figure 34: QIC exclusively inhibited signaling via $G\alpha_q$ proteins.
(**A**) HEK293 cells endogenously expressing $G\alpha_q$-mediated muscarinic M3 receptors were pretreated with increasing concentrations of QIC and concentration-response-curves were recorded after stimulation with carbachol. In higher concentrations QIC completely silenced signaling via $G\alpha_q$ proteins. pEC_{50}/E_{max} (w/o) = 5.18 ± 0.05/99%; pEC_{50}/E_{max} (0.1 nM QIC) = 5.05 ± 0.13/99%; pEC_{50}/E_{max} (1 nM QIC) = 5.02 ± 0.14/101%; pEC_{50}/E_{max} (10 nM QIC) = 4.95 ± 0.12/103%; pEC_{50}/E_{max} (30 nM QIC) = 4.95 ± 0.10/103%; pEC_{50}/E_{max} (100 nM QIC) = 4.95 ± 0.50/37%; pEC_{50}/E_{max} (178 nM QIC) = 5.19 ± 0.57/21%.
(**B**) QIC was not able to silence cAMP signaling of the $G\alpha_s$-sensitive EP2/4 receptors in HEK293 cells. pEC_{50} (w/o) = 8.25 ± 0.05; pEC_{50} (0.3 µM QIC) = 8.34 ± 0.03; pEC_{50} (1 µM QIC) = 8.28 ± 0.04.
(**C**) Signaling via $G\alpha_i$ proteins was detected with cAMP accumulation assays and QIC showed no inhibitory effect on $G\alpha_i$-sensitive CRTH2 receptors. pEC_{50} (w/o) = 7.99 ± 0.21; pEC_{50} (0.3 µM QIC) = 7.73 ± 0.21; pEC_{50} (1 µM QIC) = 7.69 ± 0.17.
(**A**)-(**C**) All data are means ± SEM of three to eight independent experiments, each conducted in triplicate.

3.2.5 BRET assays revealed QIC as selective inhibitor of $G\alpha_q$ and $G\alpha_{11}$ proteins

With the following experiments it was analyzed whether QIC was specific to silence $G\alpha_q$ subunits in bioluminescence energy transfer (BRET) assays. In a first approach $logIC_{50}$ value of QIC for this assay system was determined (**Fig. 35**). Therefore HEK293 cells were transfected to coexpress h-Flag-AT1 receptor, the energy donor $G\alpha_q$-*R*LucII and the energy acceptor $G\gamma_1$-GFP[10]. AT1 receptors were stimulated with angiotensin II (5 min) after a preincubation with increasing concentrations of QIC (30 min). With low QIC concentrations up to 0.1 nM a substantial agonist-promoted decrease in BRET was recorded which was completely blunted at a concentration of 0.1 µM QIC (pIC_{50} = 8.50 ± 0.09). This BRET decrease reflected the separation of the Gα-helical domain from the N terminus of Gγ which then enables GDP exit and GTP entry (Galés et al., 2006; Saulière et al., 2012) and was blocked concentration-dependent due

to pretreatment with QIC. Based on these findings further BRET experiments were performed after preincubation with 0.1 µM QIC for 30 min.

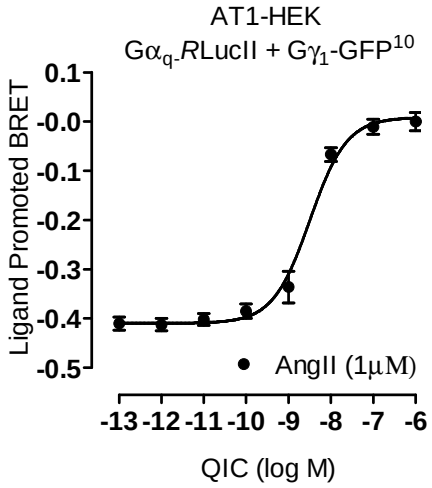

Figure 35: QIC blunted AT1-mediated BRET decrease in a concentration-dependent manner.
HEK293 cells transiently expressed h-Flag-AT1 receptor, $G\alpha_q$-*R*LucII and $G\gamma_1$-GFP^{10} and opening of the nucleotide binding pocket could be detected as BRET decrease after receptor activation (5 min, 1 µM angiotensin II) but was blocked after pretreatment with QIC for 30 min (pIC_{50} 8.50 ± 0.09). Presented data are means ± SEM of seven independent experiments. Data were kindly provided by Sylvain Armando, Division of Endocrinology and Metabolism, Department of Medicine, Montreal, Canada.

As depicted in **Figure 36** the inhibitory effect of QIC was investigated using several Gα subunits. First, two members of the $G\alpha_q$ family, $G\alpha_q$ (**Fig. 36A**) and $G\alpha_{11}$ (**Fig. 36B**), were investigated. Therefore, HEK293 cells were forced to express transiently AT1 receptor, energy donor $G\alpha_q$-*R*LucII (**Fig. 36A**) or $G\alpha_{11}$-*R*Luc8 (**Fig. 36B**) and energy acceptor $G\gamma_1$-GFP^{10} or $G\gamma_2$-GFP^{10}. Preincubation with QIC blunted AT1-mediated BRET decrease via $G\alpha_q$ and $G\alpha_{11}$ subunits. $G\alpha_s$ signaling was analyzed expressing the $G\alpha_s$-*R*LucII sensor as energy donor, $G\gamma_1$-GFP^{10} as energy acceptor (**Fig. 36C**). Human vasopressin2 (V2) receptors were stimulated with vasopressin (AVP) and concentration-dependent BRET decrease was detectable which was regardless of QIC pretreatment. The three Gα subunits $G\alpha_{i1}$, $G\alpha_{i2}$ and $G\alpha_{i3}$ were studied by transfecting $G\alpha_{i1}$-*R*LucII (**Fig. 36D**), $G\alpha_{i2}$-*R*LucII (**Fig. 36E**) or $G\alpha_{i3}$-*R*LucII (**Fig. 36F**) as energy donor together with $G\gamma_2$-GFP^{10} as energy acceptor. $G\alpha_i$ signaling was recorded using angiotensin II and its transiently expressed target receptor AT1 but pretreatment with QIC did not inhibit AT1-$G\alpha_i$ activation. $G\alpha_{oA}$-*R*Luc8 (**Fig. 36G**) and $G\alpha_{oB}$-*R*Luc8 (**Fig. 36H**) were used as energy donors to explore Myc-α2c-mediated BRET decrease triggered with UK-14304 as an agonist and $G\gamma_2$-GFP^{10} as energy acceptor but BRET decrease was insensitive to

QIC pretreatment. It was possible to record an angiotensin II-promoted decrease in BRET in cells transiently expressing AT1 receptor, $G\alpha_{12}$-*R*LucII as energy donor and $G\gamma_1$-GFP[10] as energy acceptor (**Fig. 36I**) which was unaltered after preincubation with QIC. $G\alpha_{13}$ signaling was analyzed expressing the $G\alpha_{13}$-*R*Luc8 sensor as energy donor, $G\gamma_2$-GFP[10] as energy acceptor (**Fig. 36J**). Thromboxane TPα receptors were stimulated with its ligand U-46619 and concentration-dependent BRET decrease was detectable which was regardless of QIC pretreatment.

In summary, QIC selectively silenced ligand promoted BRET via $G\alpha_q$ and $G\alpha_{11}$ proteins which was also in line with the findings for YM of Nishimura et al in 2010 because they found out that Gα residues directly interacting with the inhibitor YM were completely conserved in $G\alpha_q$, $G\alpha_{11}$ and $G\alpha_{14}$ proteins but not in other Gα members. The BRET assays were performed to gain a deeper insight into the specificity of QIC within the family members of the four main G protein subclasses. Nishimura et al. investigated the selectivity of QIC with [^{35}S]GTPγS binding assays using purified $G\alpha_q$, $G\alpha_s$, $G\alpha_{i1}$, $G\alpha_o$ and $G\alpha_{13}$ proteins (Nishimura et al., 2010). The BRET constructs enabled exploring of inhibitory effects on further members of the G protein subclasses. Thus, it was possible to distinguish between $G\alpha_q$ and $G\alpha_{11}$-mediated signaling and it could be clearly shown that QIC inhibits both Gα subunits equally. Experiments with $G\alpha_{i2}$, $G\alpha_{i3}$ and $G\alpha_{12}$ proteins were lacking and their investigation in BRET assays revealed that QIC does not interfere with these Gα subunits.

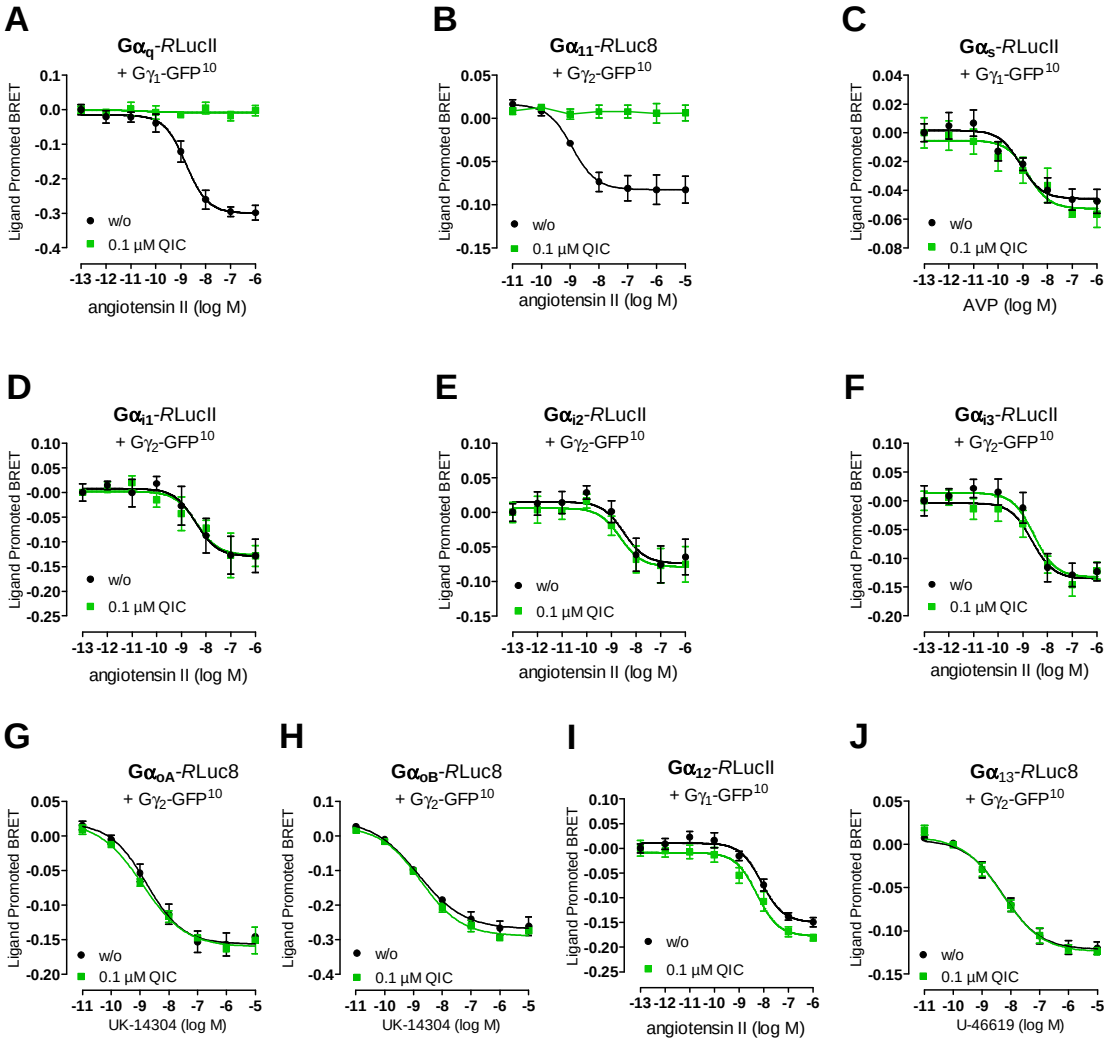

Figure 36: BRET assays revealed QIC as selective inhibitor of $G\alpha_q$ and $G\alpha_{11}$ proteins.

(**A**)-(**B**) HEK293 cells were transiently transfected to coexpress $G\alpha_q$-*R*LucII + $G\gamma_1$-GFP^{10} (pEC_{50} (w/o) = 8.79 ± 0.14) (**A**) or $G\alpha_{11}$-*R*Luc8 + $G\gamma_2$-GFP^{10} (pEC_{50} (w/o) = 8.94) (**B**) and AT1 receptor. Opening of the nucleotide binding pocket was detected as BRET decrease which was completely blocked after QIC pretreatment.

(**C**) $G\alpha_s$-*R*LucII + $G\gamma_1$-GFP^{10} were expressed together with the $G\alpha_s$-sensitive V2 receptor and recorded BRET decrease was unaffected by QIC preincubation. pEC_{50} (w/o) = 9.09 ± 0.29; pEC_{50} (0.1 µM QIC) = 8.79 ± 0.38.

(**D**)-(**F**) BRET between $G\alpha_{i1}$-, $G\alpha_{i2}$, $G\alpha_{i3}$-*R*LucII and $G\gamma_2$-GFP^{10} was determined using angiotensin II with its target receptor AT1 and was insensitive to QIC pretreatment. pEC_{50} (w/o) = 8.42 ± 0.41; pEC_{50} (0.1 µM QIC) = 8.39 ± 0.37 (**D**). pEC_{50} (w/o) = 8.50 ± 0.44; pEC_{50} (0.1 µM QIC) = 8.65 ± 0.42 (**E**). pEC_{50} (w/o) = 8.56 ± 0.29; pEC_{50} (0.1 µM QIC) = 8.63 ± 0.27 (**F**).

(**G**)-(**H**) QIC did not block molecular rearrangement of activated $G\alpha_{oA}$ or $G\alpha_{oB}$. BRET decrease was measured after α2c activation in HEK293 cells transfected to express $G\alpha_{oA}$*R*Luc8 + $G\gamma_2$-GFP^{10} or $G\alpha_{oB}$-*R*Luc8 + $G\gamma_2$-GFP^{10}. pEC_{50} (w/o) = 8.77 ± 0.20; pEC_{50} (0.1 µM QIC) = 8.92 ± 0.15 (**G**). pEC_{50} (w/o) = 8.84 ± 0.17; pEC_{50} (0.1 µM QIC) = 8.74 ± 0.11 (**H**).

(**I**) HEK293 cells were transiently transfected to coexpress $G\alpha_{12}$-*R*LucII + $G\gamma_1$-GFP^{10} and as well as AT1 receptor. Opening of the nucleotide binding pocket was detected as BRET decrease which was unaltered after QIC pretreatment. pEC_{50} (w/o) = 8.09 ± 0.13; pEC_{50} (0.1 µM QIC) = 8.28 ± 0.17.
(**J**) $G\alpha_{13}$-*R*Luc8 + $G\gamma_2$-GFP^{10} were expressed together with the $G\alpha_{13}$-sensitive TP α receptor. The recorded BRET decrease was unaffected by QIC preincubation. pEC_{50} (w/o) = 8.27 ± 0.14; pEC_{50} (0.1 µM QIC) = 8.29 ± 0.13.
(**A**)-(**J**) Data shown are means ± SEM of at least three independent experiments. Data were kindly provided by Sylvain Armando (**A**), (**C**)-(**F**), (**I**), Division of Endocrinology and Metabolism, Department of Medicine, Montreal, Canada and Ségolène Galandrin (**B**), (**G**)+(**H**), (**J**), Institut des Maladies Métaboliques et Cardiovasculaires, Institut National de la Santé et de la Recherche Médicale, Université Toulouse III, France.

3.2.6 Analyzing the inhibitory profile of QIC in label-free assays

Since QIC exclusively silenced signaling via $G\alpha_q$ (and $G\alpha_{11}$, a member of the G_q-family) in second-messenger and BRET studies it was the aim to analyze the effect of QIC on the four main Gα protein subclasses in two label-free assay systems: Dynamic mass redistribution and impedance.

3.2.6.1 Dynamic mass redistribution

QIC was analyzed according to its ability to influence $G\alpha_s$, $G\alpha_i$, dual $G\alpha_{q/i}$ and $G\alpha_{12/13}$-mediated signaling in dynamic mass redistribution (DMR) assays using the Epic system. Therefore HEK293 cells endogenously expressing EP2/4 receptors were chosen to study the influence of QIC on signaling via $G\alpha_s$ proteins (**Fig. 37A**). Prior to the assay cells were seeded into biosensor microplates as described in section 2.2.3.3. Cells were preincubated with 0.3 µM or 1 µM QIC for 1 h and challenged with 100 nM PGE_1 and the DMR response was recorded. The results show that the PGE_1-mediated cell response was not affected by QIC pretreatment but a preincubation with cholera toxin (CTX) (16-20 h) to mask $G\alpha_s$ signaling was able to inhibit signaling of the $G\alpha_s$-sensitive EP2/4 receptors. $G\alpha_i$ signaling was investigated using HEK cells stably transfected to express CRTH2 receptors which are coupling via $G\alpha_i$ proteins (**Fig. 37B**). Cells were pretreated with QIC or the $G\alpha_i$ inhibitor pertussis toxin (PTX) (16-18 h) and challenged with the CRTH2 agonist DK-PGD_2 (100 nM). PTX inhibited signaling of the $G\alpha_i$-sensitive CRTH2 receptor but the cell response was completely unaffected by QIC pretreatment. Next, FFA1-HEK cells stably transfected to express the FFA1 receptor, a dual $G\alpha_{q/i}$ coupling receptor, were analyzed (**Fig. 37C**). Cells were preincubated with QIC, PTX or a combination of both before cells were challenged with the FFA1 agonist

TUG424 (3 µM) (Schmidt et al., 2011). PTX reduced the cell response from 300 pm to about 200 pm, QIC decreased the wavelength shift from 300 pm to about 50 pm but a combination of PTX and QIC completely blocked dual FFA1-mediated signaling. To explore the influence of QIC on the signaling of the fourth Gα family member $G\alpha_{12/13}$, HEK cells stably transfected to express GPR55, a GPCR with exclusive bias toward the $G\alpha_{12/13}$ pathway (Ryberg et al., 2007; Henstridge et al., 2009; Ross, 2009), were challenged with lysophosphatidylinositol (LPI) after pretreatment with QIC (**Fig 37D**). Due to the fact that a specific $G\alpha_{12/13}$ inhibitor is not available to date cells were pretreated with the pan-G protein activator aluminum fluoride (AlF_4^-) to underline that the GPR55 trace was mediated via G proteins. The GPR55-mediated cell response was insensitive to a QIC pretreatment but was silenced after a preincubation with AlF_4^-.

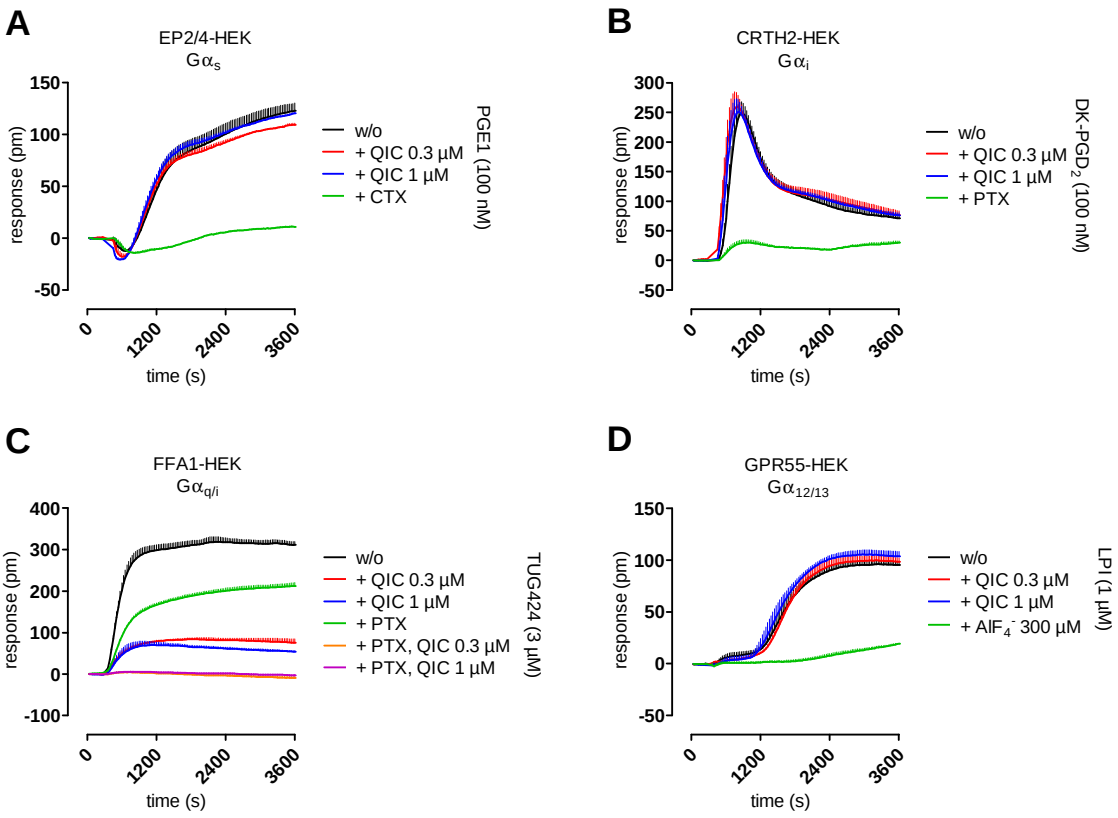

Figure 37: Dynamic mass redistribution revealed QIC as selective inhibitor of $G\alpha_q$ signaling.
(**A**) HEK293 cells endogenously expressing EP2/4 receptors were challenged with 100 nM PGE_1. Pretreatment of cells with CTX (200 ng/ml) inhibited signaling of the $G\alpha_s$-sensitive EP2/4 receptors whereas wavelength shift was unaffected by pretreatment with QIC.
(**B**) HEK293 cells stably expressing CRTH2 were treated with the agonist DK-PGD_2 to visualize $G\alpha_i$-mediated signaling. Pretreatment with QIC showed no inhibitory effect but PTX (50 ng/ml) silenced $G\alpha_i$ signaling.
(**C**) The cell response obtained with the FFA1 agonist TUG424 in stable FFA1-HEK cells was partly sensitive to PTX (50 ng/ml) or QIC pretreatment but completely silenced in the presence of a combination of PTX and QIC. For receptor expression cells were treated with 1 µg/ml doxycycline (16 h).
(**D**) Stable GPR55-HEK cells were challenged with the GPR55 agonist LPI. LPI-mediated wavelength shift was not blunted by pretreatment with QIC but was sensitive to preincubation with the pan-G protein activator AlF_4^- (300 µM).
(**A**)-(**D**) Data shown are representative data (means + SEM) of at least three independent experiments, each performed in triplicate.

With further experiments it should be investigated whether QIC was functional on every cell line analyzed in **Figure 37** and whether PTX and CTX were specific to silence $G\alpha_i$ or $G\alpha_s$ proteins, respectively. Therefore HEK293 (**Fig 38A**) and CRTH2-HEK (**Fig. 38B**) cells were challenged with ATP to stimulate $G\alpha_q$-sensitive P2Y receptors. Pretreatment with QIC completely blocked the cell response whereas preincubation

with CTX had no effect on the $G\alpha_q$-mediated trace. These findings underlined that QIC was a selective inhibitor for the $G\alpha_q$ pathway with a proper functionality in both cell lines and PTX exclusively silenced $G\alpha_i$ proteins and did not affect cell viability. In FFA1-HEK cells the functionality of QIC and PTX was already proven with the experiments in **Figure 38C** but it should be analyzed whether QIC and PTX were specific to silence $G\alpha_q$ and $G\alpha_i$ proteins in this cell line without a negative influence on cell viability. Therefore, $G\alpha_s$-mediated signaling via endogenously expressed EP2/4 receptors (**Fig. 38C**) was investigated. GPR55-HEK cells endogenously expressing muscarinic M3 receptors were treated with carbachol after a preincubation with QIC or AlF_4^- (**Fig. 38D**). Also in this cell line QIC was functional to silence $G\alpha_q$ signaling and pretreatment with AlF_4^- showed that the detected cell response was mediated via G proteins.

In summary, QIC selectively silenced signaling via $G\alpha_q$ proteins in DMR comparable to the well-known $G\alpha_q$ inhibitor YM (Schröder et al., 2010).

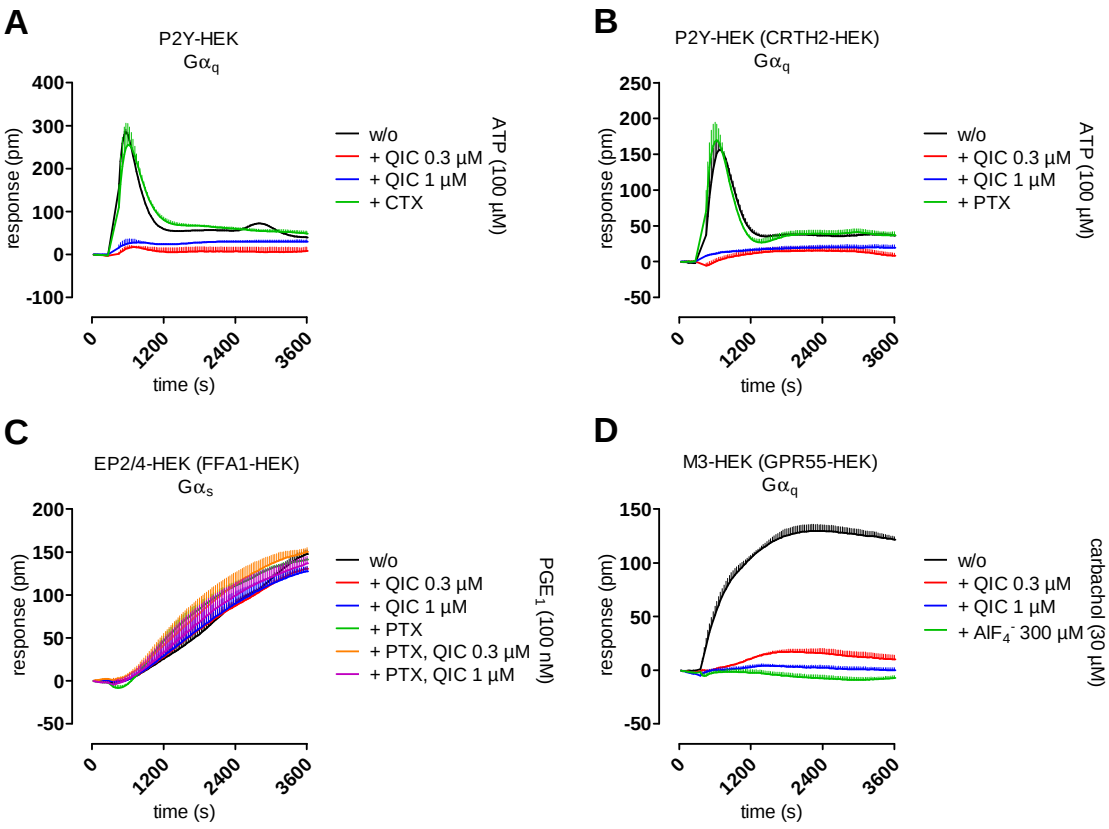

Figure 38: $G\alpha_q$ signaling was selectively blocked after QIC preincubation and PTX or CTX pretreatment was specific for $G\alpha_i$ or $G\alpha_s$, respectively.
(**A**)-(**B**) HEK293 and CRTH2-HEK cells endogenously expressing $G\alpha_q$-sensitive P2Y receptors were challenged with ATP. Pretreatment with QIC blocked $G\alpha_q$ signaling but CTX had no effect on the cell response.
(**C**) FFA1-HEK cells endogenously expressing $G\alpha_s$-sensitive EP2/4 receptors were challenged with PGE_1. Cell responses were insensitive to QIC, PTX or a combination of QIC and PTX.
(**D**) GPR55-HEK cells endogenously expressing M3 receptors were stimulated with carbachol. Wavelength shift was silenced by QIC and pan-G protein activator AlF_4^- pretreatment.
(**A**)-(**D**) Data shown are representative data (means + SEM) of at least three independent experiments, each performed in triplicate.

3.2.6.2 Impedance

QIC was analyzed according to its ability to influence $G\alpha_s$, $G\alpha_i$, dual $G\alpha_{q/i}$ and $G\alpha_{12/13}$-mediated signaling with a second label-free technology, detecting changes in impedance assays with the CellKey system. HEK293 cells endogenously expressing $G\alpha_s$-sensitive EP2/4 receptors were challenged with PGE_1 after a preincubation with QIC or CTX (**Fig. 39A**). PGE_1-triggerd cell response was blocked by CTX but was insensitive to QIC pretreatment. To study the effect of QIC on the $G\alpha_i$ pathway CRTH2-HEK cells were treated with the specific agonist DK-PGD2 (**Fig. 39B**). The detected wavelength shift could be silenced with a PTX pretreatment but was unaffected by QIC preincubation. Next, HEK cells stably transfected to express the FFA1 receptor (FFA1-HEK), a receptor with dual $G\alpha_{q/i}$ protein coupling, were investigated (**Fig. 39C**). Cells were preincubated with QIC, PTX or a combination of both before cells were challenged with the FFA1 agonist TUG424 (3 µM). PTX or QIC alone only diminished the cell response but a combination of PTX and QIC completely blocked dual FFA1-mediated signaling.

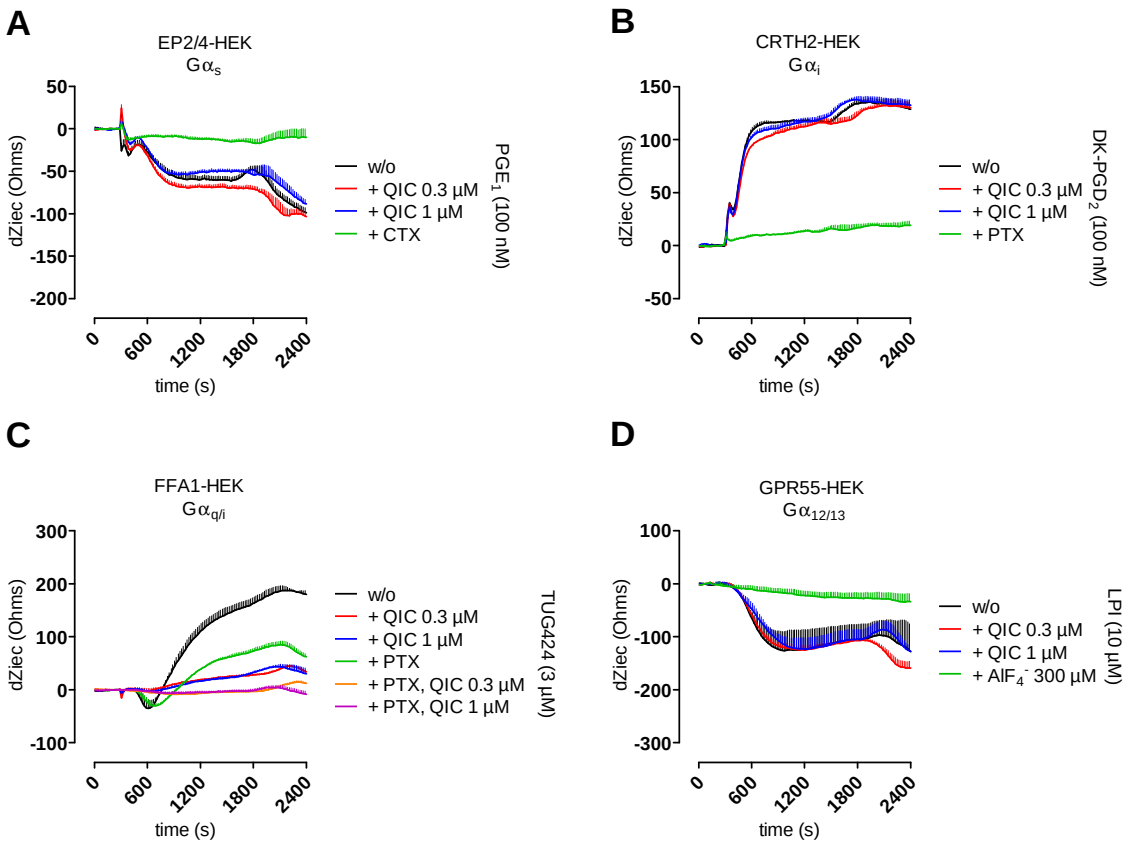

Figure 39: Impedance measurements revealed QIC as a selective inhibitor of $G\alpha_q$ signaling.

(**A**) HEK293 cells endogenously expressing EP2/4 receptors were challenged with 100 nM PGE_1. Pretreatment of cells with CTX (100 ng/ml) inhibited signaling of the $G\alpha_s$-sensitive EP2/4 receptors whereas changes in impedance were unaffected by pretreatment with QIC.

(**B**) HEK293 cells stably expressing CRTH2 were treated with the agonist DK-PGD_2 to visualize $G\alpha_i$-mediated signaling. Pretreatment with QIC showed no inhibitory effect but PTX (50 ng/ml) silenced $G\alpha_i$ signaling.

(**C**) The cell response obtained with the FFA1 agonist TUG424 in stable FFA1-HEK cells was partly sensitive to PTX (50 ng/ml) or QIC pretreatment but completely silenced in the presence of a combination of PTX and QIC. For receptor expression cells were treated with 1 µg/ml doxycycline for 16 h.

(**D**) Stable GPR55-HEK cells were challenged with the GPR55 agonist LPI. LPI-mediated changes in impedance were not blunted by pretreatment with QIC but were sensitive to preincubation with the pan-G protein activator AlF_4^- (300 µM).

(**A**)-(**D**) Data shown are representative data (means + SEM) of at least three independent experiments, each performed in triplicate.

With the following experiments it should be investigated whether QIC was functional on every cell line analyzed in **Figure 39** and whether PTX and CTX were specific to silence $G\alpha_i$ or $G\alpha_s$ proteins, respectively. Therefore HEK293 (**Fig 40A**) and CRTH2-HEK (**Fig. 40B**) cells were challenged with carbachol to stimulate $G\alpha_q$-sensitive M3 receptors. Pretreatment with QIC completely blocked the cell response whereas preincubation with CTX had no effect on the $G\alpha_q$-mediated trace. These findings underline that QIC is a selective inhibitor for the $G\alpha_q$ pathway with a proper functionality in both cell lines and CTX exclusively masked $G\alpha_s$ proteins without a negative effect on cell viability. In FFA1-HEK cells the functionality of QIC and PTX was already proven with the experiments in **Figure 39C** but it should be analyzed whether QIC and PTX were specific to silence $G\alpha_q$ and $G\alpha_i$ proteins in this cell line and that detected effects were not due to negative effects on cell viability. $G\alpha_s$-mediated signaling via endogenously expressed β2 receptors (**Fig. 40C**) was detected and the cell response was comparable between different pretreatments. GPR55-HEK cells endogenously expressing muscarinic M3 receptors were treated with carbachol after a preincubation with QIC or AlF_4^- (**Fig. 40D**). QIC was functional in this cell line to silence $G\alpha_q$ signaling and pretreatment with AlF_4^- revealed that the detected cell response was mediated via G proteins.

Taken together, experiments determining changes in impedance revealed QIC as a selective $G\alpha_q$ inhibitor equivalent to the results obtained in DMR assays (see chapter 3.2.6.1). These data were very valuable because both label-free technologies detect an overall cellular response capturing cellular events downstream of the GPCR (Kenakin, 2009, Fang et al., 2006; Fang et al., 2007) whereas traditional second-messenger assays only partially determine the overall response (Schröder et al., 2010).

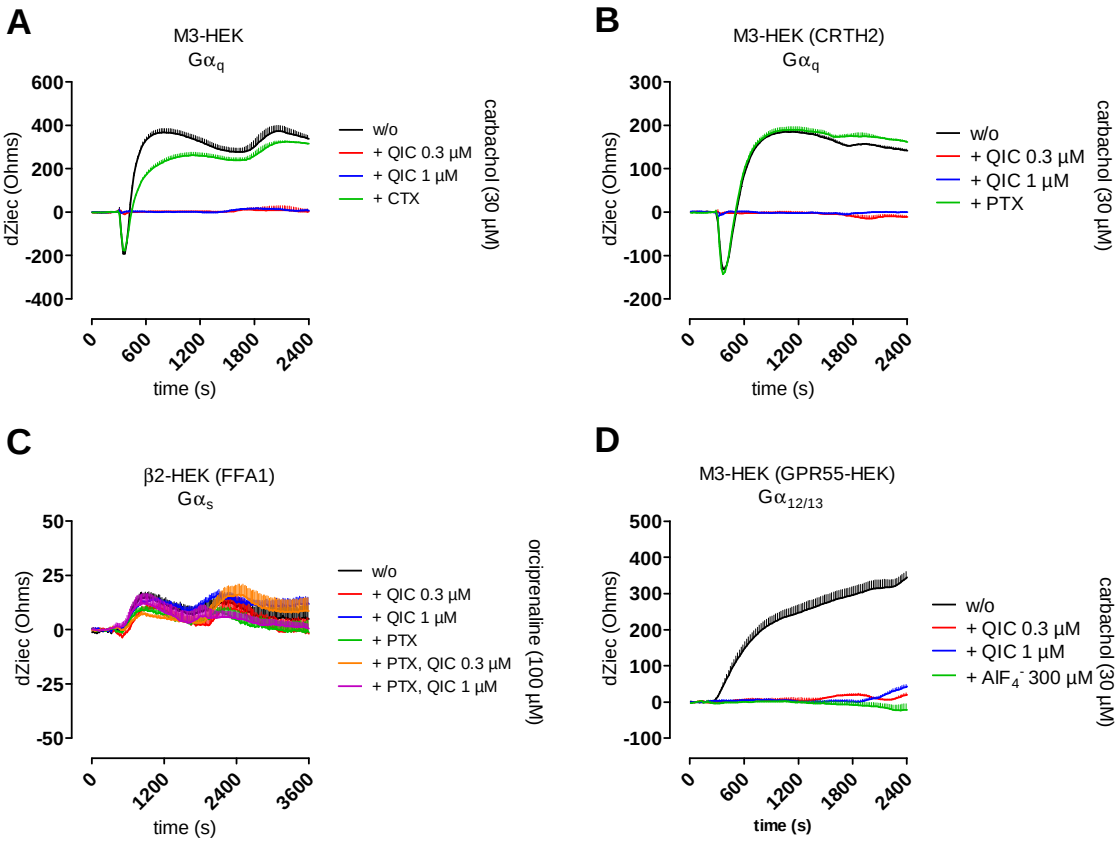

Figure 40: QIC showed functionality on all utilized cell lines and PTX or CTX pretreatment was specific for $G\alpha_i$ or $G\alpha_s$, respectively.
(**A**)-(**B**) HEK293 and CRTH2-HEK cells endogenously expressing $G\alpha_q$-sensitive M3 receptors were challenged with carbachol. Pretreatment with QIC blocked $G\alpha_q$ signaling but CTX had no effect on the cell response.
(**C**) FFA1-HEK cells endogenously expressing $G\alpha_s$-sensitive β2 receptors were challenged with orciprenaline (100 µM). Cell responses were insensitive to preincubation with QIC, PTX or a combination of QIC and PTX.
(**D**) GPR55-HEK cells endogenously expressing M3 receptors were stimulated with carbachol. Wavelength shift was silenced by QIC and pan-G protein activator AlF_4^- pretreatment.
(**A**)-(**D**) Presented data are representative data (means + SEM) of at least three independent experiments, each performed in triplicate.

3.2.7 Characterizing the influence of QIC in the patient-derived MZ7 cells

Due to the fact that BIM-dimer worked as selective $G\alpha_q$ inhibitor in a HEK cell background but silenced $G\alpha_q$, $G\alpha_s$ and $G\alpha_i$ proteins in the patient-derived cancer cell line MZ7 it was also of interest to analyze QIC in this melanoma cell line.

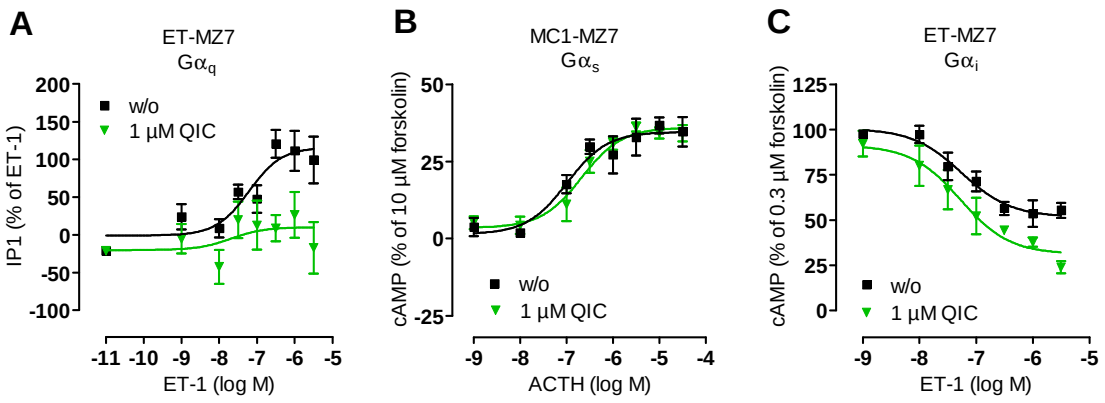

Figure 41: QIC exclusively inhibited $G\alpha_q$-mediated IP1 production in MZ7 cells.
(**A**) QIC completely blunted IP1 accumulation triggered with ET-1 via endogenously expressed endothelin receptors. pEC_{50} (w/o) = 7.21 ± 0.31.
(**B**) $G\alpha_s$-mediated cAMP production induced via ACTH and its cognate $G\alpha_s$-linked and endogenously expressed MC1 receptor was insensitive to QIC pretreatment. pEC_{50} (w/o) = 6.99 ± 0.21; pEC_{50} (QIC) = 6.68 ± 0.15.
(**C**) cAMP reduction via endogenously expressed endothelin receptors using $G\alpha_i$ proteins was unaffected by QIC preincubation. pEC_{50} (w/o) = 7.26 ± 0.21; pEC_{50} (QIC) = 7.28 ± 0.25.
(**A**)-(**C**) Data shown are means ± SEM of at least three independent experiments, each conducted in triplicate. Data were kindly provided by Ramona Schrage, Pharmacology and Toxicology Section, Institute of Pharmacy, University of Bonn, Germany.

To explore $G\alpha_q$ dependent signaling IP1 accumulation was determined in the presence or absence of QIC using endogenously expressed endothelin receptors (**Fig. 41A**). ET-1-mediated IP1 production was completely silenced after preincubation with 1 µM QIC. Furthermore, QIC pretreatment prevented IP1 production triggered with the pan-G protein activator AlF_4^- (**Fig 42**) which underlined that QIC inhibition occurred specifically at the level of G proteins.

The influence of QIC on the $G\alpha_s$ und $G\alpha_i$ pathway was investigated by determining changes in cAMP levels. After a preincubation with QIC MZ7 cells were stimulated with the adrenocorticotropic hormone (ACTH), an agonist for the $G\alpha_s$-sensitive melanocortin1 (MC1) receptor. cAMP accumulation was unaffected by QIC

pretreatment (**Fig. 41B**). Endogenous ET-1 receptors were stimulated with endothelin to verify the effect of QIC on $G\alpha_i$ dependent signaling (**Fig 41C**). The results indicate that $G\alpha_i$ coupling of ET-1 receptors in a MZ7 cell background was insensitive to QIC. Together, QIC was specific to silence $G\alpha_q$ proteins in this cancer cell line.

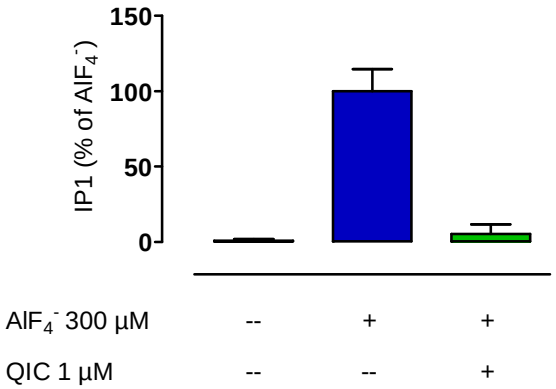

Figure 42: QIC blocked AlF_4^- triggered IP1 accumulation in MZ7 cells.
MZ7 cells were stimulated with the pan-G protein activator AlF_4^- and in the presence of QIC IP1 accumulation was completely blocked. Data shown are means + SEM of at least three independent experiments, each conducted in triplicate. Data were kindly provided by Ramona Schrage, Pharmacology and Toxicology Section, Institute of Pharmacy, University of Bonn, Germany.

3.2.8 Selectivity of QIC in second-messenger assays in CHO cells

A large number of different experiments performed in HEK and MZ7 cells revealed QIC as a selective tool to silence $G\alpha_q$-mediated signaling. Regarding the fact that CHO cells represent a commonly used cell line together with the plan to perform radioligand competition binding studies in this cellular background the selectivity of QIC should be additionally analyzed in CHO cells. After a preincubation with QIC for 1 h IP1 production mediated via stably expressed muscarinic M1 receptors was completely blocked (**Fig. 43A**). $G\alpha_s$ and $G\alpha_i$ signaling was determined using endogenously expressed $G\alpha_s$-sensitive EP2/4 receptors (**Fig. 43B**) and $G\alpha_i$-sensitive serotonin receptors (**Fig. 43C**) but cAMP production was unaffected by a preincubation with QIC.

These results were in line with the findings in other cellular backgrounds and therefore CHO cells were a suitable cell line for binding experiments.

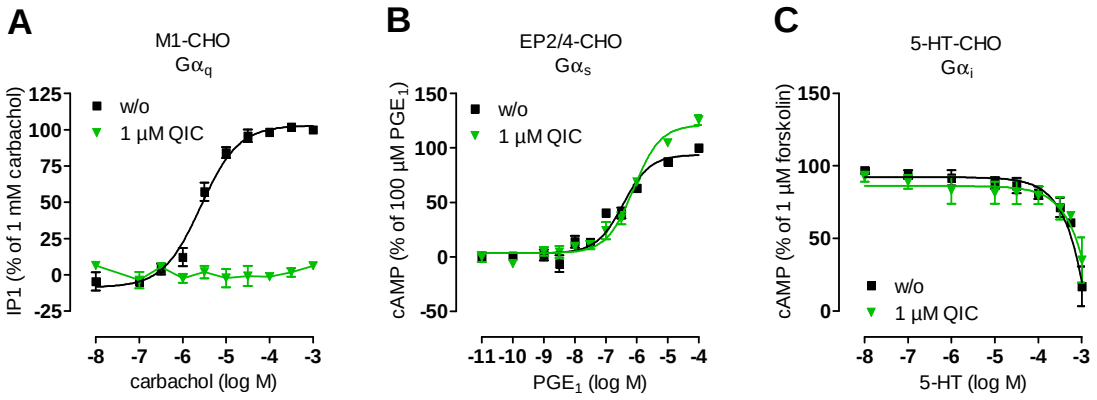

Figure 43: QIC exclusively inhibited signaling via $G\alpha_q$ proteins in CHO cells
(**A**) QIC blunted $G\alpha_q$ signaling of the muscarinic M1 receptor stably transfected in CHO cells in IP1 accumulation assays. pEC_{50} (w/o) = 5.58 ± 0.07.
(**B**) cAMP levels were detected to analyze the influence of QIC on endogenous $G\alpha_s$-coupled EP2/4 receptors. QIC did not diminish signaling of this pathway. pEC_{50} (w/o) = 6.44 ± 0.09; pEC_{50} (1 µM QIC) = 6.11 ± 0.07
(**C**) To explore the effect of QIC on $G\alpha_i$ proteins, endogenous $G\alpha_i$-coupled serotonin (5-HT) receptors were stimulated with serotonin in the presence or absence of QIC. QIC showed no inhibitory effect on the $G\alpha_i$ pathway.
(**A**)-(**C**) Presented data are means ± SEM of at least three independent experiments, each performed in triplicate.

3.2.9 Analyzing QIC in radioligand competition binding assays

QIC silenced $G\alpha_q$ signaling in different cellular environments and it should be investigated whether QIC could interfere with the agonist binding. In a control experiment it was tested whether QIC had an influence on the antagonist recognition of the muscarinic M1 receptor (**Fig. 44A**). The results depict that QIC did not interfere with antagonist recognition. Next, whole CHO-M1 cells were analyzed in radioligand competition assays using carbachol as a ligand (**Fig. 44B**). QIC did not impair carbachol displacement of the radio-antagonist [^{3}H]NMS. From these data one could conclude that the inhibition of $G\alpha_q$-mediated signaling was not due to QIC interference with agonist binding but with agonist function.

Due to the fact that the structure of QIC is quite similar to the structure of the well-known selective $G\alpha_q$ inhibitor YM one could assume the same mode of action. YM was recently described as a $G\alpha_q$-specific guanine nucleotide dissociation inhibitor (GDI) (Nishimura et al., 2010) in contrast to BIM-dimer which allowed GDP dissociation but prevented GTP entry (see chapter 3.1.8). Therefore, QIC was analyzed in radioligand binding studies with CHO-M1 cell membranes using [^{3}H]NMS as radio-antagonist to distinguish between these two mode of actions. CHO-M1 membranes were labelled with 0.2 nM [^{3}H]NMS and then increasing amounts of the M1 agonist carbachol were added. If QIC functions as GDI, it would disrupt the high-affinity agonist binding. **Figure 44C** shows binding data generated in the presence and absence of 1 µM QIC. In the absence of QIC one could detect high-affinity binding (51%) of carbachol to G protein-coupled GPCRs and low-affinity binding to uncoupled M1 receptors. If the cells were treated with QIC 35% of the high-affinity sites were converted to low-affinity sites (**Tab. 3**). Thus, QIC interferes with the high-affinity agonist binding but still 33% of the receptors remained in the high-affinity binding fraction. Based on these findings it is likely that QIC has the same mode of action as it was described for YM.

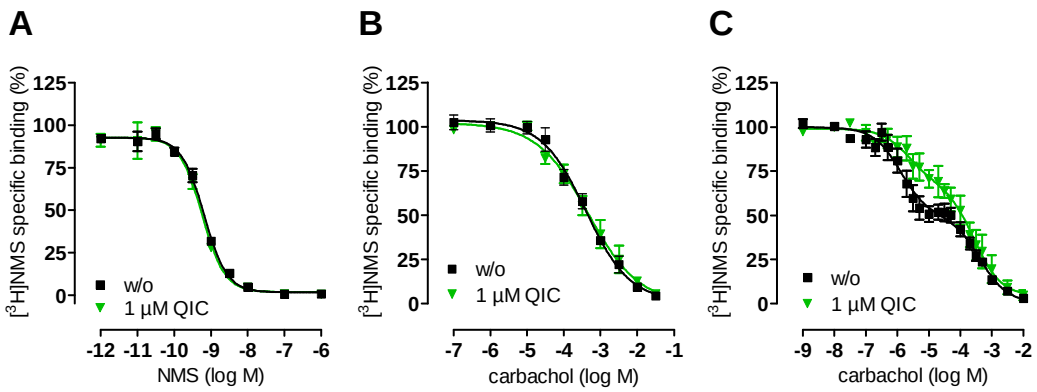

Figure 44: Effect of QIC on carbachol recognition of the muscarinic M1 receptor.
(**A**) CHO-M1 membranes were labelled with 0.2 nM [^{3}H]NMS and homologous competition experiments were conducted after a preincubation with 1 µM QIC (1 h). pKD (w/o) = 9.45 ± 0.07; pKD (QIC) = 9.52 ± 0.08.
(**B**) CHO-M1 cells were analyzed in whole cell radioligand competition assays using carbachol as ligand. Displacement of the radio-antagonist [^{3}H]NMS was insensitive to QIC preincubation. pKD (w/o) = 3.61 ± 0.08; pKD (QIC) = 3.50 ± 0.23.
(**C**) Carbachol competed [^{3}H]NMS sites with high and low affinity in membrane preparations from CHO-M1 cells. If 1 µM QIC was present, 35 % of the high-affinity sites were converted to the low-affinity sites.
(**A**)-(**C**) Data are means ± SEM of three to six independent experiments, each conducted at least in duplicates and were kindly provided by Ramona Schrage, Pharmacology and Toxicology Section, Institute of Pharmacy, University of Bonn, Germany.

Condition	log (Ki) high	SEM	log (Ki) low	SEM	fraction	SEM	n
w/o	-6.04	0.16	-3.54	0.02	0.51	0.05	4
QIC 1 µM	-5.85	0.24	-3.73	0.19	0.33	0.07	4

Table 3: Related to **Figure 44**. Binding affinities of carbachol to [^{3}H]NMS-labelled CHO-M1 receptors as determined in membrane preparations in the absence or presence of 1 µM QIC. Data were kindly provided by Ramona Schrage, Pharmacology and Toxicology Section, Institute of Pharmacy, University of Bonn, Germany.

3.2.10 Co-incubation of HEK293 cells with QIC and BIM-dimer

As depicted in chapter 3.2.9 QIC exhibited another mode of action as BIM-dimer. For further modelling investigations it was of interest whether QIC and BIM could bind on similar regions of the $G\alpha_q$ protein. Therefore, IP1 levels were determined in HEK293 cells co-incubated with BIM-dimer and QIC in concentrations which alone were not sufficient to silence $G\alpha_q$ signaling but led to a rightward shift of the concentration response curve (**Fig. 45**). Following scenarios were imaginable (1) QIC and BIM-dimer used similar binding regions interfering with each other, (2) they use different binding regions resulting in a synergistic effect or (3) in an additive mechanism. The results show that co-incubation with BIM-dimer and QIC led to a rightward shift in an additive manner (addition of $logEC_{50}$ shift of BIM-dimer and QIC alone amounted 0.898, combination of BIM-dimer and QIC revealed a rightward shift of 0.839) indicating that QIC and BIM-dimer probably do not share the same target structure within the $G\alpha_q$ protein.

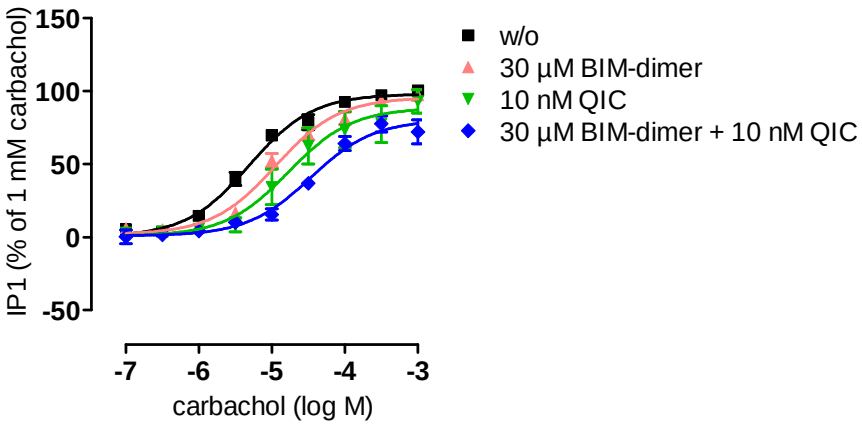

Figure 45: Inhibitory effects of BIM-dimer and QIC were additive.
HEK293 cells endogenously expressing muscarinic M3 receptors were pretreated with BIM-dimer (30 µM: pEC_{50} 4.95), QIC (10 nM: pEC_{50} 4.77) or a combination of both (pEC_{50} 4.47) and IP1 accumulation was determined (w/o: pEC_{50} 5.31). pEC_{50} values were shifted in an additive manner (Shifting of pEC_{50} values, BIM-dimer: 0.36, QIC: 0.54, BIM-dimer + QIC: 0.84). Data shown were means ± SEM of at least three independent experiments, each conducted in triplicate.

3.2.11 Characterizing QIC red, a hydrogenated derivative of QIC

As it was recently described for YM (Taniguchi et al., 2004) the chemical structure of QIC was modified to obtain semisynthetic hydrogenated QIC hereafter referred to as QIC red (**Fig. 46**).

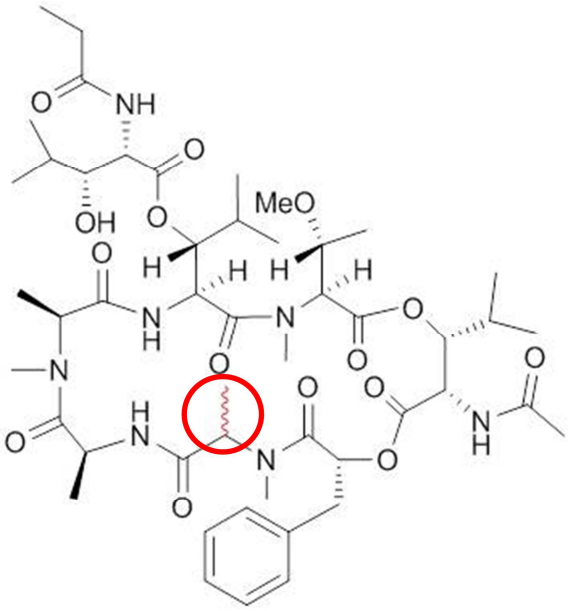

Figure 46: Chemical structure of hydrogenated QIC (QIC red)
The structure was synthesized and purified by Anne Stößel and Marion Schneider Pharmaceutical Chemistry, Institute of Pharmacy, University of Bonn, Germany.

In a first approach the inhibitory activity of QIC red should be evaluated in comparison to QIC by determining IP1 levels after preincubation with increasing concentrations of QIC or QIC red, respectively (**Fig. 47**). The inhibitory activity of QIC red was reduced and the logIC_{50} value was rightward shifted by about half a decade (QIC logIC_{50}: -6.58; QIC red log EC_{50}: -6.05) compared to QIC. The activity of the semisynthetic analogues in Tangiuchi et al revealed great differences within the two diastereomers, one derivative showed nearly the same inhibitory activity as YM, but the other diasteromer exhibited significantly less activity. Our semisynthetic derivative consisted of a mixture of two diastereomers which could explain reduced activity in comparison to QIC.

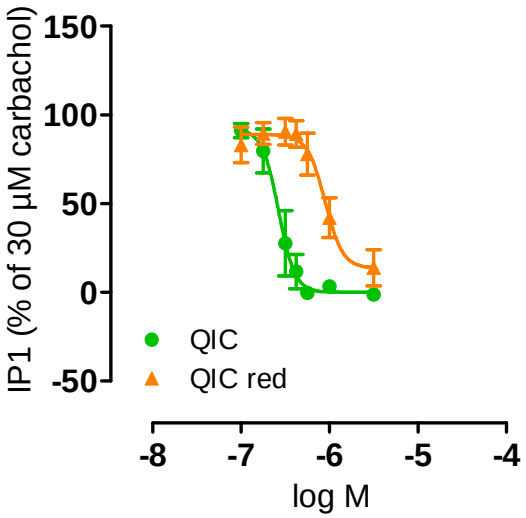

Figure 47: Determining inhibitory activity of QIC red.
CHO cells stably transfected to express muscarinic M1 receptors were preincubated with increasing concentrations QIC (pIC_{50} 6.58 ± 0.05) or QIC red (pIC_{50} 6.05 ± 0.06), stimulated with carbachol (30 µM) and IP1 accumulation was determined. QIC red exhibited less activity to silence $G\alpha_q$-mediated signaling than QIC. Data shown are means ± SEM of at least three independent experiments.

With further experiments it should be analyzed whether the effect of QIC red was selective for inhibition of $G\alpha_q$ proteins. Therefore IP1 and cAMP accumulation was detected in the presence or absence of 5 µM QIC red. Pretreatment with QIC red completely silenced IP1 production mediated via stably expressed M1 receptors in CHO cells (**Fig. 48A**) but cAMP production triggered via $G\alpha_s$-sensitive endogenously expressed EP2/4 receptors (**Fig. 48B**) or $G\alpha_i$-sensitive endogenous serotonin receptors (**Fig. 48C**) in CHO cells was completely unaffected by preincubation with QIC red. Together, second-messenger assays revealed QIC red as selective $G\alpha_q$-inhibitory compound.

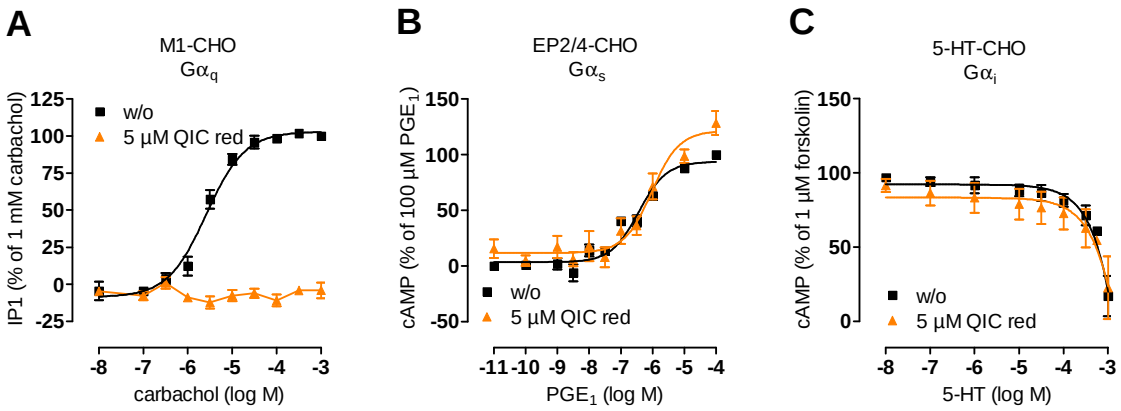

Figure 48: QIC red selectively silenced Gα$_q$-mediated signaling in CHO cells.
(**A**) CHO cells stably transfected to express M1 receptors were pretreated with QIC red, stimulated with carbachol and IP1 accumulation was detected. pEC$_{50}$ (w/o) = 5.58 ± 0.07
(**B**)-(**C**) cAMP levels were detected to analyze the influence of QIC red on endogenous Gα$_s$-coupled EP2/4 receptors (pEC$_{50}$ (w/o) = 6.44 ± 0.09; pEC$_{50}$ (QIC red) = 6.03 ± 0.14) (**B**) and endogenous Gα$_i$-coupled serotonin (5-HT) receptors (**C**). Both pathways were insensitive to QIC red pretreatment.
(**A**)-(**C**) Presented data are means ± SEM of at least three independent experiments, each performed in triplicate.

To explore structure-activity relationship of QIC and QIC red washing experiments were performed. HEK293 cells were analyzed in an IP1 accumulation assay and therefore preincubated with 1 µM QIC (**Fig. 49A**) or 5 µM QIC red (**Fig. 49B**) for 1 h. After the incubation cells were washed three times for 5 min with PBS and then stimulated with carbachol. In parallel the assay was performed without the washing procedure to check for influences on the cells by the washing process itself. As depicted in **Figure 49** the washing procedure had no effect on the concentration response curve in the absence of QIC or QIC red, respectively. If the cells were washed in the presence of QIC or QIC red the inhibitory effect on the Gα$_q$ pathway was nearly unaltered. From these results one could conclude that QIC did not interact with the Gα$_q$ protein via Michael addition which was also described for YM recently (Taniguchi et al., 2004). It was imaginable that QIC inhibitory effect would be caused due to a Michael addition of a nucleophilic residue in the Gα$_q$ protein (Taniguchi et al., 2004). This hypothesis could not be confirmed because it was also impossible to remove the inhibitory effect of hydrogenated QIC with washing procedures although the chemical structure of QIC red did not reveal structural conditions for Michael addition.

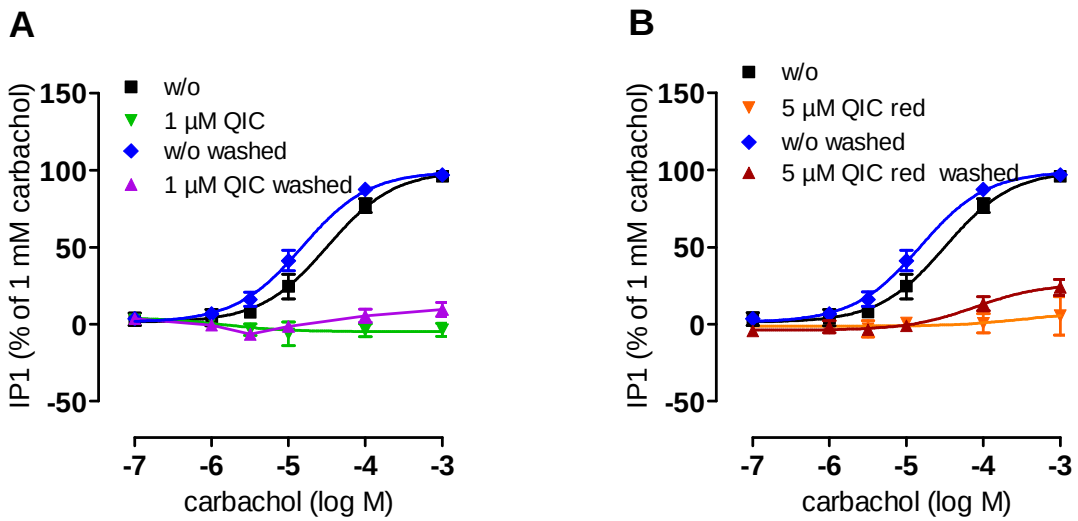

Figure 49: QIC and QIC red inhibitory effect was still detectable after washing procedure. HEK293 cells endogenously expressing muscarinic M3 receptors were preincubated with QIC (1 µM) or QIC red (5 µM) and after that cells were washed three times for 5 minutes with 750 µl PBS. Then cells were stimulated with the muscarinic agonist carbachol in increasing concentrations und IP1 accumulation was detected. As a control IP1 accumulation was also determined without the washing procedure. pEC_{50} (w/o) = 4.50 ± 0.12; pEC_{50} (w/o washed) = 4.82 ± 0.08. Data shown are means ± SEM of at least three independent experiments, each performed in triplicate.

3.2.12 Screening of QIC-derivatives

The working group of Prof. Imhof (Pharmaceutical Chemistry I, Institute of Pharmacy, University of Bonn, Germany) synthesized compounds which resemble the chemical structure of QIC. C-terminally amidated decapeptide CCAP-vill (hereafter referred to as CCAP) (**Fig. 50A**), originally discovered in the marine cone snail *Conus villepinii*, was originally synthesized for experiments for another publication of their working group (Miloslavina et al., 2010) but was still available and should be tested because ring size shows similarity to the chemical structure of QIC. EK2 cyclo (**Fig. 50B**) and EK2 linear (**Fig. 50C**) were synthesized on basis of recently published X-ray crystal structure analysis of the $G\alpha_q\beta\gamma$-YM complex (Nishimura et al., 2010). QIC-derivatives were synthesized to become independent from plant material, to identify the pharmacophore and to get a possibility to develop specific inhibitory compounds for other Gα subunits. Nishimura et al. identified aromatic phenyl group of YM as an important structure because this group can dock into a small hydrophobic pocket and forms contacts with residues from Switch I which stabilize Switch I in the inactive GDP-bound conformation. It is important to know that each Gα subunit preserves such an interdomain cleft but with different surface shapes and properties which could be used as basis for the development of specific inhibitors for other Gα subunits (Nishimura et al., 2010)

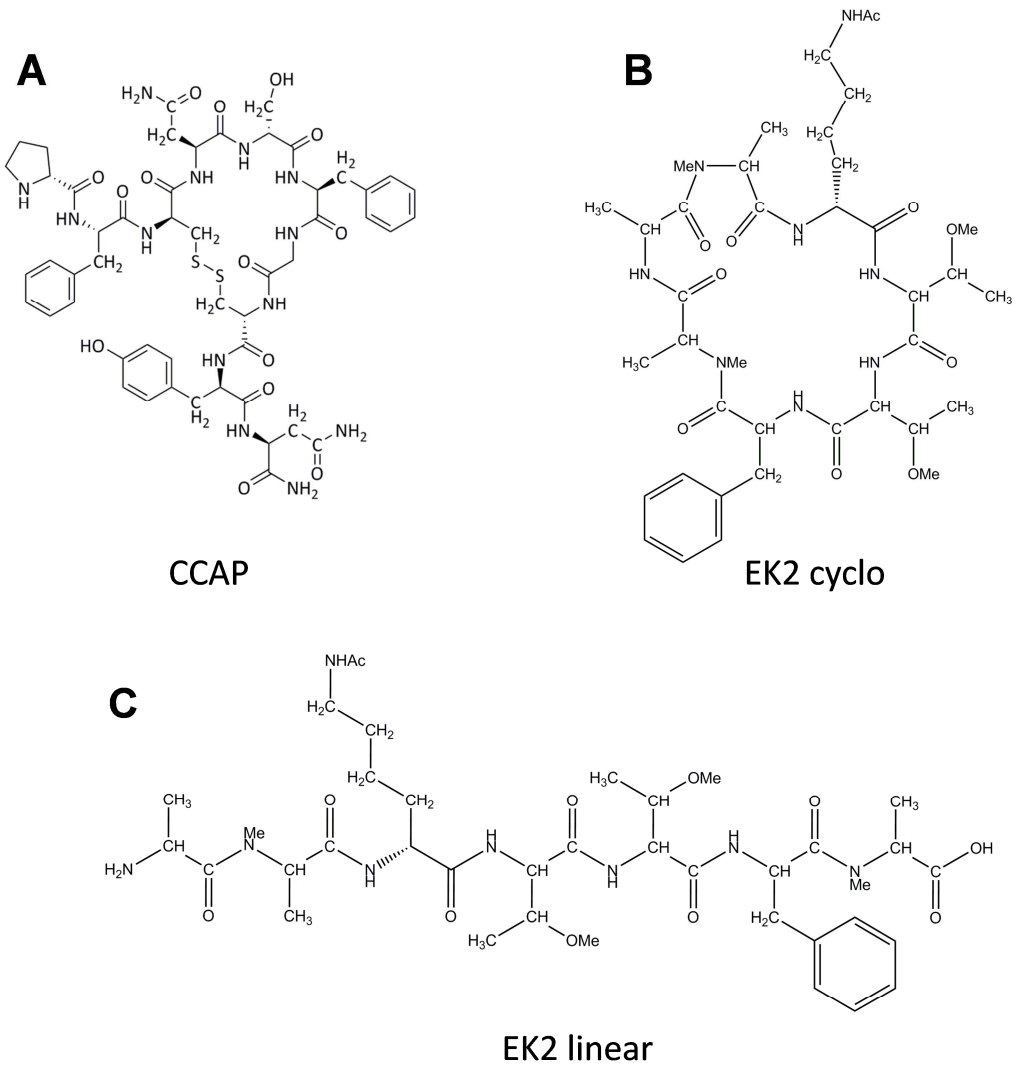

Figure 50: Chemical structures of QIC derivatives. The compounds were kindly provided by the working group of Prof. Imhof, Pharmaceutical Chemistry I, Institute of Pharmacy, University of Bonn, Germany.

All of the three synthesized QIC analogs exhibit an aromatic phenyl group and the depsipeptide structure is lacking. The amino acid sequence of EK2 linear and EK2 cyclo resembled QIC but were partially modified due to increased complexity of peptide production. Their ability to silence $G\alpha_q$-mediated signaling was analyzed in IP1 accumulation assays. Therefore CHO M1 cells were preincubated for 2 h with CCAP (**Fig. 51A**), EK2 linear (**Fig. 51B**) or EK2 cyclo (**Fig. 51C**) in increasing concentrations. Signaling via $G\alpha_q$ proteins was silenced after pretreatment with QIC but was completely unaffected by preincubation with CCAP, EK2 linear or EK2 cyclo, respectively. Based on these findings one could conclude that structural similarities were not sufficient enough to blunt $G\alpha_q$ signaling.

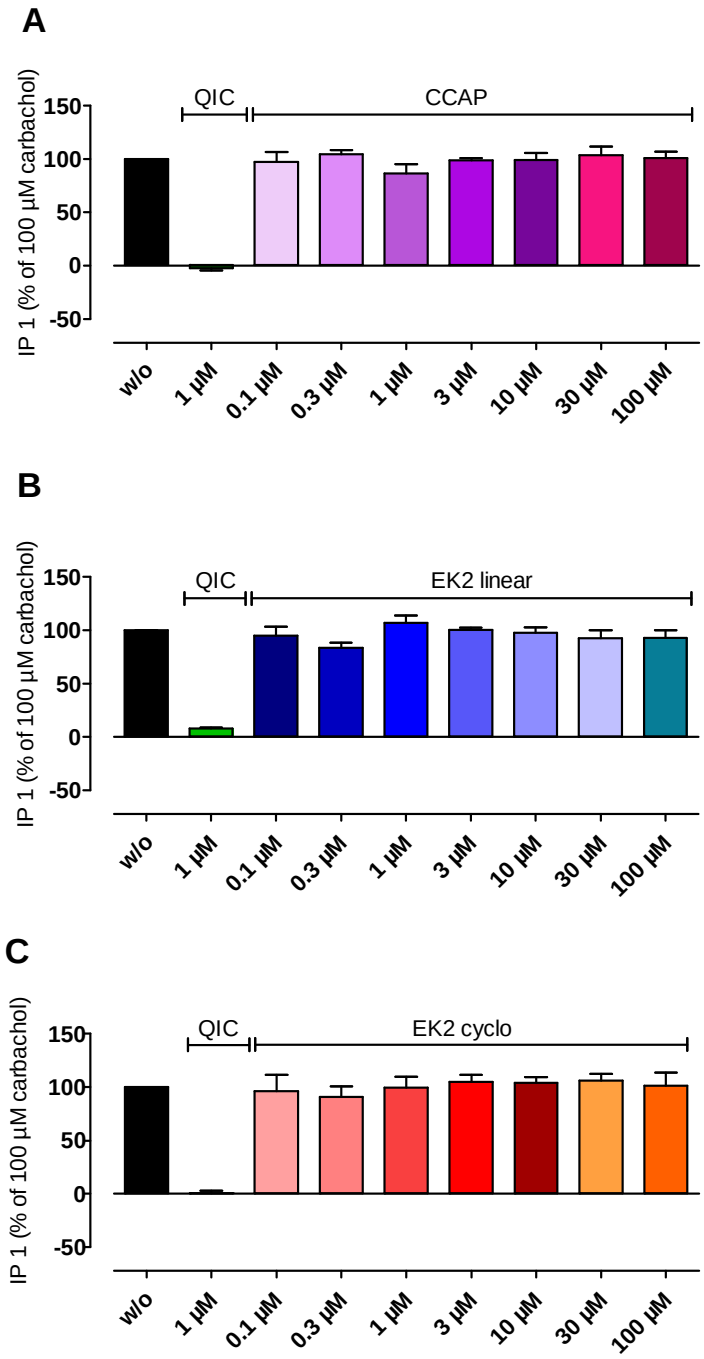

Figure 51: Testing of QIC analogs in IP1 accumulation assays.
(**A**)-(**C**) CHO cells stably transfected to express muscarinic M1 receptors were used to screen CCAP (**A**), EK2 linear (**B**) or EK2 cyclo (**C**) on their ability to silence $G\alpha_q$ signaling after preincubation for 2 h in IP1 accumulation assays. Each substance was tested in a concentration of 0.1, 0.3, 1, 3, 10, 30 and 100 µM. QIC (1 µM) was used as positive control. $G\alpha_q$-mediated signaling was insensitive to pretreatment with CCAP, EK2 linear or EK2 cyclo, respectively. Data are means + SEM of at least three independet experiments, each conducted in triplicate. Data were generated by Tigisti Beraki-Schauff as part of her Master´s thesis, Institute for Pharmaceutical Biology, University of Bonn, Germany.

With further experiments it should be analyzed whether EK2 linear and EK2 show inhibitory effects on $G\alpha_i$ or $G\alpha_s$ proteins. cAMP levels were determined in the presence or absence of 100 µM EK2 linear or EK2 cyclo (**Fig. 52**) in CHO cells stably transfected to express GPR17. It was possible to analyze $G\alpha_i$ and $G\alpha_s$ signaling simultaneously because by application of higher MDL29,951 concentrations stimulatory signaling cascade predominated the inhibitory effect resulting in a bell-shaped concentration response curve. This was a major advantage due to the fact that QIC analogues were available in limited quantities. CCAP had already been used up in IP1 accumulation assays and could not be analyzed in experiments determining cAMP levels. As depicted in **Figure 52** GPR17-mediated cAMP production was unaltered after preincubation with EK2 linear or EK2 cyclo.

Together, signaling via $G\alpha_q$, $G\alpha_i$ and $G\alpha_s$ proteins was insensitive to pretreatment with synthesized QIC analogs indicating that performed changes in the chemical structure of QIC destroyed its ability to silence $G\alpha_q$ proteins but also did not lead to inhibitory effects on $G\alpha_i$ or $G\alpha_s$ proteins.

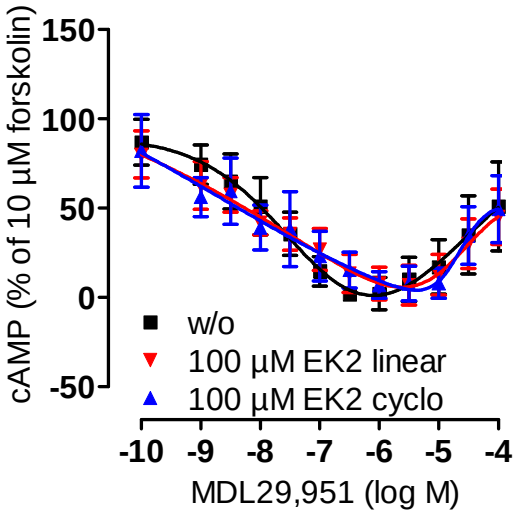

Figure 52: Testing of QIC analogs in cAMP accumulation assays.
CHO cells stably transfected to express GPR17 were used to test EK2 linear or EK2 cyclo on their ability to silence $G\alpha_i$ or $G\alpha_s$ signaling after preincubation for 2 h in cAMP accumulation assays. Both compounds were tested in a concentration of 100 µM. $G\alpha_s$- and $G\alpha_i$-mediated signaling was insensitive to pretreatment with EK2 linear or EK2 cyclo, respectively. For receptor expression CHO-GPR17 cells were treated with 1 µg/ml doxycycline for 16 h. Data are means ± SEM al least three independent experiments, each conducted in triplicate. Data were generated by Tigisti Beraki-Schauff as part of her Master´s thesis, Institute for Pharmaceutical Biology, University of Bonn, Germany.

4 Discussion

4.1 Advantages of small molecule G protein inhibitors vs siRNA

Small molecule inhibitors like BIM and QIC represent an important approach for selective inhibition of Gα subunits. The pharmacological manipulation of G protein signaling with small molecules has many specific advantages against knockdown strategies such as small interfering RNA (siRNA) for the application in cell-based test systems as well as for use as potential drugs (Weiss et al., 2007). Typically, small molecules are able to cross cell membranes and therefore, it is imaginable that they can be used as orally active drug. In contrast to siRNA they can be easily applied in cell-based assays without transfection procedures. Based on this fact, small molecules show a rapid onset of action while knockdown is typically observed 24-48 h after transfection (Weiss et al., 2007). In case that small molecules reversibly bind to their target protein the inhibitory effects can be rapidly removed which is not possible after siRNA application. Additionally, small molecules allow performing titration experiments and therefore, one can use concentrations ranging from complete inhibition to only slight effects. This feature could be exploited for co-incubation experiments described in chapter 3.2.10. In this setting it was possible to explore the inhibitory effect after a co-incubation with BIM-dimer and QIC to find out whether these two compounds interfere with each other. To this end, it was of great importance to work with concentrations which cause only a rightward shift of the concentration-response curve but are not sufficient for complete inhibition. The extent of inhibitory effects after siRNA application is likely to vary due to different transfection efficiencies. It should be noted that siRNA molecules can be obtained quickly whereas the generation of selective small molecule inhibitors can be a long-term process (Weiss et al., 2007).

4.2 Context-dependent pharmacology of BIM

This thesis reveals an inhibition profile for the BIM-dimer ranging from selective $G\alpha_q$ protein inhibition to pan-G protein inhibition in a cell-type-specific manner which is in apparent contrast to the findings of Ayoub et al.. They recently described BIM-dimer acting as a specific pan-G protein inhibitor in various cancer cell lines and in COS7 cells (Ayoub et al., 2009). However, in the commonly used HEK293 and CHO cell background BIM-dimer as well as the BIM-monomer specifically silenced signaling via $G\alpha_q$ proteins but acted as a pan-G protein inhibitor in COS7 cells and in the patient-

derived melanoma MZ7 cells. Regarding the fact that context-dependent pharmacology represents a well-described phenomenon which can often be explained by differences in the relative amount or stoichiometry of signaling components (Kenakin and Christopoulos, 2013) the mechanistic link between sensitivity toward BIM-dimer inhibition and the level of expression of BIM target proteins was investigated. In HEK293 cells BIM-dimer functioned as specific $G\alpha_q$ inhibitor and it was hypothesized that this effect could be caused by a lower expression level of $G\alpha_q$ proteins in comparison to $G\alpha_i$ and $G\alpha_s$ proteins. Indeed, enrichment with increasing amounts of $G\alpha_q$ proteins led to a reduced inhibitory effect of BIM-dimer on the $G\alpha_q$ pathway. From these data it was imaginable that differing endogenous expression levels of Gα subunits might contribute to the cell-type-dependent inhibitory profile of BIM-dimer. Many recent publications suggest that G proteins can interact with receptors before agonist binding, an effect which is called precoupling or preassembly. One opposing model to this is represented by the collision coupling model which assumes that an agonist binds to the free receptor, activates it and then the agonist-bound receptor collides with free G proteins as a result of free lateral diffusion within the plasma membrane. The literature gives accumulating evidence for both, collision coupling and precoupling model (Qin et al., 2011; Oldham & Hamm, 2008; Jakubik et al., 2011). The precoupling model can account for the rapid intracellular response of G protein-mediated signaling (Oldham and Hamm, 2008). Therefore, it is imaginable that enrichment of HEK cells with $G\alpha_q$ leads to an increase in the number of preassembled, GPCR-$G\alpha_q$ protein complexes. This phenomenon is expected to increase the likelihood that cellular signaling via preformed BIM-free $G\alpha_q$-GPCR complexes would be enhanced, because in our experiments receptor amounts were kept constant but $G\alpha_q$ levels varied. Immunoblot detection of endogenous expression levels of Gα subunits of HEK293 and MZ7 cells revealed equal amounts for the expression of $G\alpha_q$ proteins which is compatible with the postulated mechanistic link we observed as BIM-dimer was able to silence $G\alpha_q$-mediated signaling in both cellular backgrounds. Significantly lower expression of $G\alpha_s$ proteins in MZ7 cells additionally supports the hypothesis because in HEK293 cells $G\alpha_s$ signaling was unaffected by BIM-dimer preincubation. This can be explained by a higher expression level of $G\alpha_s$ subunits in a HEK293 cell background compared to MZ7 cells. Immunoblot quantification of $G\alpha_i$ proteins revealed a higher expression level in MZ7 cells which is incompatible with the postulated hypothesis. Taken together, different expression levels of Gα subunits may serve as explanation approach for cell-type-

dependent pharmacology of BIM-dimer but are not sufficient to explain $G\alpha_q$ selective inhibition in some cells and pan-G protein inhibition in other cellular backgrounds.

Pan-G protein inhibition represents an interesting approach for the treatment of malignant diseases because GPCRs are described as crucial players in tumor growth and metastasis (Dorsam and Gutkind, 2007; Smrcka, 2013). Prévost et al. recently described monomeric BIM as a compound with promising antitumor activity (Prévost et. al., 2006). Regarding the fact, that depending on the type of cancer different Gα subunits may be affected by mutations it is important to pay particular attention to the cell-type-dependent inhibitory profile. For example $G\alpha_s$ mutations have been found in pancreatic cancers or $G\alpha_s$ upregulation in ovarian and breast cancers (Kan et al, 2010) while mutations in $G\alpha_q$ or $G\alpha_{11}$ were found to be prevalent in certain types of melanomas (Van Raamsdonk et al., 2009; Van Raamsdonk et al. 2010). It is likely that additional cell lines exist, in which BIM does not function as a pan-G protein inhibitor. Therefore, it will be of great importance to determine the selectivity profile of BIM for every cellular background used.

It is noteworthy that Prévost et al. determined the antiproliferative activity of BIM-monomer on HEK293 cells to have an IC_{50} value of 7.8 µM (Prévost et al., 2006). BIM-monomer showed antiproliferative activity inspite of the fact that this thesis revealed monomeric BIM to preferentially silence $G\alpha_q$ proteins in HEK293 cells. This implies that pan-G protein inhibition does not seem to be necessary for antiproliferative activity and indicates that inhibition of $G\alpha_q$ proteins might be sufficient to achieve antiproliferative activity, at least in this cellular background. With regard to the application of small molecules as anticancer agents, it would be of great benefit to silence only as many Gα subunits as necessary to reduce toxic and side effects. The IC_{50} value of BIM-monomer on cell growth is lower than concentrations needed to block G protein-activated second-messenger accumulation (Prévost et al., 2006) which was also confirmed in cell growth experiments performed in MZ7 cells as described previously (Schmitz et al., 2014). Inhibition of cell growth by BIM-dimer reached its maximum at 10 µM but a 10-fold increase of BIM concentration was required to silence signaling via $G\alpha_q$, $G\alpha_s$ and $G\alpha_i$ proteins (Schmitz et al., 2014). This discrepancy can be explained by short (second-messenger assays, 2 h) versus long (cell growth assays, 72 h) BIM preincubation times and/or abrogation of ligand-stimulated signaling (second-messenger assays) versus endogenous receptor signaling (cell growth assays) (Prévost et al., 2006; Schmitz et al, 2014).

4.3 BIM-dimer functions as GTP entry inhibitor

Further studies identified BIM to completely prevent G protein activation in [^{35}S]GTPγS binding assays independent if activation was obtained with a ligand-occupied GPCR, either the $G\alpha_i$ mimetic FUB132, or the direct G protein activators AlF_4^- or mastoparan (Prévost et al., 2006; Ayoub et al., 2009). These findings underline a direct action of BIM on the Gα protein but leave the question whether BIM prevents GDP dissociation or GTP entry. Prior to investigations concerning the mode of action, the influence of BIM on agonist recognition of the muscarinic M1 receptor was analyzed. BIM did not impair but rather enhanced carbachol displacement of the radio-antagonist [^{3}H]NMS confirming that agonist binding is unaffected by BIM pretreatment. It was possible to explore the mode of action with the use of radioligand binding assays in which one can visualize nucleotide-sensitive binding states of GPCRs. Agonist binding to GPCRs triggers GDP release from the Gα subunit and until GTP binds, a high-affinity complex is formed between the receptor and G protein (Oldham and Hamm, 2008). These nucleotide-free G proteins stabilize the agonist-bound active state of the receptor. They can only be visualized in the absence of guanine nucleotides and are transient conformational intermediates in intact cells where guanine nucleotides are richly available (Rodbell et al., 1971, De Lean et al., 1980, Seifert et al., 1999). This phenomenon was used to study the mechanism of interference of BIM for the nucleotide-bound state of Gα. The high-affinity binding can be disrupted with high concentrations of guanine nucleotides such as GTP. High concentrations of GTP force to a rapid exchange of GDP for GTP and therefore the empty-pocket conformation is no longer detectable. The high-affinity sites induced by the empty-pocket conformation are converted to low-affinity sites (De Lean et al., 1980). Additionally, molecules which stabilize GDP-bound Gα, so called guanine nucleotide dissociation inhibitors (GDIs) would prohibit the empty-pocket conformation resulting in a similar loss of high-affinity sites. Assuming that BIM would act as guanine nucleotide dissociation inhibitor high-affinity agonist sites would have been converted to low-affinity sites after preincubation with BIM-dimer. Inhibition of heterotrimer signaling can only be achieved with compounds precluding nucleotide exchange. Due to the fact that in the presence of BIM high-affinity agonist binding was unaffected it must consequently allow GDP exit but prevent GTP entry. This postulated mode of action is entirely new and has not been described for any other small molecule G protein α subunit inhibitor to date (**Fig. 51**).

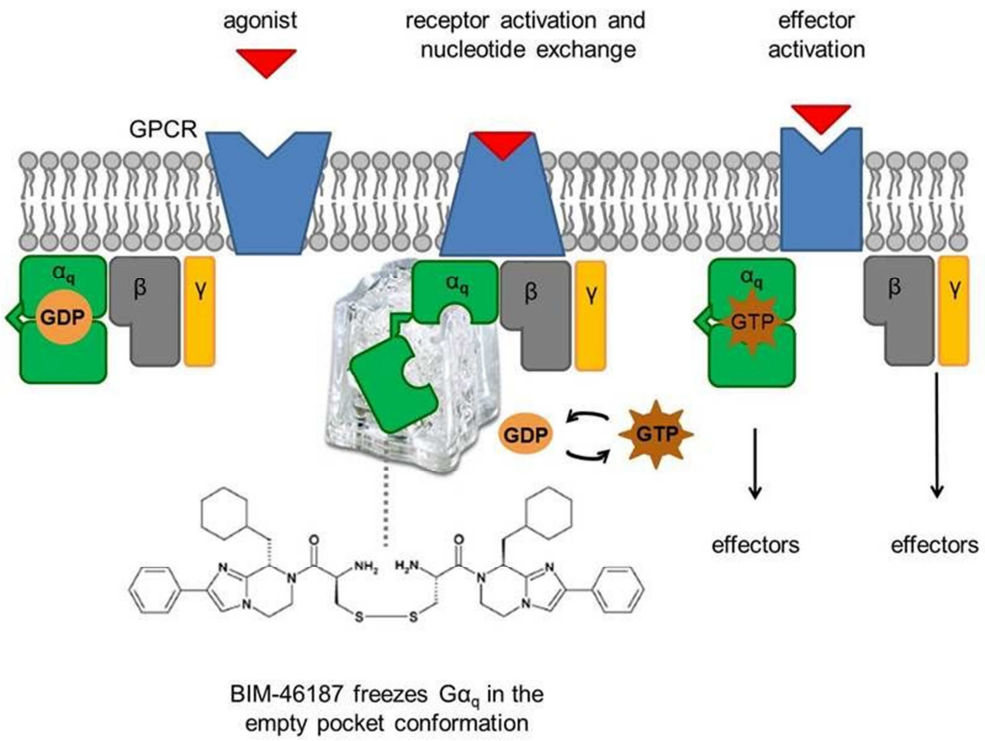

Figure 53: Mechanism of action of BIM-dimer. Upon receptor stimulation, conformational changes trigger the release of GDP. The subsequent binding of GTP is blocked because BIM-dimer traps $G\alpha_q$ in the empty pocket conformation.

All previously developed small molecule Gα subunit inhibitors have common mechanism of action. They bind to G protein α subunits where they prevent intrinsic and receptor-stimulated GDP release (Smrcka, 2013). Only the $G\alpha_q$-selective inhibitor YM warrants a credible mechanism for inhibition of GDP exit by virtue of the mechanistic details available at the structural level (Nishiumura et al., 2010). A similar mode of action has been described for suramin which represents a relatively specific inhibitor of GDP release on the G_s family G protein α subunits, but the utility of suramin in cell-based assays or as drug is limited because it cannot cross cell membranes due to its strong negative charge (Smrcka, 2013; Hohenegger et al., 1998).

Further experiments investigating GDP dissociation from purified $G\alpha_q$ proteins confirmed the hypothesis that BIM-dimer permits GDP exit because GDP dissociation remained uninfluenced by pretreatment with BIM-dimer.

Binding experiments in which membranes were preincubated with a combination of BIM and GTP prove that BIM prevents GTP entry because BIM counteracts the effect of GTP on the high-affinity agonist binding. Additionally, it would be possible to check this hypothesis by the use of [^{35}S]GTPγS assays with purified $G\alpha_q$ proteins. This setting could detect spontaneous GTPγS binding to $G\alpha_q$ in the presence and absence of BIM

and one would expect that BIM does not permit GTPγS binding (Nishimura et al., 2010).

This unique mode of action also explains why carbachol binding to whole CHO-M1 cells was enhanced in the presence of BIM, because a GTP entry inhibitor prolongs the lifetime of active-state complexes.

Additionally, this mechanism elucidates the fact that BIM-dimer was incapable of completely preventing the opening of the nucleotide binding pocket of activated $G\alpha_q$-βγ proteins in the BRET assays. In this approach HEK293 cells were transfected to express $G\alpha_q$-*R*Luc as energy donor together with $G\gamma_2$-GFP^{10} as energy acceptor. M3 receptor activation resulted in a negative BRET which illustrates the separation of the Gα helical domain from the N terminus of Gγ. This process demonstrates opening of the nucleotide binding pocket, enabling GDP dissociation followed by GTP entry (Galés et al., 2006; Saulière et al., 2012). Receptor antagonists or inhibitors of G protein function acting as GDIs, for example pertussis toxin, were able to completely prevent agonist-mediated BRET decrease (Galés et al., 2006). In contrast, BIM significantly reduced agonist-mediated BRET decrease but did not completely abrogate opening of the nucleotide binding pocket which indicates rearrangements between Gα and Gγ that allow GDP exit.

Based on the results generated in HEK293 and CHO cells, BIM was identified as a $G\alpha_q$-specific GTP entry inhibitor in this cellular background which represents a new and unique molecular mechanism not yet assigned to any other small molecule Gα inhibitor to date. The structure of BIM might be a suitable starting point for development of more potent, cell permeable and highly specific inhibitors for $G\alpha_q$ and/or the remaining Gα subfamilies. Furthermore, this new molecular mechanism could be exploited to gain deeper insight into the empty pocket conformation of Gα proteins by the use of cocrystallization experiments.

4.4 Mode of action and structure activity relationship of QIC

The chemical structure of QIC shows high similarity to that of YM and features a unique amino acid composition, including the uncommon amino acid N-methyldehydroalanine and the novel amino acid N,O-dimethylthreonine (Nesterov et al., 2010). Several assays, ranging from second-messenger assays to whole cell label-free analyses, were performed in the commonly used HEK293 and CHO cell

background which all revealed QIC as a selective $G\alpha_{q/11}$ inhibitor. Due to the fact that BIM-dimer preferentially silences $G\alpha_q$ proteins in HEK293 and CHO cells but functions as pan-G protein inhibitor in the skin cancer cell line MZ7 the inhibitory profile of QIC was also analyzed in MZ7 cells. In contrast to BIM, QIC specifically silences $G\alpha_q$-mediated signaling in MZ7 cells as well as in HEK and CHO cells. For YM, complex structural information is available which allows for the understanding of its mode of action on an atomic level, providing a plausible mechanism for inhibiting GDP release (Nishimura et al., 2010; Smrcka, 2013). Because of the high structural similarity between QIC and YM it is likely that QIC silences $G\alpha_q$ proteins according to a mechanism that is identical to that of YM. Nesterov et al. investigated QIC for its ability to prevent GTP binding. Their experiments revealed that QIC inhibited CCK-induced GDP for GTP exchange (Nesterov et al., 2010). From these experiments it is not possible to conclude whether GDP dissociation was blocked or whether $G\alpha_q$ was "frozen" in the high-affinity empty pocket conformation. To discriminate between these possibilities, radioligand binding studies on CHO-M1 membranes were performed in the same way when tested with BIM. In the absence of QIC, active-state ternary complexes could be observed, but in the presence of QIC 35% of them were converted to low-affinity agonist sites indicating that QIC interferes with GDP exit and thereby decreases the high-affinity fraction. In binding experiments performed in the presence of 1 mM GTP 49% of the high-affinity sites were converted to low-affinity sites (see chapter 3.1.8). Thus, in comparison to GTP, QIC only partially converts the high-affinity sites to low-affinity sites. This fact does not refute the hypothesis that QIC might function as GDI but gives rise to the question which could be the reason for the different conversion rates observed upon GTP and QIC pretreatment, respectively. According to the literature, muscarinic M1 receptors preferentially activate $G\alpha_{q/11}$ proteins but they can also couple via $G\alpha_{i/o}$ and $G\alpha_s$ proteins (Offermanns et al., 1994; Burford and Nahorski, 1996; Akam et al., 2001). In DMR experiments, performed in CHO-M1 cells, a negative DMR response was detectable after pretreatment with QIC and stimulation with carbachol (see chapter 3.2.1 and 3.2.2). This negative cell response likely indicates the ability of the M1 receptor to couple via $G\alpha_s$ proteins. In the absence of a $G\alpha_q$-inhibitory compound this signal is masked by the positive $G\alpha_q$-mediated wavelength shift. Therefore, it is imaginable that the remaining high-affinity fraction is due to ternary complexes between M1 receptor and $G\alpha_{i/o}$ or $G\alpha_s$ proteins. In order to check this hypothesis, one could repeat the experiments with membranes which are

pretreated with PTX and QIC, CTX and QIC or a combination of PTX, CTX and QIC. This setting would be useful to grasp the contribution of $G\alpha_{i/o}$ and $G\alpha_s$ proteins to high affinity agonist binding.

In order to substantiate the hypothesis that QIC functions as GDI, one could perform [^{3}H]GDP dissociation assays on purified $G\alpha_q$ proteins. In this setting, a GDI would prevent GDP dissociation and it would enable exploring the mode of action in isolated $G\alpha_q$ proteins. Thus, confounding effects of other Gα subunits can be excluded.

Based on the chemical structure of YM it is imaginable that the $G\alpha_{q/11}$ inhibitory activity might be caused by Michael addition of a nucleophilic residue of the $G\alpha_{q/11}$ protein to the N-methyldehydroalanine residue of YM. With this in mind, YM was hydrogenated to provide two diastereomers which have lost the structural requirement for Michael addition (Taniguchi et al., 2004). One of the diastereomers showed almost the same IC_{50} value as YM, thereby negating the hypothesis that YM interacts with the $G\alpha_{q/11}$ protein by covalent Michael addition (Taniguchi et al., 2004). The other diastereomer had significantly reduced activity which might be explained by conformational differences between both diastereomers. The conformation of YM and the more active diastereomer were similar while the less active diastereomer revealed a different conformation (Taniguchi et al., 2004). As the selective $G\alpha_q$ inhibitor QIC also shows the N-methyldehydroalanine structure, it was hydrogenated analogously to YM to examine whether QIC interacts with the $G\alpha_q$ protein via Michael addition. The resulting QIC red could not be further separated into its two diastereomers because of an insufficient yield of the chemical reaction. This could be an explanation for the fact that the inhibitory activity of hydrogenated QIC was reduced compared to QIC. The mixture of the two diastereomers in comparison to QIC was analyzed concerning its inhibitory effect after washing procedures followed by an IP1 accumulation assay. In a first step it was investigated whether it is possible to remove the inhibitory effect of QIC by washing procedures. These experiments revealed that QIC cannot be washed out and the reason for this could be a covalent modification via Michael addition. To verify this hypothesis it was analyzed whether QIC red, which has lost the structural requirement for Michael addition, was removable by washing procedures. Regarding the fact that it was also impossible to remove the inhibitory effect of QIC red, it must, consequently, be concluded that QIC as well as YM interact with the $G\alpha_{q/11}$ protein without covalent modification by Michael addition.

4.5 $G\alpha_q$-selective inhibitors: an important tool to study G protein signaling pathways and a promising approach for cancer treatment

Heterotrimeric G proteins are central to G protein-coupled receptor signal transduction, and as such, are involved in nearly every physiological pathway and organ system. Of the four families of heterotrimeric G proteins, the $G\alpha_{i/o}$ family can be silenced with the specific inhibitor PTX, which provides an enormous benefit as it allows the unraveling of the contribution of $G\alpha_{i/o}$ signaling to complex cellular responses. Until quite recently, no selective inhibitors were available for the remaining Gα families with the exception of YM, a cyclic depsipeptide isolated from *Chromobacterium* sp. QS3666 and described as selective tool to specifically silence $G\alpha_q$ signaling. It has the disadvantage that it is not commercially available, and only accessible to very few research laboratories. YM binding to $G\alpha_q$ is the only example of a small molecule-G protein complex for which structural information is available and therefore, allows understanding its mode of action on an atomic level (Smrcka, 2013). X-ray crystal structure analysis revealed that YM binds at the hydrophobic cleft between two interdomain linkers connecting the GTPase and helical domains of the $G\alpha_q$ protein. Each Gα subunit preserves such an interdomain cleft, which is similar to that of $G\alpha_q$ but displays unique surface shapes and properties. This observation suggests that YM derivatives could be developed for the specific inhibition of each Gα subunit (Nishimura et al., 2010). Based on the fact that the chemical structure of QIC shows high similarity to the chemical structure of YM and additionally, an identical selective inhibitory profile, the structure of QIC could similarly be exploited as a lead structure for the development of Gα protein subfamily selective inhibitors. The key benefit is that QIC is accessible to research groups worldwide and therefore, it could also be used as starting point for the generation of semi-synthetic derivatives.

As only few cell permeable Gα inhibitors are in existence, it is of great relevance that this thesis identified BIM-dimer as a selective $G\alpha_q$ inhibitor in mammalian HEK293 and CHO cells, two cell lines commonly used to examine signaling of recombinant or endogenous GPCRs. In these cellular backgrounds, BIM-dimer blocks $G\alpha_q$-mediated signaling by exhibiting a unique mechanism, not yet described for any small molecule inhibitor of Gαβγ heterotrimers to date. Therefore, BIM molecules could serve as lead structures for the development of inhibitors for the other G protein α subunit family members. It is of great advantage that BIM molecules can be manufactured through chemical synthesis which prevents dependency on plant material.

An interesting potential application of G protein inhibitors would be the treatment of malignant diseases which are under the control of a complex array of GPCR ligands regulating multiple steps in the development of primary tumors and metastasis. (Dorsam and Gutkind, 2007; Lappano and Maggiolini, 2011). Therefore, manipulating one receptor may not be sufficient for an effective treatment (Smrcka, 2013). Remarkably, Prévost et al reported antiproliferative effects in HEK293 cells after a pretreatment with BIM-monomer although this thesis revealed a preference for inhibition of $G\alpha_q$ signaling. Thus, it can be assumed that pan-G protein inhibition is not responsible for the antiproliferative effects in a HEK293 background and inhibition of $G\alpha_q$-mediated events may be sufficient to cause these effects. Cell growth experiments in the patient derived MZ7 cell line showed that BIM-dimer induced cell death, but in this cell line BIM-dimer also dampened cellular signaling via $G\alpha_q$, $G\alpha_s$ and $G\alpha_i$ pathways, which can be referred to as pan-G protein inhibition (Schmitz et al., 2014). Consequently, it would be of great interest to investigate the effect of a selective $G\alpha_q$ inhibitor on MZ7 cells in cell growth experiments to decipher whether silencing $G\alpha_q$ proteins would also be sufficient for antiproliferative effects in this cell line. To implement these experiments, it is of high importance that a selective $G\alpha_q$ inhibitor such as QIC is available for research.

The literature describes a constitutively active form of $G\alpha_q$ which was found in ocular melanoma of the uvea. This mutations affects the glutamine at codon 209 (Q209) in the GNAQ and GNA11 gene (van Raamsdonk et al., 2010). Takasaki et al. investigated the effect of YM on the active $G\alpha_q$ mutant $G\alpha_q$Q209L (Takasaki et al., 2004). In the Q209L mutant glutamine is replaced by leucine. The glutamine at codon 209 lies within the ras-like domain of GNAQ and is essential for GTP hydrolysis. As a consequence, $G\alpha_q$Q209L shows deficient GTPase activity (van Raamsdonk et al., 2009). Takasaki et al. performed serum response element (SRE) luciferase gene reporter assays with YM. They found out that YM had only a modest effect on the constitutive activity of $G\alpha_q$Q209L. In a further experiment they co-transfected HEK293 cells with $G\alpha_q$-I, a minigene corresponding to the C-terminal peptide sequence of $G\alpha_q$ which can selectively inhibit the receptor-$G\alpha_q$ interaction. Notably, the serum response factor (SRF)-mediated gene transcription induced by Q209L could not be prevented by co-transfection of the $G\alpha_q$-I minigene. Based on these findings they conclude that Q209L activation occurred independently of receptor stimulation but was generated after translation in cytoplasm in a receptor-independent manner. This could be explained with a higher affinity for GTP than for GDP (Takasaki et al., 2004). In this context, it

would be of great interest to explore the effect of BIM on this constitutively active mutant. Due to the mode of action of BIM it would be imaginable that the initial GTP entry after translation could be blocked. In the gene reporter assays of Takasaki et al. YM was added directly after transfection and then incubated for 18 h. It could be difficult to perform such assays with BIM in HEK293 cells because within this time period cell-toxic effects can already be observed. To investigate whether BIM in principle can prevent GTP entry into the constitutive active $G\alpha_qQ209L$ one could perform [^{35}S]GTPγS assays with purified $G\alpha_qQ209L$ proteins analogous to the experiments suggested in chapter 4.3 (Nishimura et al., 2010). Since there is not yet any inhibitor for the constitutive $G\alpha_qQ209L$ mutant available it would be a great benefit to discover an inhibitor having this property.

5 Summary

Selective silencing of Gα protein subfamilies by small molecules is of great value to explore the contribution of G protein signaling in physiology and disease. It also represents a new opportunity to treat diseases, such as cancer, in which multiple receptors are involved. Consequently, signaling of a large number of receptors could be silenced with a single tool. Only few small cell-permeable molecules acting as Gα-selective inhibitors have been reported to date.

The present thesis classifies BIM-46187, previously reported as pan-G protein inhibitor, as a compound which preferentially silences $G\alpha_q$-mediated signaling in a cellular context-dependent manner. In particular, BIM functions as selective $G\alpha_q$ inhibitor in HEK and CHO cells but silences $G\alpha_q$, $G\alpha_i$ and $G\alpha_s$ proteins in the human skin cancer cell line MZ7. Cell-context pharmacology might be explained with differences in the relative amount or stoichiometry of signaling components. Gene dosing experiments revealed a correlation between BIM inhibition and $G\alpha_q$ expression. However, immunoblot detection, which compared expression levels of $G\alpha_q$, $G\alpha_s$ and $G\alpha_i$ proteins in HEK and MZ7 cells, indicated that different Gα expression levels cannot exclusively account for cell-type-dependent pharmacology of BIM. Investigations concerning the mode of action uncovered an entirely new molecular mechanism: BIM permits GDP exit but precludes GTP entry thereby “freezing” the $G\alpha_q$ protein in the empty pocket conformation.

The second part of this thesis uncovers the cyclic depsipeptide FR900359 as a suitable tool for selective silencing of $G\alpha_{q/11}$ proteins. A great variety of assays, such as classical second-messenger assays, BRET assays and label-free methods, demonstrate the selectivity of FR900359. Experiments in the commonly used HEK and CHO backgrounds, as well as in the human skin cancer cell line MZ7, reveal its utility in cell-based assays. FR900359 does not compromise agonist binding but interacts with agonist function. Based on radioligand competition experiments, it can be assumed that FR900359 functions as a guanine-nucleotide dissociation inhibitor as it impairs the formation of the high-affinity agonist binding.

6 Abbreviations

AC	adenylyl cyclase
ADP	adenosine 5’-diphosphate
ATP	adenosine 5’-triphosphate
BIM-dimer	BIM-46187
BIM-monomer	BIM-46174
bp	base pairs
BRET	bioluminescence resonance energy transfer
BSA	bovine serum albumin
cAMP	cyclic adenosine monophosphate
cDNA	complementary DNA
°C	Celsius
CHO	chinese hamster ovary
CTX	cholera toxin
CRTH2	chemo attractant receptor homologous molecule expressed on T-helper type 2 cells
DAG	diacylglycerol
DMEM	Dulbecco´s modified eagle medium
DMR	dynamic mass redistribution
DMSO	dimethyl sulfoxid
DNA	deoxyribonucleic acid
E.coli	*Escherichia coli*
EC_{50}	concentration of half maximum effect
EDTA	ethylene diamine tetraacetic acid
EP	E-prostanoid receptor
ERK	extracellular-signal regulated kinase
FCS	fetal calf serum
FFA1	free fatty acid receptor 1
FFA2	free fatty acid receptor 2
FFA3	free fatty acid receptor 3
FRET	fluorescence resonance energy transfer
Fsk	forskolin
g	acceleration by gravity; gram
G418	geneticin
GDP	guanosine 5′-diphosphate
GEF	guanine nucleotide exchange factor

GFP	green fluorescent protein
GPCR	G protein-coupled receptor
G protein	guanine nucleotide-binding protein
GRK	G protein-coupled receptor kinases
GTP	guanosine 5′-triphosphate
h	hour(s), human
HA	haemagglutinin
HBSS	Hank´s balanced salt solution
HEK	human embryonic kidney
HEPES	N-(2-Hydroxyethyl)piperazine-N-ethanesulforinic acid
5-HT	5-hydroxytryptamine, serotonin
HTRF	homogeneous time resolved fluorescence
IBMX	3-isobutyl-1-methylxanthine
IC_{50}	concentration of half maximum inhibition
IP1	inositol 4-phosphate
IP3	inositol 1,3,4-triphosphate
JNK	c-Jun N-terminal kinase
kb	kilo base(s)
LB-medium	Luria Bertani medium
l	liter
log M	logarithm of molar concentration to base 10
M	molar concentration (mol/liter)
MAPK	mitogen-activated protein kinase
mBRET	milliBRET
min	minute(s)
ml	milliliter
ms	millisecond
M1	muscarinic receptor 1
M3	muscarinic receptor 3
µl	microliter
µM	micromolar
n	number
nm	nanometer
nM	nanomolar
NMS	N-methylscopolamine
ns	non-significant

N-terminus	amino terminus
OD	optical density
PKA	protein kinase A
PKC	protein kinase C
PLC	phospholipase C
PBS	phosphate buffered saline
PTX	pertussis toxin
QIC	FR900359
RhoA	Ras homolog gene family, member A
*R*Luc	*Renilla* luciferase
RNA	ribonucleic acid
rpm	rounds per minute
RPMI	Roswell Park Memorial Institute
RT	room temperature
sec	second(s)
s	second(s)
SEM	standard error of mean
TE	Tris EDTA
TM	transmembrane
Tris	Tris(hydroxymethyl)aminomethane
U	unit
UV	ultraviolet
V	volt
w/o	without
YM	YM-254890

7 References

Ahmed-Belkacem, A., Pozza, A., Muñoz-Martínez, F., Bates, S.E., Castanys, S., Gamarro, F., Di Pietro, A., and Pérez-Victoria, J.M. (2005). Flavonoid structure-activity studies identify 6-prenylchrysin and tectochrysin as potent and specific inhibitors of breast cancer resistance protein ABCG2. Cancer Res 65, 4852-4860.

Akam, E.C., Challiss, R.A., and Nahorski, S.R. (2001). G(q/11) and G(i/o) activation profiles in CHO cells expressing human muscarinic acetylcholine receptors: dependence on agonist as well as receptor-subtype. Br. J. Pharmacol 132, 950-958.

Ayoub, M.A., Damian, M., Gespach, C., Ferrandis, E., Lavergne, O., Wever, O. de, Banères, J.-L., Pin, J.-P., and Prévost, G.P. (2009). Inhibition of heterotrimeric G protein signaling by a small molecule acting on Galpha subunit. J. Biol. Chem 284, 29136-29145.

Berman, D.M., Wilkie, T.M., and Gilman, A.G. (1996). GAIP and RGS4 are GTPase-activating proteins for the Gi subfamily of G protein alpha subunits. Cell 86, 445-452.

Bohm, A., Gaudet, R., and Sigler, P.B. (1997). Structural aspects of heterotrimeric G-protein signaling. Curr. Opin. Biotechnol 8, 480-487.

Bornancin, F., Pfister, C., and Chabre, M. (1989). The transitory complex between photoexcited rhodopsin and transducin. Reciprocal interaction between the retinal site in rhodopsin and the nucleotide site in transducin. Eur. J. Biochem 184, 687-698.

Breton, B., Sauvageau, É., Zhou, J., Bonin, H., Le Gouill, C., and Bouvier, M. (2010). Multiplexing of multicolor bioluminescence resonance energy transfer. Biophys. J 99, 4037-4046.

Brown, A.J., Goldsworthy, S.M., Barnes, A.A., Eilert, M.M., Tcheang, L., Daniels, D., Muir, A.I., Wigglesworth, M.J., Kinghorn, I., Fraser, N.J., Pike, N.B., Strum, J.C., Steplewski, K.M., Murdock, P.R., Holder, J.C., Marshall, F.H., Szekeres, P.G., Wilson, S., Ignar, D.M., Foord, S.M., Wise, A., and Dowell, S.J. (2003). The Orphan G protein-coupled receptors GPR41 and GPR43 are activated by propionate and other short chain carboxylic acids. J. Biol. Chem 278, 11312-11319.

Burford, N.T., and Nahorski, S.R. (1996). Muscarinic m1 receptor-stimulated adenylate cyclase activity in Chinese hamster ovary cells is mediated by Gs alpha and is not a consequence of phosphoinositidase C activation. Biochem. J 315 (Pt 3), 883-888.

Burns, D.L. (1988). Subunit structure and enzymic activity of pertussis toxin. Microbiol. Sci *5*, 285-287.

Caulfield, M.P., and Birdsall, N.J. (1998). International Union of Pharmacology. XVII. Classification of muscarinic acetylcholine receptors. Pharmacol. Rev 50, 279-290.

Cheng, Y., and Prusoff, W.H. (1973). Relationship between the inhibition constant (K1) and the concentration of inhibitor which causes 50 per cent inhibition (I50) of an enzymatic reaction. Biochem. Pharmacol 22, 3099-3108.

Chidiac, P., Markin, V.S., and Ross, E.M. (1999). Kinetic control of guanine nucleotide binding to soluble Galpha(q). Biochem. Pharmacol 58, 39-48.

Clapham, D.E., and Neer, E.J. (1997). G protein beta gamma subunits. Annu. Rev. Pharmacol. Toxicol 37, 167-203.

Cockcroft, S., and Gomperts, B.D. (1985). Role of guanine nucleotide binding protein in the activation of polyphosphoinositide phosphodiesterase. Nature 314, 534-536.

Cordeaux, Y., and Hill, S.J. (2002). Mechanisms of cross-talk between G-protein-coupled receptors. Neurosignals 11, 45-57.

Defea, K. (2008). Beta-arrestins and heterotrimeric G-proteins: collaborators and competitors in signal transduction. Br. J. Pharmacol 153 Suppl 1, S298-309.

Defer, N., Best-Belpomme, M., and Hanoune, J. (2000). Tissue specificity and physiological relevance of various isoforms of adenylyl cyclase. Am. J. Physiol. Renal Physiol 279, F400-16.

Dixon, R.A., Kobilka, B.K., Strader, D.J., Benovic, J.L., Dohlman, H.G., Frielle, T., Bolanowski, M.A., Bennett, C.D., Rands, E., Diehl, R.E., Mumford, R.A., Slater, E.E., Sigal, I.S., Caron, M.G., Lefkowitz, R.J., and Strader, C.D. (1986). Cloning of the gene and cDNA for mammalian beta-adrenergic receptor and homology with rhodopsin. Nature 321, 75-79.

Dorsam, R.T., and Gutkind, J.S. (2007). G-protein-coupled receptors and cancer. Nat. Rev. Cancer 7, 79-94.

Emeis, D., Kühn, H., Reichert, J., and Hofmann, K.P. (1982). Complex formation between metarhodopsin II and GTP-binding protein in bovine photoreceptor membranes leads to a shift of the photoproduct equilibrium. FEBS Lett 143, 29-34.

Fang, Y., Ferrie, A.M., Fontaine, N.H., Mauro, J., and Balakrishnan, J. (2006). Resonant waveguide grating biosensor for living cell sensing. Biophys. J 91, 1925-1940.

Fang, Y., Li, G., and Ferrie, A.M. (2007). Non-invasive optical biosensor for assaying endogenous G protein-coupled receptors in adherent cells. J Pharmacol Toxicol Methods 55, 314-322.

Felder, C.C., Briley, E.M., Axelrod, J., Simpson, J.T., Mackie, K., and Devane, W.A. (1993). Anandamide, an endogenous cannabimimetic eicosanoid, binds to the cloned human cannabinoid receptor and stimulates receptor-mediated signal transduction. Proc. Natl. Acad. Sci. U.S.A 90, 7656-7660.

Fredriksson, R., Lagerström, M.C., Lundin, L.-G., and Schiöth, H.B. (2003). The G-protein-coupled receptors in the human genome form five main families. Phylogenetic analysis, paralogon groups, and fingerprints. Mol. Pharmacol 63, 1256-1272.

Freissmuth, M., Boehm, S., Beindl, W., Nickel, P., Ijzerman, A.P., Hohenegger, M., and Nanoff, C. (1996). Suramin analogues as subtype-selective G protein inhibitors. Mol. Pharmacol 49, 602-611.

Fujioka, M., Koda, S., and Morimoto, Y. (1988). Structure of FR900359, a Cyclic Depsipeptide from Ardisia crenata sims. J. Org. Chem., 2820-2825.

Galés, C., van Durm, J.J.J., Schaak, S., Pontier, S., Percherancier, Y., Audet, M., Paris, H., and Bouvier, M. (2006). Probing the activation-promoted structural rearrangements in preassembled receptor-G protein complexes. Nat. Struct. Mol. Biol 13, 778-786.

Guichard, A., Cruz-Moreno, B., Cruz-Moreno, B.C., Aguilar, B., van Sorge, N.M., Kuang, J., Kurkciyan, A.A., Wang, Z., Hang, S., Pineton Chambrun, G.P. de, McCole, D.F., Watnick, P., Nizet, V., and Bier, E. (2013). Cholera toxin disrupts barrier function by inhibiting exocyst-mediated trafficking of host proteins to intestinal cell junctions. Cell Host Microbe 14, 294-305.

Haan, L. de, and Hirst, T.R. (2004). Cholera toxin: a paradigm for multi-functional engagement of cellular mechanisms (Review). Mol. Membr. Biol 21, 77-92.

Hanyaloglu, A.C., and Zastrow, M. von (2008). Regulation of GPCRs by endocytic membrane trafficking and its potential implications. Annu. Rev. Pharmacol. Toxicol 48, 537-568.

Hennen, S., Wang, H., Peters, L., Merten, N., Simon, K., Spinrath, A., Blättermann, S., Akkari, R., Schrage, R., Schröder, R., Schulz, D., Vermeiren, C., Zimmermann, K., Kehraus, S., Drewke, C., Pfeifer, A., König, G.M., Mohr, K., Gillard, M., Müller, C.E., Lu, Q.R., Gomeza, J., and Kostenis, E. (2013). Decoding signaling and function of the orphan G protein-coupled receptor GPR17 with a small-molecule agonist. Sci Signal 6, ra93.

Henstridge, C.M., Balenga, N.A.B., Ford, L.A., Ross, R.A., Waldhoer, M., and Irving, A.J. (2009). The GPR55 ligand L-alpha-lysophosphatidylinositol promotes RhoA-dependent Ca2+ signaling and NFAT activation. FASEB J 23, 183-193.

Hohenegger, M., Waldhoer, M., Beindl, W., Böing, B., Kreimeyer, A., Nickel, P., Nanoff, C., and Freissmuth, M. (1998). Gsalpha-selective G protein antagonists. Proc. Natl. Acad. Sci. U.S.A 95, 346-351.

Jacoby, E., Bouhelal, R., Gerspacher, M., and Seuwen, K. (2006). The 7 TM G-protein-coupled receptor target family. ChemMedChem 1, 761-782.

Jakubík, J., Janíčková, H., Randáková, A., El-Fakahany, E.E., and Doležal, V. (2011). Subtype differences in pre-coupling of muscarinic acetylcholine receptors. PLoS ONE 6, e27732.

Johnston, C.A., and Siderovski, D.P. (2007). Receptor-mediated activation of heterotrimeric G-proteins: current structural insights. Mol. Pharmacol 72, 219-230.

Johnston, C.A., Lobanova, E.S., Shavkunov, A.S., Low, J., Ramer, J.K., Blaesius, R., Fredericks, Z., Willard, F.S., Kuhlman, B., Arshavsky, V.Y., and Siderovski, D.P. (2006). Minimal determinants for binding activated G alpha from the structure of a G alpha(i1)-peptide dimer. Biochemistry 45, 11390-11400.

Johnston, C.A., Willard, F.S., Jezyk, M.R., Fredericks, Z., Bodor, E.T., Jones, M.B., Blaesius, R., Watts, V.J., Harden, T.K., Sondek, J., Ramer, J.K., and Siderovski, D.P. (2005). Structure of Galpha(i1) bound to a GDP-selective peptide provides insight into guanine nucleotide exchange. Structure 13, 1069-1080.

Kan, Z., Jaiswal, B.S., Stinson, J., Janakiraman, V., Bhatt, D., Stern, H.M., Yue, P., Haverty, P.M., Bourgon, R., Zheng, J., Moorhead, M., Chaudhuri, S., Tomsho, L.P., Peters, B.A., Pujara, K., Cordes, S., Davis, D.P., Carlton, V.E.H., Yuan, W., Li, L., Wang, W., Eigenbrot, C., Kaminker, J.S., Eberhard, D.A., Waring, P., Schuster, S.C., Modrusan, Z., Zhang, Z., Stokoe, D., Sauvage, F.J. de, Faham, M., and Seshagiri, S. (2010). Diverse somatic mutation patterns and pathway alterations in human cancers. Nature 466, 869-873.

Kenakin, T., and Christopoulos, A. (2013). Signalling bias in new drug discovery: detection, quantification and therapeutic impact. Nat Rev Drug Discov 12, 205-216.

Kenakin, T.P. (2009). Cellular assays as portals to seven-transmembrane receptor-based drug discovery. Nat Rev Drug Discov 8, 617-626.

Kimple, A.J., Bosch, D.E., Giguère, P.M., and Siderovski, D.P. (2011). Regulators of G-protein signaling and their Gα substrates: promises and challenges in their use as drug discovery targets. Pharmacol. Rev 63, 728-749.

Kimple, R.J., Kimple, M.E., Betts, L., Sondek, J., and Siderovski, D.P. (2002). Structural determinants for GoLoco-induced inhibition of nucleotide release by Galpha subunits. Nature 416, 878-881.

Kobilka, B.K. (2007). G protein coupled receptor structure and activation. Biochim. Biophys. Acta 1768, 794-807.

Kobilka, B.K., MacGregor, C., Daniel, K., Kobilka, T.S., Caron, M.G., and Lefkowitz, R.J. (1987). Functional activity and regulation of human beta 2-adrenergic receptors expressed in Xenopus oocytes. J. Biol. Chem 262, 15796-15802.

Kostenis, E., Waelbroeck, M., and Milligan, G. (2005). Techniques: promiscuous Galpha proteins in basic research and drug discovery. Trends Pharmacol. Sci 26, 595-602.

Kozasa, T., Jiang, X., Hart, M.J., Sternweis, P.M., Singer, W.D., Gilman, A.G., Bollag, G., and Sternweis, P.C. (1998). p115 RhoGEF, a GTPase activating protein for Galpha12 and Galpha13. Science 280, 2109-2111.

Kreutz, B., Yau, D.M., Nance, M.R., Tanabe, S., Tesmer, J.J.G., and Kozasa, T. (2006). A new approach to producing functional G alpha subunits yields the activated and deactivated structures of G alpha(12/13) proteins. Biochemistry 45, 167-174.

Kurose, H. (2003). Galpha12 and Galpha13 as key regulatory mediator in signal transduction. Life Sci 74, 155-161.

Lagerström, M.C., and Schiöth, H.B. (2008). Structural diversity of G protein-coupled receptors and significance for drug discovery. Nat Rev Drug Discov 7, 339-357.

Lambert, N.A., Johnston, C.A., Cappell, S.D., Kuravi, S., Kimple, A.J., Willard, F.S., and Siderovski, D.P. (2010). Regulators of G-protein signaling accelerate GPCR signaling kinetics and govern sensitivity solely by accelerating GTPase activity. Proc. Natl. Acad. Sci. U.S.A 107, 7066-7071.

Lambright, D.G., Noel, J.P., Hamm, H.E., and Sigler, P.B. (1994). Structural determinants for activation of the alpha-subunit of a heterotrimeric G protein. Nature 369, 621-628.

Lappano, R., and Maggiolini, M. (2011). G protein-coupled receptors: novel targets for drug discovery in cancer. Nat Rev Drug Discov 10, 47-60.

Le Poul, E., Loison, C., Struyf, S., Springael, J.-Y., Lannoy, V., Decobecq, M.-E., Brezillon, S., Dupriez, V., Vassart, G., van Damme, J., Parmentier, M., and Detheux, M. (2003). Functional characterization of human receptors for short chain fatty acids and their role in polymorphonuclear cell activation. J. Biol. Chem 278, 25481-25489.

Lean, A. de, Stadel, J.M., and Lefkowitz, R.J. (1980). A ternary complex model explains the agonist-specific binding properties of the adenylate cyclase-coupled beta-adrenergic receptor. J. Biol. Chem 255, 7108-7117.

Leyers, S., Häcker, H.-G., Wiendlocha, J., Gütschow, M., and Wiese, M. (2008). A 4-aminobenzoic acid derivative as novel lead for selective inhibitors of multidrug resistance-associated proteins. Bioorg. Med. Chem. Lett 18, 4761-4763.

Loening, A.M., Fenn, T.D., Wu, A.M., and Gambhir, S.S. (2006). Consensus guided mutagenesis of Renilla luciferase yields enhanced stability and light output. Protein Eng. Des. Sel 19, 391-400.

Lutz, S., Shankaranarayanan, A., Coco, C., Ridilla, M., Nance, M.R., Vettel, C., Baltus, D., Evelyn, C.R., Neubig, R.R., Wieland, T., and Tesmer, J.J.G. (2007). Structure of Galphaq-p63RhoGEF-RhoA complex reveals a pathway for the activation of RhoA by GPCRs. Science 318, 1923-1927.

Mangmool, S., and Kurose, H. (2011). G(i/o) protein-dependent and -independent actions of Pertussis Toxin (PTX). Toxins (Basel) 3, 884-899.

Masu, Y., Nakayama, K., Tamaki, H., Harada, Y., Kuno, M., and Nakanishi, S. (1987). cDNA cloning of bovine substance-K receptor through oocyte expression system. Nature 329, 836-838.

McGuinness, R. (2007). Impedance-based cellular assay technologies: recent advances, future promise. Curr Opin Pharmacol 7, 535-540.

Middlebrook, J.L., and Dorland, R.B. (1984). Bacterial toxins: cellular mechanisms of action. Microbiol. Rev 48, 199-221.

Miller, C.E., Majewski, J., Watkins, E.B., and Kuhl, T.L. (2008). Part I: an x-ray scattering study of cholera toxin penetration and induced phase transformations in lipid membranes. Biophys. J 95, 629-640.

Milligan, G., and Kostenis, E. (2006). Heterotrimeric G-proteins: a short history. Br. J. Pharmacol 147 Suppl 1, S46-55.

Miloslavina, A., Ebert, C., Tietze, D., Ohlenschläger, O., Englert, C., Görlach, M., and Imhof, D. (2010). An unusual peptide from Conus villepinii: synthesis, solution structure, and cardioactivity. Peptides 31, 1292-1300.

Nesterov, A., Hong, M., Hertel, C., Jiao, P., Brownell, L., and Cannon, E. (2010). Screening a plant extract library for inhibitors of cholecystokinin receptor CCK1 pathways. J Biomol Screen 15, 518-527.

Nilsson, N.E., Kotarsky, K., Owman, C., and Olde, B. (2003). Identification of a free fatty acid receptor, FFA2R, expressed on leukocytes and activated by short-chain fatty acids. Biochem. Biophys. Res. Commun 303, 1047-1052.

Nishimura, A., Kitano, K., Takasaki, J., Taniguchi, M., Mizuno, N., Tago, K., Hakoshima, T., and Itoh, H. (2010). Structural basis for the specific inhibition of heterotrimeric Gq protein by a small molecule. Proc. Natl. Acad. Sci. U.S.A 107, 13666-13671.

Offermanns, S. (2003). G-proteins as transducers in transmembrane signalling. Prog. Biophys. Mol. Biol 83, 101-130.

Offermanns, S., Wieland, T., Homann, D., Sandmann, J., Bombien, E., Spicher, K., Schultz, G., and Jakobs, K.H. (1994). Transfected muscarinic acetylcholine receptors selectively couple to Gi-type G proteins and Gq/11. Mol. Pharmacol 45, 890-898.

Oldham, W.M., and Hamm, H.E. (2008). Heterotrimeric G protein activation by G-protein-coupled receptors. Nat. Rev. Mol. Cell Biol 9, 60-71.

Pierce, K.L., Premont, R.T., and Lefkowitz, R.J. (2002). Seven-transmembrane receptors. Nat. Rev. Mol. Cell Biol 3, 639-650.

Pitcher, J.A., Freedman, N.J., and Lefkowitz, R.J. (1998). G protein-coupled receptor kinases. Annu. Rev. Biochem 67, 653-692.

Pittman, M. (1979). Pertussis toxin: the cause of the harmful effects and prolonged immunity of whooping cough. A hypothesis. Rev. Infect. Dis 1, 401-412.

Prévost, G.P., Lonchampt, M.O., Holbeck, S., Attoub, S., Zaharevitz, D., Alley, M., Wright, J., Brezak, M.C., Coulomb, H., Savola, A., Huchet, M., Chaumeron, S., Nguyen, Q.-D., Forgez, P., Bruyneel, E., Bracke, M., Ferrandis, E., Roubert, P., Demarquay, D., Gespach, C., and Kasprzyk, P.G. (2006). Anticancer activity of BIM-46174, a new inhibitor of the heterotrimeric Galpha/Gbetagamma protein complex. Cancer Res 66, 9227-9234.

Qin, K., Dong, C., Wu, G., and Lambert, N.A. (2011). Inactive-state preassembly of G(q)-coupled receptors and G(q) heterotrimers. Nat. Chem. Biol 7, 740-747.

Rodbell, M., Krans, H.M., Pohl, S.L., and Birnbaumer, L. (1971). The glucagon-sensitive adenyl cyclase system in plasma membranes of rat liver. IV. Effects of guanylnucleotides on binding of 125I-glucagon. J. Biol. Chem 246, 1872-1876.

Ross, R.A. (2009). The enigmatic pharmacology of GPR55. Trends Pharmacol. Sci 30, 156-163.

Ryberg, E., Larsson, N., Sjögren, S., Hjorth, S., Hermansson, N.-O., Leonova, J., Elebring, T., Nilsson, K., Drmota, T., and Greasley, P.J. (2007). The orphan receptor GPR55 is a novel cannabinoid receptor. Br. J. Pharmacol 152, 1092-1101.

Sack, D.A., Sack, R.B., Nair, G.B., and Siddique, A.K. (2004). Cholera. Lancet 363, 223-233.

Saulière, A., Bellot, M., Paris, H., Denis, C., Finana, F., Hansen, J.T., Altié, M.-F., Seguelas, M.-H., Pathak, A., Hansen, J.L., Sénard, J.-M., and Galés, C. (2012). Deciphering biased-agonism complexity reveals a new active AT1 receptor entity. Nat. Chem. Biol 8, 622-630.

Schmidt, J., Liebscher, K., Merten, N., Grundmann, M., Mielenz, M., Sauerwein, H., Christiansen, E., Due-Hansen, M.E., Ulven, T., Ullrich, S., Gomeza, J., Drewke, C., and Kostenis, E. (2011). Conjugated linoleic acids mediate insulin release through islet G protein-coupled receptor FFA1/GPR40. J. Biol. Chem 286, 11890-11894.

Schmitz, A.-L., Schrage, R., Gaffal, E., Charpentier, T.H., Wiest, J., Hiltensperger, G., Morschel, J., Hennen, S., Häußler, D., Horn, V., Wenzel, D., Grundmann, M., Büllesbach, K.M., Schröder, R., Brewitz, H.H., Schmidt, J., Gomeza, J., Galés, C., Fleischmann, B.K., Tüting, T., Imhof, D., Tietze, D., Gütschow, M., Holzgrabe, U., Sondek, J., Harden, T.K., Mohr, K., and Kostenis, E. (2014). A cell-permeable inhibitor to trap Gαq proteins in the empty pocket conformation. Chem. Biol 21, 890-902.

Schröder, R., Janssen, N., Schmidt, J., Kebig, A., Merten, N., Hennen, S., Müller, A., Blättermann, S., Mohr-Andrä, M., Zahn, S., Wenzel, J., Smith, N.J., Gomeza, J., Drewke, C., Milligan, G., Mohr, K., and Kostenis, E. (2010). Deconvolution of complex G protein-coupled receptor signaling in live cells using dynamic mass redistribution measurements. Nat. Biotechnol 28, 943-949.

Seifert, R., Gether, U., Wenzel-Seifert, K., and Kobilka, B.K. (1999). Effects of guanine, inosine, and xanthine nucleotides on beta(2)-adrenergic receptor/G(s) interactions: evidence for multiple receptor conformations. Mol. Pharmacol 56, 348-358.

Simon, M.I., Strathmann, M.P., and Gautam, N. (1991). Diversity of G proteins in signal transduction. Science 252, 802-808.

Simonds, W.F. (1999). G protein regulation of adenylate cyclase. Trends Pharmacol. Sci 20, 66-73.

Smrcka, A.V. (2013). Molecular targeting of Gα and Gβγ subunits: a potential approach for cancer therapeutics. Trends Pharmacol. Sci 34, 290-298.

Stoddart, L.A., Smith, N.J., Jenkins, L., Brown, A.J., and Milligan, G. (2008). Conserved polar residues in transmembrane domains V, VI, and VII of free fatty acid receptor 2 and free fatty acid receptor 3 are required for the binding and function of short chain fatty acids. J. Biol. Chem 283, 32913-32924.

Takasaki, J., Saito, T., Taniguchi, M., Kawasaki, T., Moritani, Y., Hayashi, K., and Kobori, M. (2004). A novel Galphaq/11-selective inhibitor. J. Biol. Chem 279, 47438-47445.

Taniguchi, M., Suzumura, K.-I., Nagai, K., Kawasaki, T., Takasaki, J., Sekiguchi, M., Moritani, Y., Saito, T., Hayashi, K., Fujita, S., Tsukamoto, S.-I., and Suzuki, K.-I. (2004). YM-254890 analogues, novel cyclic depsipeptides with Galpha(q/11) inhibitory activity from Chromobacterium sp. QS3666. Bioorg. Med. Chem 12, 3125-3133.

Tesmer, V.M., Kawano, T., Shankaranarayanan, A., Kozasa, T., and Tesmer, J.J.G. (2005). Snapshot of activated G proteins at the membrane: the Galphaq-GRK2-Gbetagamma complex. Science 310, 1686-1690.

van Raamsdonk, C.D., Bezrookove, V., Green, G., Bauer, J., Gaugler, L., O'Brien, J.M., Simpson, E.M., Barsh, G.S., and Bastian, B.C. (2009). Frequent somatic mutations of GNAQ in uveal melanoma and blue naevi. Nature 457, 599-602.

van Raamsdonk, C.D., Griewank, K.G., Crosby, M.B., Garrido, M.C., Vemula, S., Wiesner, T., Obenauf, A.C., Wackernagel, W., Green, G., Bouvier, N., Sozen, M.M., Baimukanova, G., Roy, R., Heguy, A., Dolgalev, I., Khanin, R., Busam, K., Speicher, M.R., O'Brien, J., and Bastian, B.C. (2010). Mutations in GNA11 in uveal melanoma. N. Engl. J. Med 363, 2191-2199.

Waldo, G.L., Ricks, T.K., Hicks, S.N., Cheever, M.L., Kawano, T., Tsuboi, K., Wang, X., Montell, C., Kozasa, T., Sondek, J., and Harden, T.K. (2010). Kinetic scaffolding mediated by a phospholipase C-beta and Gq signaling complex. Science 330, 974-980.

Wall, M.A., Posner, B.A., and Sprang, S.R. (1998). Structural basis of activity and subunit recognition in G protein heterotrimers. Structure 6, 1169-1183.

Weiss, W.A., Taylor, S.S., and Shokat, K.M. (2007). Recognizing and exploiting differences between RNAi and small-molecule inhibitors. Nat. Chem. Biol 3, 739-744.

Wortelboer, H.M., Usta, M., van der Velde, A.E., Boersma, M.G., Spenkelink, B., van Zanden, J.J., Rietjens, I.M.C.M., van Bladeren, P.J., and Cnubben, N.H.P. (2003). Interplay between MRP inhibition and metabolism of MRP inhibitors: the case of curcumin. Chem. Res. Toxicol 16, 1642-1651.

Worzfeld, T., Wettschureck, N., and Offermanns, S. (2008). G(12)/G(13)-mediated signalling in mammalian physiology and disease. Trends Pharmacol. Sci 29, 582-589.

8 Appendix

Chemical structures of BIM-dimer analogs tested in CHO-M1 cells (see chapter 3.1.14).

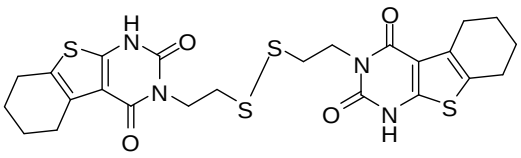

Gü237

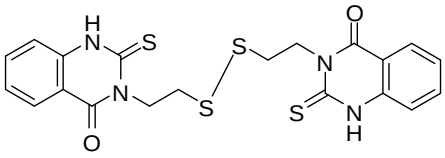

Gü257

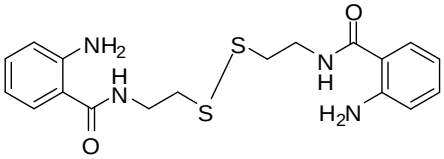

Gü260

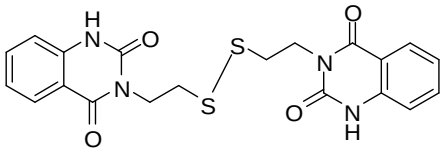

Gü267

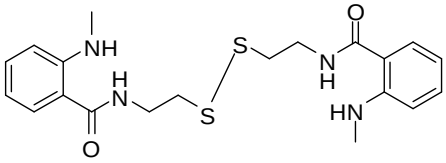

Gü269

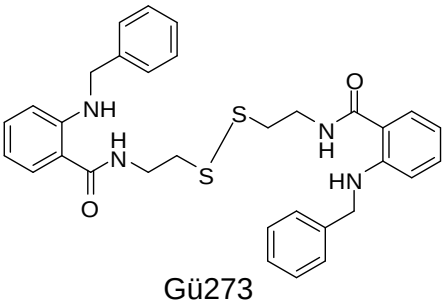

Gü273

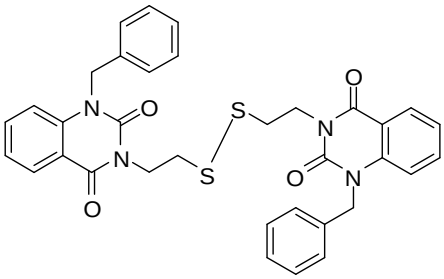

Gü276

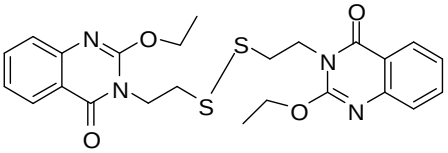

Gü366

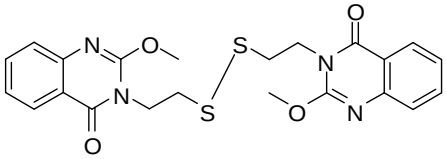

Gü287

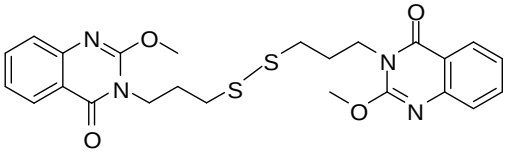

Gü368

Erklärung

Hiermit erkläre ich, dass ich die vorliegende Dissertation selbständig angefertigt habe. Es wurden nur die in der Arbeit ausdrücklich benannten Quellen und Hilfsmittel benutzt. Wörtlich oder sinngemäß übernommenes Gedankengut habe ich als solches kenntlich gemacht.

Ort, Datum	Unterschrift

Acknowledgment

Mein besonderer Dank gilt meiner Doktormutter Frau Prof. Evi Kostenis für die Aufnahme in ihre Arbeitsgruppe und die Überlassung des interessanten Themas sowie für die wissenschaftliche und persönliche Unterstützung während der Doktorarbeit.

Frau Prof. G. M. König möchte ich herzlich für die Bereitschaft zur Übernahme des Koreferrats der Arbeit danken.

Bei Herrn Prof. K. Mohr und Frau Professor H. Wägele möchte ich mich dafür bedanken, dass sie als weitere Mitglieder der Prüfungskommission zur Verfügung stehen.

Zudem danke ich der Arbeitsgruppe von Herrn Prof. K. Mohr für die gute und inspirierende Zusammenarbeit. Hierbei gilt ein besonderer Dank Frau Dr. Ramona Schrage für die Durchführung der Bindungsexperimente und die Untersuchungen an MZ7 Zellen, sowie für die stetige Gesprächsbereitschaft.

Der Arbeitsgruppe von Frau Prof. U. Holzgrabe (Pharmazeutische Chemie, Universität Würzburg) und hierbei insbesondere Herrn Dr. Georg Hiltensperger und Johannes Wiest für die Synthese von BIM und die Durchführung von Stabilitätsuntersuchungen.

Bei der Arbeitsgruppe von Herrn Prof. M. Gütschow bedanke ich mich für die Nachsynthese von BIM, sowie für die Bereitstellung der BIM-Analoga und Hemmstoffe für Multidrug-Transporter.

Ich danke der Arbeitsgruppe von Dr. C. Galés (INSERM, Toulouse, Frankreich) und hierbei besonders der Mitarbeiterin Ségolène Galandrin für die Durchführung von BRET Assays, sowie für die Bereitstellung der BRET-Konstrukte.

Der Arbeitsgruppe von Dr. S. Laporte (McGill Universität, Montréal, Kanada) und Dr. M. Bouvier und dem Mitarbeiter Sylvain Armando danke ich für die Durchführung von BRET Experimenten.

Ich möchte mich bei der Arbeitsgruppe von Dr. J. Sondek (University of North Carolina, Chapel Hill, USA) und Dr. T. K. Harden danken und hierbei insbesondere dem Mitarbeiter Dr. T. H. Charpentier, der die Versuche zur GDP Dissoziation durchgeführt hat.

Bei der Arbeitsgruppe von Herrn Prof. B. K. Fleischmann und bei Dr. D. Wenzel möchte ich mich für die Daten des Einzellcalciumassays bedanken.

Frau Dr. E. Gaffal danke ich für die Bereitstellung der MZ7 Zellen und die konstruktive Zusammenarbeit im Rahmen des Projekts.

Der Arbeitsgruppe von Frau Prof. C. E. Müller danke ich für die Synthese von QIC red.

Ich möchte mich bei der Arbeitsgruppe von Frau Prof. G. König und hier besonders bei Dr. S. Kehraus für die Bereitstellung von QIC und die stets freundliche und unkomplizierte Zusammenarbeit während der Promotion bedanken.

Ich bedanke mich bei Nina Heycke für die großartige Unterstützung der praktischen Arbeit, die wunderbare Teamarbeit und für viele motivierende Gespräche über Probleme jeglicher Art.

Bei Dr. S. Blättermann möchte ich mich für die Durchführung der Calciumassays im Rahmen des Stabilitätstests von QIC und bedanken.

Julia Morschel danke ich für die Western Blot Analysen und darüber hinaus für die schöne gemeinsame Bürozeit und stetige Unterstützung in allen Belangen.

Bei Katrin Büllesbach bedanke ich mich für cAMP Daten, das Korrekturlesen der Arbeit, die stets motivierenden Gespräche und die angenehme Atmosphäre im Büro.

Ich danke Manuel Grundmann für cAMP und IP1 Daten, für sehr konstruktive Gespräche, das Korrekturlesen der Arbeit und die nette Zeit im gemeinsamen Büro.

Tigisti Beraki-Schauff danke ich für die Versuche mit QIC-Derivaten im Rahmen ihrer Masterarbeit.

Dr. N. Merten, Dr. S. Hennen und Dr. R. Schröder danke ich dafür, dass sie bei Fragen zu neuen Methoden immer ansprechbar waren und viele hilfreiche Hinweise geben konnten.

Ich danke Herrn T. Kögler für seine Hilfe bei Problemen aller Art mit den technischen Geräten und Frau E. Gassen für die freundliche Hilfe bei allen verwaltungstechnischen Aufgaben und Problemen.

Der ehemaligen Leiterin des Kurses „Pharmazeutische Biologie II“, Frau Dr. M. Koch, sowie dem jetzigen Leiter Dr. R. Schröder und den anderen Assistenten des Kurses danke ich für die angenehme Atmosphäre in der Zeit als Betreuer.

Frau Dr. C. Drewke und Herrn Dr. J. Gomeza danke ich für die Gesprächsbereitschaft und Unterstützung während der Arbeit.

Allen namentlich und nicht namentlich erwähnten Kollegen/Innen des Instituts für Pharmazeutische Biologie in Bonn danke ich für die gute Zusammenarbeit und die schöne Atmosphäre in den letzten Jahren.

Für die vielen motivierenden Worte und unendliche Geduld während der Promotionszeit danke ich meinem Mann Alexander Schmitz, ohne den ich die Arbeit nicht hätte vollenden können. Zudem danke ich ihm für das Korrekturlesen der Arbeit.

Meinen Eltern und meiner Schwester danke ich ganz besonders für die stetige Unterstützung und für die vielen motivierenden Gespräche während der Doktorarbeit.